

Introduction

3. Introduction to Carbon Nanotubes

Carbon nanotubes are remarkable objects that look set to revolutionize the technological landscape in the near future. Tomorrow's society will be shaped by nanotube applications, just as silicon-based technologies dominate society today. Space elevators tethered by the strongest of cables; hydrogen-powered vehicles; artificial muscles: these are just a few of the technological marvels that may be made possible by the emerging science of carbon nanotubes.

Of course, this prediction is still some way from becoming reality; we are still at the stage of evaluating possibilities and potential. Consider the recent example of fullerenes – molecules closely related to nanotubes. The anticipation surrounding these molecules, first reported in 1985, resulted in the bestowment of a Nobel Prize for their discovery in 1996. However, a decade later, few applications of fullerenes have reached the market, suggesting that similarly enthusiastic predictions about nanotubes should be approached with caution.

There is no denying, however, that the expectations surrounding carbon nanotubes are very high. One of the main reasons for this is the anticipated application of nanotubes to electronics. Many believe that current techniques for miniaturizing microchips are about to reach their lowest limits, and that nanotube-based technologies are the best hope for further miniaturization. Carbon nanotubes may therefore provide the building blocks for further technological progress, enhancing our standards of living.

In this chapter, we first describe the structures, syntheses, growth mechanisms and properties of carbon nanotubes. Then we discuss nanotube-related nano-objects, including those formed by reactions and associations of all-carbon nanotubes with foreign atoms, molecules and compounds, which may provide the path to hybrid materials with even better properties than "pristine" nanotubes. Finally, we will describe the most

3.1 Structure of Carbon Nanotubes	44
3.1.1 Single-Wall Nanotubes	44
3.1.2 Multiwall Nanotubes	47
3.2 Synthesis of Carbon Nanotubes	49
3.2.1 Solid Carbon Source-Based Production Techniques for Carbon Nanotubes	49
3.2.2 Gaseous Carbon Source-Based Production Techniques for Carbon Nanotubes	57
3.2.3 Miscellaneous Techniques	63
3.2.4 Synthesis of Carbon Nanotubes with Controlled Orientation	63
3.3 Growth Mechanisms of Carbon Nanotubes	65
3.3.1 Catalyst-Free Growth	65
3.3.2 Catalytically Activated Growth	65
3.4 Properties of Carbon Nanotubes	69
3.4.1 Overview	69
3.4.2 General Properties of SWNTs	69
3.4.3 Adsorption Properties of SWNTs	69
3.4.4 Electronic and Optical Properties	72
3.4.5 Mechanical Properties	73
3.4.6 Reactivity	74
3.5 Carbon Nanotube-Based Nano-Objects	74
3.5.1 Heteronanotubes	74
3.5.2 Hybrid Carbon Nanotubes	75
3.5.3 Functionalized Nanotubes	78
3.6 Applications of Carbon Nanotubes	80
3.6.1 Current Applications	80
3.6.2 Expected Applications Related to Adsorption	84
3.6.3 Expected Applications Related to Composite Systems	88
3.7 Concluding Remarks	95
References	95

important current and potential applications of carbon nanotubes, which suggest that the future for the carbon nanotube industry looks very promising indeed.

Carbon nanotubes have long been synthesized as products of the action of a catalyst on the gaseous species originating from the thermal decomposition of hydrocarbons (see Sect. 3.2). The first evidence that the nanofilaments produced in this way were actually nanotubes – that they exhibited an inner cavity – can be found in the transmission electron microscope micrographs published by *Radushkevich* et al. in 1952 [3.1]. This was of course related to and made possible by the progress in transmission electron microscopy. It is then likely that the carbon filaments prepared by *Hughes* and *Chambers* in 1889 [3.2], which is probably the first patent ever deposited in the field, and whose preparation method was also based on the catalytically enhanced thermal cracking of hydrocarbons, were already carbon nanotube-related morphologies. The preparation of vapor-grown carbon fibers was actually reported over a century ago [3.3, 4]. Since then, the interest in carbon nanofilaments/nanotubes has been recurrent, though within a scientific area almost limited to the carbon material scientist community. The reader is invited to consult the review published by *Baker* et al. [3.5] regarding the early works. Worldwide enthusiasm came unexpectedly in 1991, after the catalyst-free formation of nearly perfect concentric multiwall carbon nanotubes (c-MWNTs, see Sect. 3.1) was reported [3.6] as by-products of the formation of fullerenes via the electric-arc technique. But the real breakthrough occurred two years later, when attempts to fill the nanotubes in situ with various metals (see

Sect. 3.5) led to the discovery – again unexpected – of single-wall carbon nanotubes (SWNTs) simultaneously by *Iijima* et al. [3.7] and *Bethune* et al. [3.8]. Single-wall carbon nanotubes were really new nano-objects with properties and behaviors that are often quite specific (see Sect. 3.4). They are also beautiful objects for fundamental physics as well as unique molecules for experimental chemistry, although they are still somewhat mysterious since their formation mechanisms are the subject of controversy and are still debated (see Sect. 3.3). Potential applications seem countless, although few have reached marketable status so far (see Sect. 3.6). Consequently, about five papers a day are currently published by research teams from around the world with carbon nanotubes as the main topic, an illustration of how extraordinarily active – and highly competitive – this field of research is. It is an unusual situation, similar to that for fullerenes, which, by the way, are again carbon nano-objects structurally closely related to nanotubes.

This is not, however, only about scientific exaltation. Economic aspects are leading the game to a greater and greater extent. According to experts, the world market was estimated to be more than 430 million dollars in 2004 and it is predicted to grow to several billion dollars before 2009. That is serious business, and it will be closely related to how scientists and engineers deal with the many challenges found on the path from the beautiful, ideal molecule to the reliable – and it is hoped, cheap – manufactured product.

3.1 Structure of Carbon Nanotubes

It is relatively easy to imagine a single-wall carbon nanotube (SWNT). Ideally, it is enough to consider a perfect graphene sheet (graphene is a polyaromatic monoatomic layer consisting of sp^2 -hybridized carbon atoms arranged in hexagons; genuine graphite consists of layers of this graphene) and to roll it into a cylinder (Fig. 3.1), making sure that the hexagonal rings placed in contact join coherently. Then the tips of the tube are sealed by two caps, each cap being a hemi-fullerene of the appropriate diameter (Fig. 3.2a–c).

3.1.1 Single-Wall Nanotubes

Geometrically, there is no restriction on the tube diameter. However, calculations have shown that collapsing the single-wall tube into a flattened two-layer rib-

bon is energetically more favorable than maintaining the tubular morphology beyond a diameter value of ≈ 2.5 nm [3.9]. On the other hand, it is easy to grasp intuitively that the shorter the radius of curvature, the higher the stress and the energetic cost, although SWNTs with diameters as low as 0.4 nm have been synthesized successfully [3.10]. A suitable energetic compromise is therefore reached for ≈ 1.4 nm, the most frequent diameter encountered regardless of the synthesis technique (at least for those based on solid carbon sources) when conditions ensuring high SWNT yields are used. There is no such restriction on the nanotube length, which only depends on the limitations of the preparation method and the specific conditions used for the synthesis (thermal gradients, residence time, and so on). Experimental data are consistent with these statements, since SWNTs

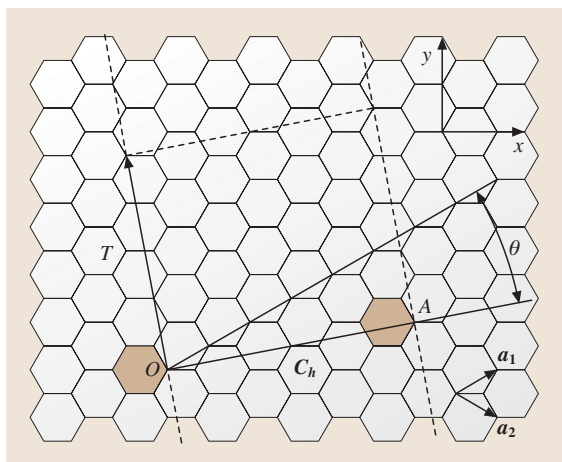


Fig. 3.1 Sketch of the way to make a single-wall carbon nanotube, starting from a graphene sheet (adapted from [3.11])

wider than 2.5 nm are only rarely reported in the literature, whatever the preparation method, while the length of the SWNTs can be in the micrometer or the millimeter range. These features make single-wall carbon nanotubes a unique example of single molecules with huge aspect ratios.

Two important consequences derive from the SWNT structure as described above:

1. All carbon atoms are involved in hexagonal aromatic rings only and are therefore in equivalent positions, except at each nanotube tip, where $6 \times 5 = 30$ atoms are involved in pentagonal rings (considering that adjacent pentagons are unlikely) – though not more, not less, as a consequence of Euler’s rule that also governs the fullerene structure. For ideal SWNTs, chemical reactivity will therefore be highly favored at the tube tips, at the locations of the pentagonal rings.
2. Although carbon atoms are involved in aromatic rings, the C=C bond angles are not planar. This means that the hybridization of carbon atoms is not pure sp^2 ; it has some degree of the sp^3 character, in a proportion that increases as the tube radius of curvature decreases. The effect is the same as for the C_{60} fullerene molecules, whose radius of curvature is 0.35 nm, and whose bonds therefore have 10% sp^3 character [3.13]. On the one hand, this is believed to make the SWNT surface a bit more reactive than regular, planar graphene, even though it still consists of aromatic ring faces. On the other hand, this some-

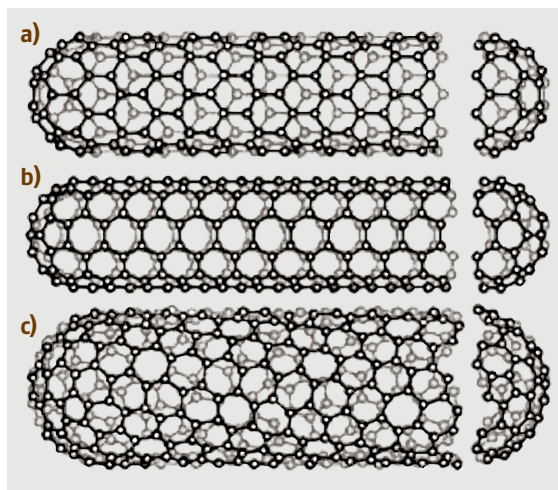


Fig. 3.2a–c Sketches of three different SWNT structures that are examples of (a) a zig-zag-type nanotube, (b) an armchair-type nanotube, (c) a helical nanotube (adapted from [3.12])

how induces variable overlapping of energy bands, resulting in unique and versatile electronic behavior (see Sect. 3.4).

As illustrated by Fig. 3.2, there are many ways to roll a graphene into a single-wall nanotube, with some of the resulting nanotubes possessing planes of symmetry both parallel and perpendicular to the nanotube axis (such as the SWNTs from Fig. 3.2a and 3.2b), while others do not (such as the SWNT from Fig. 3.2c). Similar to the terms used for molecules, the latter are commonly called “chiral” nanotubes, since they are unable to be superimposed on their own image in a mirror. “Helical” is however sometimes preferred (see below). The various ways to roll graphene into tubes are therefore mathematically defined by the vector of helicity C_h , and the angle of helicity θ , as follows (referring to Fig. 3.1):

$$OA = C_h = na_1 + ma_2$$

with

$$a_1 = \frac{a\sqrt{3}}{2}x + \frac{a}{2}y \quad \text{and} \quad a_2 = \frac{a\sqrt{3}}{2}x - \frac{a}{2}y$$

$$\text{where } a = 2.46 \text{ \AA}$$

and

$$\cos \theta = \frac{2n + m}{2\sqrt{n^2 + m^2 + nm}}$$

where n and m are the integers of the vector OA considering the unit vectors a_1 and a_2 .

The vector of helicity $C_h (= OA)$ is perpendicular to the tube axis, while the angle of helicity θ is taken with respect to the so-called zig-zag axis: the vector of helicity that results in nanotubes of the “zig-zag” type (see below). The diameter D of the corresponding nanotube is related to C_h by the relation:

$$D = \frac{|C_h|}{\pi} = \frac{a_{CC}\sqrt{3(n^2 + m^2 + nm)}}{\pi},$$

where

$$1.41 \text{ \AA} \leq a_{C=C} \leq 1.44 \text{ \AA} \quad (\text{graphite}) \quad (C_{60})$$

The C–C bond length is actually elongated by the curvature imposed by the structure; the average bond length in the C_{60} fullerene molecule is a reasonable upper limit, while the bond length in flat graphene in genuine graphite is the lower limit (corresponding to an infinite radius of curvature). Since C_h , θ , and D are all expressed as a function of the integers n and m , they are sufficient to define any particular SWNT by denoting them (n, m) . The values of n and m for a given SWNT can be simply obtained by counting the number of hexagons that separate the extremities of the C_h vector following the unit vector a_1 first and then a_2 [3.11]. In the example of Fig. 3.1, the SWNT that is obtained by rolling the graphene so that the two shaded aromatic cycles can be superimposed exactly is a (4,2) chiral nanotube. Similarly, SWNTs from Fig. 3.2a to 3.2c are (9,0), (5,5), and (10,5) nanotubes respectively, thereby providing examples of zig-zag-type SWNT (with an angle of helicity = 0°), armchair-type SWNT (with an angle of helicity of 30°) and a chiral SWNT, respectively. This also illustrates why the term “chiral” is sometimes inappropriate and should preferably be replaced with “helical”. Armchair (n, n) nanotubes, although definitely achiral from the standpoint of symmetry, exhibit a nonzero “chiral angle”. “Zig-zag” and “armchair” qualifications for



Fig. 3.3 Image of two neighboring chiral SWNTs within a SWNT bundle as seen using high-resolution scanning tunneling microscopy (courtesy of Prof. Yazdani, University of Illinois at Urbana, USA)

achiral nanotubes refer to the way that the carbon atoms are displayed at the edge of the nanotube cross-section (Fig. 3.2a and 3.2b). Generally speaking, it is clear from Figs. 3.1 and 3.2a that having the vector of helicity perpendicular to any of the three overall C=C bond directions will provide zig-zag-type SWNTs, denoted $(n, 0)$, while having the vector of helicity parallel to one of the three C=C bond directions will provide armchair-type SWNTs, denoted (n, n) . On the other hand, because of the sixfold symmetry of the graphene sheet, the angle of helicity θ for the chiral (n, m) nanotubes is such that $0 < \theta < 30^\circ$. Figure 3.3 provides two examples of what chiral SWNTs look like, as seen via atomic force microscopy.

The graphenes in graphite have π electrons which are accommodated by the stacking of graphenes, allowing van der Waals forces to develop. Similar reasons make fullerenes gather and order into fullerite crystals and SWNTs into SWNT ropes (Fig. 3.4a). Provided the SWNT diameter distribution is narrow, the SWNTs in ropes tend to spontaneously arrange into hexagonal arrays, which correspond to the highest compactness achievable (Fig. 3.4b). This feature brings new periodicities with respect to graphite or turbostratic polyaromatic carbon crystals. Turbostratic structure corresponds to

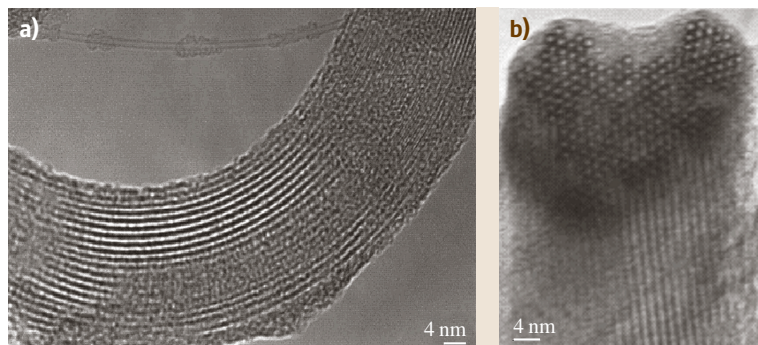


Fig. 3.4a,b High-resolution transmission electron microscopy images of a SWNT rope. (a) Longitudinal view. An isolated single SWNT also appears at the top of the image. (b) Cross-sectional view (from [3.14])

graphenes that are stacked with random rotations or translations instead of being piled up following sequential ABAB positions, as in graphite structure. This implies that no lattice atom plane exists other than the graphene planes themselves (corresponding to the (001) atom plane family). These new periodicities give specific diffraction patterns that are quite different to those of other sp^2 -carbon-based crystals, although hk reflections, which account for the hexagonal symmetry of the graphene plane, are still present. On the other hand, 00l reflections, which account for the stacking sequence of graphenes in regular, “multilayered” polyaromatic crystals (which do not exist in SWNT ropes) are absent. This hexagonal packing of SWNTs within the ropes requires that SWNTs exhibit similar diameters, which is the usual case for SWNTs prepared by electric arc or laser vaporization processes. SWNTs prepared using these methods are actually about 1.35 nm wide (diameter of a (10,10) tube, among others), for reasons that are still unclear but are related to the growth mechanisms specific to the conditions provided by these techniques (see Sect. 3.3).

3.1.2 Multiwall Nanotubes

Building multiwall carbon nanotubes is a little bit more complex, since it involves the various ways graphenes can be displayed and mutually arranged within filamentary morphology. A similar versatility can be expected to the usual textural versatility of polyaromatic solids. Likewise, their diffraction patterns are difficult to differentiate from those of anisotropic polyaromatic solids. The easiest MWNT to imagine is the concentric type (c-MWNT), in which SWNTs with regularly increasing diameters are coaxially arranged (according to a Russian-doll model) into a multiwall nanotube (Fig. 3.5). Such nanotubes are generally formed either by the electric arc technique (without the need for a catalyst), by catalyst-enhanced thermal cracking of gaseous hydrocarbons, or by CO disproportionation (see Sect. 3.2). There can be any number of walls (or coaxial tubes), from two upwards. The intertube distance is approximately the same as the intergraphene distance in turbostratic, polyaromatic solids, 0.34 nm (as opposed to 0.335 nm in genuine graphite), since the increasing radius of curvature imposed on the concentric graphenes prevents the carbon atoms from being arranged as in graphite, with each of the carbon atoms from a graphene facing either a ring center or a carbon atom from the neighboring graphene. However, two cases allow a nanotube to reach – totally or partially – the 3-D crystal periodicity of graphite. One is to consider a high num-

ber of concentric graphenes: concentric graphenes with a long radius of curvature. In this case, the shift in the relative positions of carbon atoms from superimposed graphenes is so small with respect to that in graphite that some commensurability is possible. This may result in MWNTs where both structures are associated; in other words they have turbostratic cores and graphitic outer parts [3.15]. The other case occurs for c-MWNTs exhibiting faceted morphologies, originating either from the synthesis process or more likely from subsequent heat treatment at high temperature (such as 2500 °C) in inert atmosphere. Facets allow the graphenes to resume a flat arrangement of atoms (except at the junction between neighboring facets) which allows the specific stacking sequence of graphite to develop.

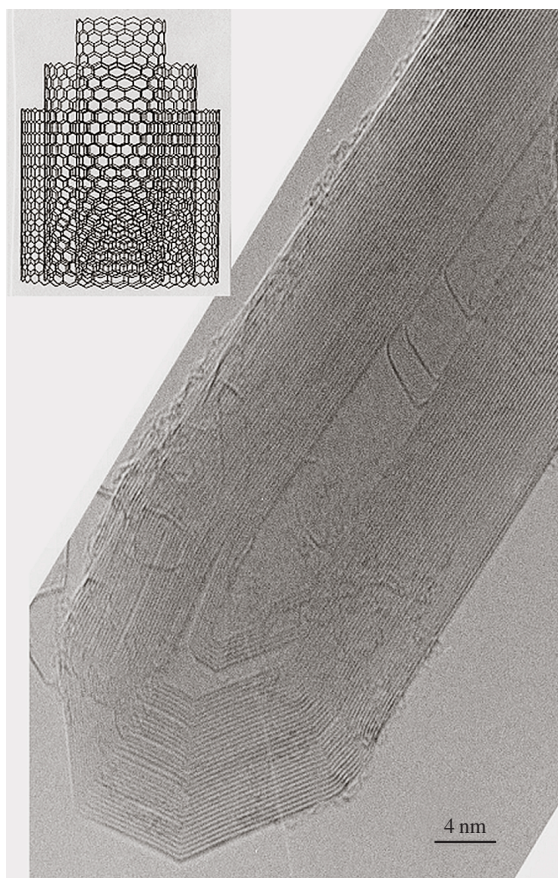


Fig. 3.5 High-resolution transmission electron microscopy image (longitudinal view) of a concentric multiwall carbon nanotube (c-MWNT) prepared using an electric arc. The *insert* shows a sketch of the Russian-doll-like arrangement of graphenes

Another frequent inner texture for multiwall carbon nanotubes is the so-called herringbone texture (h-MWNTs), in which the graphenes make an angle with respect to the nanotube axis (Fig. 3.6). The angle value varies upon the processing conditions (such as the catalyst morphology or the composition of the atmosphere), from 0 (in which case the texture becomes that of a c-MWNT) to 90° (in which case the filament is no longer a tube, see below), and the inner diameter varies so that the tubular arrangement can be lost [3.16], meaning that the latter are more accurately called nanofibers rather than nanotubes. h-MWNTs are exclusively obtained by processes involving catalysts, generally catalyst-enhanced thermal cracking of hydrocarbons or CO disproportionation. One unresolved question is whether the herringbone texture, which actually describes the texture projection rather than the overall three-dimensional texture, originates from the scroll-like spiral arrangement of a single graphene ribbon or from the stacking of independent truncated cone-like graphenes in what is also called a “cup-stack” texture.

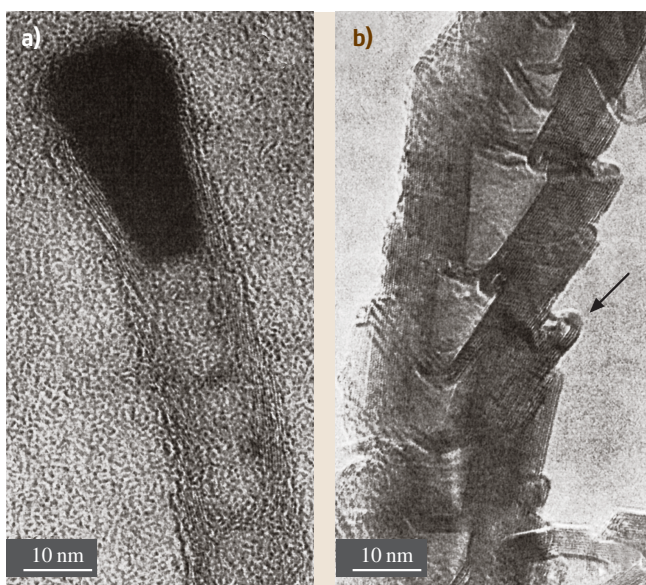


Fig. 3.6a,b Some of the earliest high-resolution transmission electron microscopy images of a herringbone (and bamboo) multiwall nanotube (bh-MWNT, longitudinal view) prepared by CO disproportionation on Fe-Co catalyst. (a) As-grown. The nanotube surface is made of free graphene edges. (b) After 2900 °C heat treatment. Both the herringbone and the bamboo textures have become obvious. Graphene edges from the surface have buckled with their neighbors (arrow), closing off access to the intergraphene space (adapted from [3.17])

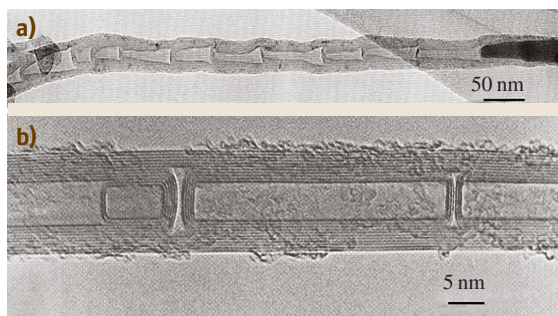


Fig. 3.7a,b Transmission electron microscopy images from bamboo multiwall nanotubes (longitudinal views). (a) Low magnification of a bamboo-herringbone multiwall nanotube (bh-MWNT) showing the nearly periodic nature of the texture, which occurs very frequently. (from [3.18]); (b) High-resolution image of a bamboo-concentric multiwall nanotube (bc-MWNT) (modified from [3.19])

Another common feature is the occurrence, to some degree, of a limited amount of graphenes oriented perpendicular to the nanotube axis, thus forming a “bamboo” texture. This is not a texture that can exist on its own; it affects either the c-MWNT (bc-MWNT) or the h-MWNT (bh-MWNT) textures (Figs. 3.6 and 3.7). The question is whether such filaments, although hollow, should still be called nanotubes, since the inner cavity is no longer open all the way along the filament as it is for a genuine tube. These are therefore sometimes referred to as “nanofibers” in the literature too.

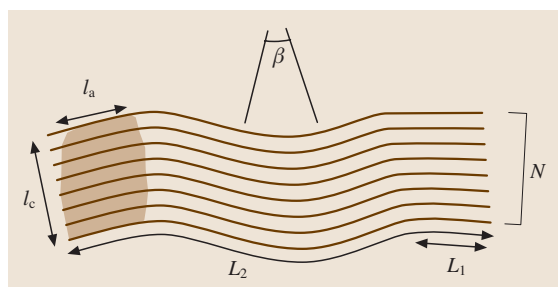


Fig. 3.8 Sketch explaining the various parameters obtained from high-resolution (lattice fringe mode) transmission electron microscopy, used to quantify nanotexture: L_1 is the average length of perfect (distortion-free) graphenes of coherent areas; N is the number of piled-up graphenes in coherent (distortion-free) areas; L_2 is the average length of continuous though distorted graphenes within graphene stacks; β is the average distortion angle. L_1 and N are related to the L_a and L_c values obtained from X-ray diffraction

One nanofilament that definitely cannot be called a nanotube is built from graphenes oriented perpendicular to the filament axis and stacked as piled-up plates. Although these nanofilaments actually correspond to h-MWNTs with a graphene/MWNT axis angle of 90° , an inner cavity is no longer possible, and such filaments are therefore often referred to as “platelet nanofibers” in the literature [3.16].

Unlike SWNTs, whose aspect ratios are so high that it is almost impossible to find the tube tips, the aspect ratios for MWNTs (and carbon nanofibers) are generally lower and often allow one to image tube ends by transmission electron microscopy. Aside from c-MWNTs derived from electric arc (see Fig. 3.5), which grow in a catalyst-free process, nanotube tips are frequently found to be associated with the catalyst crystals from which they were formed.

3.2 Synthesis of Carbon Nanotubes

Producing carbon nanotubes so that the currently planned applications currently planned become marketable will require solving some problems that are more or less restrictive depending on the case. Examples include specifically controlling the configuration (chirality), the purity, or the structural quality of SWNTs, and adapting the production capacity to the application. One objective would be to understand the mechanism of nanotube nucleation and growth perfectly, and this remains a controversial subject despite an intense, worldwide experimental effort. This problem is partly due to our lack of knowledge regarding several parameters controlling the conditions during synthesis. For instance, the exact and accurate role of the catalysts in nanotube growth is often unknown. Given the large number of experimental parameters and considering the large range of conditions that the synthesis techniques correspond to, it is quite legitimate to think of more than one mechanism intervening during nanotube formation.

3.2.1 Solid Carbon Source-Based Production Techniques for Carbon Nanotubes

Among the different SWNT production techniques, the four processes (laser ablation, solar energy, dc electric arc, and three-phase ac arc plasma) presented in this section have at least two points in common: a high-temperature ($1000\text{ K} < T < 6000\text{ K}$) medium and the

The properties of the MWNT (see Sect. 3.4) will obviously largely depend on the perfection and the orientation of the graphenes in the tube (for example, the spiral angles of the nanotubes constituting c-MWNTs has little importance). Graphene orientation is a matter of texture, as described above. Graphene perfection is a matter of nanotexture, which is commonly used to describe other polyaromatic carbon materials, and which is quantified by several parameters preferably obtained from high-resolution transmission electron microscopy (Fig. 3.8). Both texture and nanotexture depend on the processing conditions. While the texture type is a permanent, intrinsic feature which can only be completely altered upon a severe degradation treatment (such as oxidation), the nanotexture can be improved by subsequent thermal treatments at high temperatures (such as $> 2000^\circ\text{C}$) and potentially degraded by chemical treatments (such as slightly oxidizing conditions).

fact that the carbon source originates from the erosion of solid graphite. Despite these common points, the morphologies of the carbon nanostructures and the SWNT yields can differ notably with respect to the experimental conditions.

Before being utilized for carbon nanotube synthesis, these techniques permitted the production of fullerenes. Laser vaporization of graphite was actually the very first method to demonstrate the existence of fullerenes, including the most common one (because it is the most stable and therefore the most abundant), C_{60} [3.20]. On the other hand, the electric arc technique was (and still is) the first method of producing fullerenes in relatively large quantities [3.21–23]. Unlike fullerene formation, which requires the presence of carbon atoms in high-temperature media and the absence of oxygen, the utilization of these techniques for the synthesis of nanotubes (of SWNT type at least) requires an additional condition: the presence of catalysts in either the electrode or the target.

The different mechanisms (such as carbon molecule dissociation and atom recombination processes) involved in these high-temperature techniques take place at different time scales, from nanoseconds to microseconds and even milliseconds. The formation of nanotubes and other graphene-based products occurs afterward with a relatively long delay.

The methods of laser ablation, solar energy, and electric arc are all based on one essential mechanism: the energy transfer resulting from the interaction between either the target material and an external radiation source (a laser beam or radiation emanating from solar energy) or the electrode and the plasma (in case of an electric arc). This interaction causes target or anode erosion, leading to the formation of a plasma: an electrically neutral ionized gas, composed of neutral atoms, charged particles (molecules and ionized species) and electrons. The ionization degree of this plasma, defined by the ratio ($n_e/n_e + n_o$), where n_e and n_o are the electron and that of neutral atom densities respectively, highlights the importance of energy transfer between the plasma and the material. The characteristics of this plasma and notably the ranges in temperature and concentrations of the various species present in the plasma thereby depend not only on the nature and composition of the target or the electrode but also on the energy transferred.

One of the advantages of these synthesis techniques is the ability to vary a large number of parameters that modify the composition of the high-temperature medium and consequently allow the most relevant parameters to be determined so that the optimal conditions for the control of carbon nanotube formation can be obtained. However, a major drawback of these techniques – and of any other technique used to produce SWNTs – is that the SWNTs formed are not pure: they are associated with other carbon phases and remnants of the catalyst. Although purification processes have been proposed in the literature and by some commercial companies for removing these undesirable phases, they are all based on oxidation (such as acid-based) processes that are likely to significantly affect the SWNT structure [3.14]. Subsequent thermal treatments at $\approx 1200^\circ\text{C}$ under inert atmosphere, however, succeed in recovering structural quality somewhat [3.26].

Laser Ablation

After the first laser was built in 1960, physicists immediately made use of it as a means of concentrating a large quantity of energy inside a very small volume within a relatively short time. The consequence of this energy input naturally depends upon the characteristics of the device employed. During the interaction between the laser beam and the material, numerous phenomena occur at the same time and/or follow each other within the a certain time period, and each of these processes are sensitive to different parameters such as the characteristics of the laser beam, the incoming power density (also

termed the “fluence”), the nature of the target, and the environment surrounding it. For instance, the solid target can merely heat up, melt or vaporize depending on the power provided.

While this technique was successfully used to synthesize fullerene-related structures for the very first time [3.20], the synthesis of SWNTs by laser ablation took another ten years of research [3.24].

Laser Ablation – Experimental Devices

Two types of laser devices are currently utilized for carbon nanotube production: lasers operating in pulsed mode and lasers operating in continuous mode, with the latter generally providing a smaller fluence.

An example of the layout of a laser ablation device is given in Fig. 3.9. A graphite pellet containing the catalyst is placed in the middle of a quartz tube filled with inert gas and placed in an oven maintained at a temperature of 1200°C [3.24, 25]. The energy of the laser beam focused on the pellet permits it to vaporize and sublime the graphite by uniformly bombarding its surface. The carbon species, swept along by a flow of neutral gas, are then deposited as soot in different regions: on the conical water-cooled copper collector, on the quartz tube walls, and on the backside of the pellet.

Various improvements have been made to this device in order to increase the production efficiency. For example, *Thess et al.* [3.27] employed a second pulsed laser that follows the initial impulsion but at a different frequency in order to ensure a more complete and efficient irradiation of the pellet. This second impulsion vaporizes the coarse aggregates issued from the first ablation, causing them to participate in the active carbon feedstock involved in nanotube growth. Other modifications were suggested by *Rinzler et al.* [3.26], who inserted a second quartz tube of a smaller diameter coaxially inside the first one. This second tube reduces the vaporization zone and so permits an in-

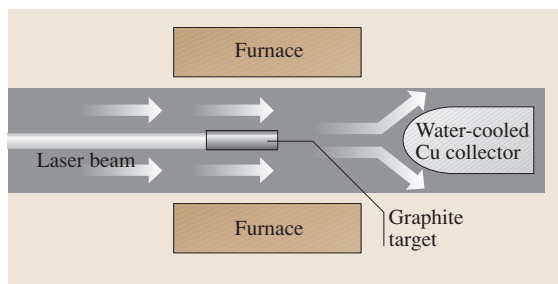


Fig. 3.9 Sketch of an early laser vaporization apparatus (adapted from [3.24, 25])

creased amounts of sublimed carbon to be obtained. They also arranged the graphite pellet on a revolving system so that the laser beam uniformly scans its whole surface.

Other groups have realized that, where the target contains both the catalyst and the graphite, the latter evaporates first and the pellet surface becomes more and more metal-rich, resulting in a decrease in the efficiency of nanotube formation during the course of the process. To solve this problem, *Yudasaka et al.* [3.29] utilized two pellets facing each other, one made entirely from the graphite powder and the other from an alloy of transition metals (catalysts), and irradiated them simultaneously.

A sketch of a synthesis reactor based on the vaporization of a target at a fixed temperature by a continuous CO₂ laser beam ($\lambda = 10.6\ \mu\text{m}$) is shown in Fig. 3.10 [3.28]. The power can be varied from 100 W to 1600 W. The temperature of the target is measured with an optical pyrometer, and these measurements are used to regulate the laser power to maintain a constant vaporization temperature. The gas, heated by contact with the target, acts as a local furnace and creates an extended hot zone, making an external furnace unnecessary. The gas is extracted through a silica pipe, and the solid products formed are carried away by the gas flow through the

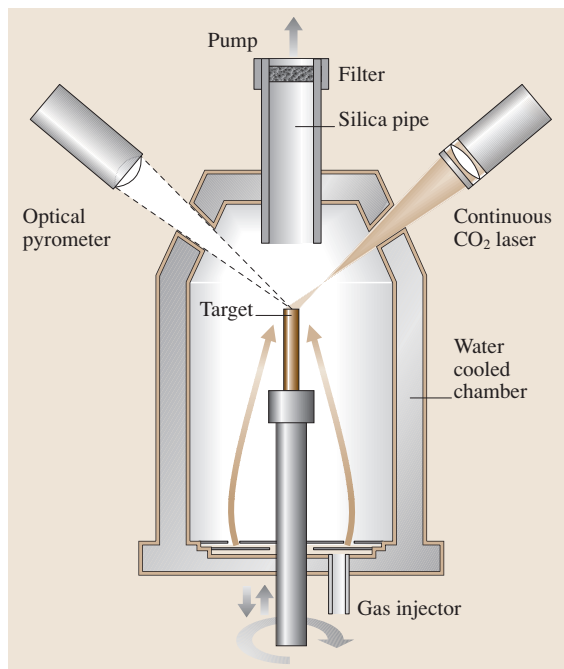


Fig. 3.10 Sketch of a synthesis reactor with a continuous CO₂ laser device (adapted from [3.28])

pipe and then collected on a filter. The synthesis yield is controlled by three parameters: the cooling rate of the medium where the active, secondary catalyst particles are formed, the residence time, and the temperature (in the range 1000–2100 K) at which SWNTs nucleate and grow [3.30].

However, devices equipped with facilities to gather data such as the target temperature in situ are scarce and, generally speaking, this is one of the numerous variables of the laser ablation synthesis technique. The parameters that have been studied the most are the nature of the target, the nature and concentration of the catalyst, the nature of the neutral gas flow, and the temperature of the outer oven.

Laser Ablation – Results

In the absence of catalysts in the target, the soot collected mainly contains multiwall nanotubes (c-MWNTs). Their lengths can reach 300 nm. Their quantity and structural quality are dependent on the oven temperature. The best quality is obtained for an oven temperature set at 1200 °C. At lower oven temperatures, the structural quality decreases, and the nanotubes start presenting many defects [3.24]. As soon as small quantities (a few percent or less) of transition metal (Ni, Co) catalysts are incorporated into the graphite pellet, the products yielded undergo significant modifications, and SWNTs are formed instead of MWNTs. The yield of SWNTs strongly depends on the type of metal catalyst used and is seen to increase with the furnace temperature, among

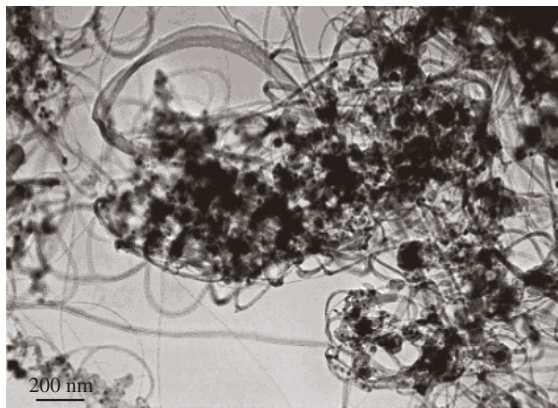


Fig. 3.11 Low-magnification TEM images of a typical raw SWNT material obtained using the laser vaporization technique. The fibrous structures are SWNT bundles, and the dark particles are remnants of the catalyst. Raw SWNT materials obtained from an electric arc exhibit similar features (from [3.14])

other factors. The SWNTs have remarkably uniform diameters and they self-organize into rope-like crystallites 5–20 nm in diameter and tens to hundreds of micrometers in length (Fig. 3.11). The ends of all of the SWNTs appear to be perfectly closed with hemispherical end-caps that show no evidence of any associated metal catalyst particle, although, as pointed out in Sect. 3.1, finding the two tips of a SWNT is rather challenging, considering the huge aspect ratio of the nanotube and their entangled nature. Another feature of the SWNTs produced with this technique is that they are supposedly “cleaner” than those produced using other techniques; in other words they are associated with smaller amounts of the amorphous carbon that either coats the SWNTs or is gathered into nanoparticles. This advantage, however, only occurs for synthesis conditions designed to ensure high-quality SWNTs. It is not true when high-yield conditions are preferred; in this case SWNTs from an electric arc may appear cleaner than SWNTs from laser vaporization [3.14].

The laser vaporization technique is one of the three methods currently used to prepare SWNTs as commercial products. SWNTs prepared this way were first marketed by Carbon Nanotechnologies Inc. (Houston, TX, USA), with prices as high as \$ 1000/g (raw materials) until December 2002. Probably because lowering the amount of impurities in the raw materials using this technique is impossible, they have recently decided to focus on fabricating SWNTs using the HiPCo technique (see Sect. 3.2.2). Laser-based methods are generally not considered to be competitive in the long term for the low-cost production of SWNTs compared to CCVD-based methods (see Sect. 3.2.2). However, prices as low as \$0.03 per gram of raw high concentration have been estimated possible from a pre-industrial project study (Acolt S.A., Yverdon, Switzerland).

Electric Arc Method

Electric arcs between carbon electrodes have been studied as light sources and radiation standards for a very long time. They have however received renewed attention more recently due to their use in the production of new fullerene-related molecular carbon nanostructures, such as genuine fullerenes or nanotubes. This technique was first brought to light by Krättschmer et al. [3.21] who utilized it to achieve the production of fullerenes in macroscopic quantities. In the course of investigating other carbon nanostructures formed along with the fullerenes, and more particularly the solid carbon deposit that formed on the cathode, Iijima [3.6] discovered the

catalyst-free formation of perfect c-MWNT-type carbon nanotubes. Then, as mentioned in the *Introduction*, the catalyst-promoted formation of SWNTs was accidentally discovered after some amounts of transition metals were introduced into the anode in an attempt to fill the c-MWNTs with metals during growth [3.7, 8]. Since then, a lot of work has been carried out by many groups using this technique in order to understand the mechanisms of nanotube growth as well as the role played by the catalysts (if any) in the synthesis of MWNTs and/or SWNTs [3.31–43].

Electric Arc Method – Experimental Devices

The principle of this technique is to vaporize carbon in the presence of catalysts (iron, nickel, cobalt, yttrium, boron, gadolinium, cerium, and so forth) in a reduced atmosphere of inert gas (argon or helium). After triggering an arc between two electrodes, a plasma is formed consisting of the mixture of carbon vapor, the rare gas (helium or argon), and the catalyst vapors. The vaporization is the consequence of energy transfer from the arc to the anode made of graphite doped with catalysts. The importance of the anode erosion rate depends on the power of the arc and also on other experimental conditions. It is worth noting that a high anode erosion does not necessarily lead to a high carbon nanotube production.

An example of a reactor layout is shown in Fig. 3.12. It consists of a cylinder about 30 cm in diameter and about 1 m in height, equipped with diametrically opposed sapphire windows located so that they face the plasma zone, observing the arc. The reactor possesses two valves, one for performing the primary evacuation (0.1 Pa) of the chamber, the other for filling it with a rare gas up to the desired working pressure.

Contrary to the solar energy technique, SWNTs are deposited (provided appropriate catalysts are used) in different regions of the reactor: (1) the collaret, which forms around the cathode; (2) the web-like deposits found above the cathode; (3) the soot deposited all around the reactor walls and the bottom. On the other hand, MWNTs are formed in a hard deposit adherent to the cathode whether catalysts are used or not. The cathode deposits form under the cathode. The formation of collaret and web is not systematic and depends on the experimental conditions, as indicated in Table 3.1, as opposed to the cathode deposit and soot, which are obtained consistently.

Two graphite rods of few millimeters in diameter constitute the electrodes between which a potential difference is applied. The dimensions of these electrodes

vary according to the authors. In certain cases, the cathode has a greater diameter than the anode in order to facilitate their alignment [3.34, 44]. Other authors utilize electrodes of the same diameter [3.43]. The whole device can be designed horizontally [3.35, 43] or vertically [3.36, 38–40]. The advantage of the latter is the symmetry brought by the verticality with respect to gravity, which facilitates computer modeling (regarding convection flows, for instance).

Two types of anode can be utilized when catalysts are introduced: (1) a graphite anode containing a coaxial hole several centimeters in length into which a mixture of the catalyst and the graphite powder is placed; (2) a graphite anode within which the catalysts are homogeneously dispersed [3.45]. The former are by far the most popular, due to their ease of fabrication.

Optimizing the process in terms of the nanotube yield and quality is achieved by studying the roles of various parameters such as the type of doped anode (homogeneous or heterogeneous catalyst dispersion), the nature as well as the concentration of the catalyst, the nature of the plasmagen gas, the buffer gas pressure, the arc current intensity, and the distance between electrodes. Investigating the influences of these parameters on the type and amount of carbon nanostructures formed is, of course, the preliminary work that has been done. Although electric arc reactors equipped with the facilities to perform such investigations are scarce (see Fig. 3.12), investigating the missing link (the effect of

varying the parameters on the plasma characteristics – the species concentrations and temperature) is likely to provide a more comprehensive understanding of the phenomena involved during nanotube formation. This has been recently performed using atomic and molecular optical emission spectroscopy [3.36, 38–41, 43].

Finally, we should mention attempts to create an electric arc in liquid media, such as liquid nitrogen [3.46] or water [3.47, 48]. The goal here is to make processing easier, since such systems should not require pumping devices or a closed volume and so they are more likely to allow continuous synthesis. This adaptation has not, however, reached the stage of mass production.

Electric Arc Method – Results

In view of the numerous results obtained with this electric arc technique, it is clear that both the morphology and the production efficiency of nanotubes strongly depends upon the experimental conditions used and, in particular, upon the nature of the catalysts. It is worth noting that the products obtained do not consist solely of carbon nanotubes. Nontubular forms of carbon, such as nanoparticles, fullerene-like structures including C_{60} , poorly organized polyaromatic carbons, nearly amorphous nanofibers, multiwall shells, single-wall nanocapsules, and amorphous carbon have all been obtained, as reported in Table 3.1 [3.37, 39, 40]. In addition, remnants of the catalyst are found all over the place – in the soot, the collaret, the web and the cathode deposit – in various concentrations. Generally, at a helium pressure of about 600 mbar, for an arc current of 80 A and for an electrode gap of 1 mm, the synthesis of SWNTs is favored by the use of Ni/Y as coupled catalysts [3.7, 35, 49]. In these conditions, which give high SWNT yields, SWNT concentrations are highest in the collaret (50–70%), then in the web ($\approx 50\%$ or less) and then in the soot. On the other hand, c-MWNTs are found in the cathode deposit. SWNT lengths are micrometric and, typical outer diameters are around 1.4 nm. Using the latter conditions (Table 3.1, column 4), Table 3.1 illustrates the consequence of changing the parameters. For instance (Table 3.1, column 3), using Ni/Co instead of Ni/Y as catalysts prevents the formation of SWNTs. But when the Ni/Co catalysts are homogeneously dispersed in the anode (Table 3.1, column 1), the formation of nanotubes is promoted again, but MWNTs with two or three walls prevail over SWNTs, among which DWNTs (double-wall nanotubes) dominate. However, decreasing the ambient pressure from 60 to 40 kPa (Table 3.1, column 2) again suppresses nanotube formation.

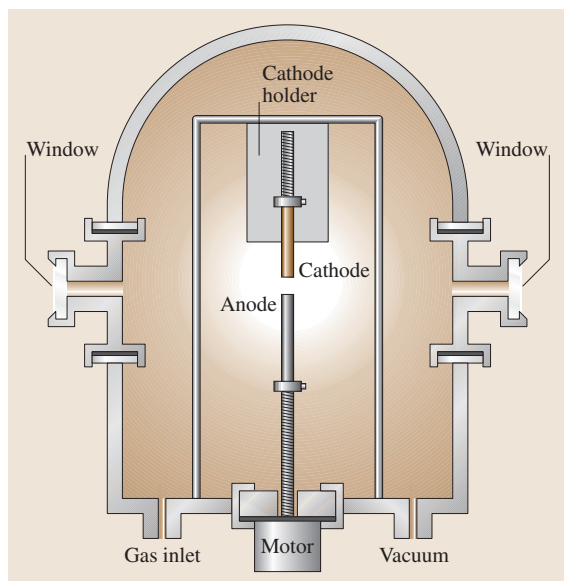


Fig. 3.12 Sketch of an electric arc reactor

Table 3.1 Different carbon morphologies obtained by changing the type of anode, the type of catalyst and the pressure in a series of arc discharge experiments (electrode gap = 1 mm)

Catalyst (atom%) Arc conditions	0.6Ni + 0.6Co (homogeneous anode) $P \sim 60$ kPa $I \sim 80$ A	0.6Ni + 0.6Co (homogeneous anode) $P \sim 40$ kPa $I \sim 80$ A	0.5Ni + 0.5Co $P \sim 60$ kPa $I \sim 80$ A	4.2Ni + 1Y $P \sim 60$ kPa $I \sim 80$ A
Soot	<ul style="list-style-type: none"> • MWNT + MWS + POPAC or Cn ± catalysts $\phi \sim 3$–35 nm • NANF + catalysts • AC particles + catalysts • [DWNT], [SWNT], ropes or isolated, + POPAC 	<ul style="list-style-type: none"> • POPAC and AC particles + catalysts $\phi \sim 2$–20 nm • NANF + catalysts $\phi \sim 5$–20 nm + MWS • [SWNT] $\phi \sim 1$–1.4 nm, distorted or damaged, isolated or ropes + Cn 	<ul style="list-style-type: none"> • AC and POPAC particles + catalysts $\phi \sim 3$–35 nm • NANF + catalysts $\phi \sim 4$–15 nm • [SWNT] $\phi \sim 1.2$ nm, isolated or ropes 	<ul style="list-style-type: none"> • POPAC and AC + particles + catalysts $\phi \leq 30$ nm • SWNT $\phi \sim 1.4$ nm, clean + Cn, short with tips, [damaged], isolated or ropes $\phi \leq 25$ nm • [SWNC] particles
Web	<ul style="list-style-type: none"> • [MWNT], DWNT, $\phi 2.7$–4–5.7 nm SWNT $\phi 1.2$–1.8 nm, isolated or ropes $\phi < 15$ nm, + POPAC ± Cn • AC particles + catalysts $\phi \sim 3$–40 nm + MWS • [NANF] 	None	None	<ul style="list-style-type: none"> • SWNT, $\phi \sim 1.4$ nm, isolated or ropes $\phi \leq 20$ nm, + AC • POPAC and AC particles + catalysts $\phi \sim 3$–10–40 nm + MWS
Collaret	<ul style="list-style-type: none"> • POPAC and SWNC particles • Catalysts $\phi \sim 3$–250 nm, < 50 nm + MWS • SWNT $\phi 1$–1.2 nm, [opened], distorted, isolated or ropes $\phi < 15$ nm, + Cn • [AC] particles 	<ul style="list-style-type: none"> • AC and POPAC particles + catalysts $\phi \sim 3$–25 nm • SWNT $\phi \sim 1$–1.4 nm clean + Cn, [isolated] or ropes $\phi < 25$ nm • Catalysts $\phi \sim 5$–50 nm + MWS, • [SWNC] 	<ul style="list-style-type: none"> • Catalysts $\phi \sim 3$–170 nm + MWS • AC or POPAC particles + catalysts $\phi \sim 3$–50 nm • SWNT $\phi \sim 1.4$ nm clean + Cn isolated or ropes $\phi < 20$ nm 	<ul style="list-style-type: none"> • SWNT $\phi \sim 1.4$–2.5 nm, clean + Cn, [damaged], isolated or ropes $\phi < 30$ nm • POPAC or AC particles + catalysts $\phi \sim 3$–30 nm • [MWS] + catalysts or catalyst-free.
Cathode deposit	<ul style="list-style-type: none"> • POPAC and SWNC particles • Catalysts $\phi \sim 5$–300 nm MWS • MWNT $\phi < 50$ nm • [SWNT] $\phi \sim 1.6$ nm clean + Cn, isolated or ropes 	<ul style="list-style-type: none"> • POPAC and SWNC particles + Cn • Catalysts $\phi \sim 20$–100 nm + MWS 	<ul style="list-style-type: none"> • MWS, catalyst-free • MWNT $\phi < 35$ nm • POPAC and PSWNC particles • [SWNT], isolated or ropes • [Catalysts] $\phi \sim 3$–30 nm 	<ul style="list-style-type: none"> • SWNT $\phi \sim 1.4$–4.1 nm, clean + Cn, short with tips, isolated or ropes $\phi \leq 20$ nm. • POPAC or AC particles + catalysts $\phi \sim 3$–30 nm • MWS + catalysts $\phi < 40$ nm or catalyst-free • [MWNT]

Abundant – Present – [**Rare**]

Glossary: **AC:** amorphous carbon; **POPAC:** poorly organized polyaromatic carbon; **Cn:** fullerene-like structure, including C_{60} ; **NANF:** nearly amorphous nanofiber; **MWS:** multiwall shell; **SWNT:** single-wall nanotube; **DWNT:** double-wall nanotube, **MWNT:** multiwall nanotube; **SWNC:** single-wall nanocapsule.

Recent works have attempted to replace graphite powder (sp^2 hybridized carbon) by diamond powder (sp^3 hybridized carbon). This is mixed with the catalyst powder and placed in hollowed-type graphite anodes. The result is an unexpected but quite significant increase (up to +230%) in the **SWNT** yield [3.41, 42]. Such experiments have revealed, as in the comparison between the results from using homogeneous instead of heterogeneous anodes, that the physical phenomena (charge and heat transfers) that occur in the anode during the arc are of the utmost importance, a factor which was neglected before this.

It is clear that while the use of a rare earth element (such as Y) as a single catalyst does not provide the right conditions to grow **SWNTs**, associating it with a transition metal (Ni/Y for instance) seems to lead to the best combinations that give the highest **SWNT** yields [3.44]. On the other hand, using a single rare earth element may lead to unexpected results, such as the closure of graphene edges from a **c-MWNT** wall with the neighboring graphene edges from the same wall side, leading to the preferred formation of telescope-like and open **c-MWNTs** that are able to contain nested Gd crystals [3.38, 40]. The effectiveness of bimetallic catalysts is believed to be due to the transitory formation of nickel particles coated with yttrium carbide, which has a lattice constant that is somewhat commensurable with that of graphene [3.50].

Figure 3.13 illustrates the kind of information provided by analyzing the plasma using emission spectroscopy, including profiles of radial temperature (Fig. 3.13a) or C_2 species concentration (Fig. 3.13b) in the plasma. A common feature is that a huge vertical gradient (≈ 500 K/mm) rapidly establishes (≈ 0.5 mm from the center in the radial direction) from the bottom to the top of the plasma, probably due to convection phenomena (Fig. 3.13a). The zone of actual **SWNT** formation is beyond the limit of the volume analyzable in the radial direction, corresponding to colder areas. The C_2 concentration increases dramatically from the anode to the cathode and decreases dramatically in the radial direction (Fig. 3.13b). This demonstrates that C_2 moieties are secondary products resulting from the recombination of primary species formed from the anode. It also suggests that C_2 moieties may be the building blocks for **MWNTs** (formed at the cathode) but not for **SWNTs** [3.40, 42].

Although many aspects of it still need to be understood, the electric arc method is one of the three methods currently used to produce **SWNTs** as commercial products. Though not selling bare nanotubes

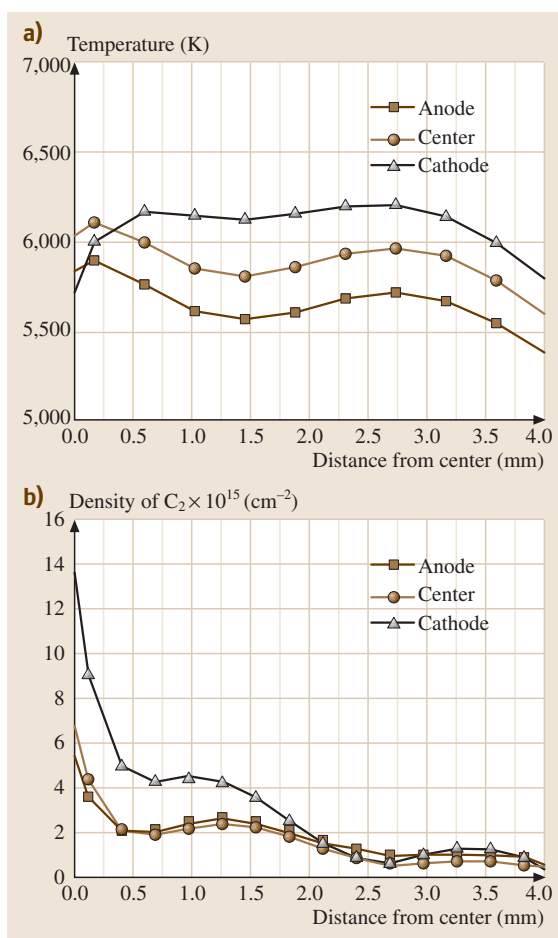


Fig. 3.13a,b Typical temperature (a) and C_2 concentration (b) profiles for plasma at the anode surface (*squares*), at the center of the plasma (*dots*), and at the cathode surface (*triangles*) at “standard” conditions (see text). Gradients are similar whichever catalyst is used, although absolute values may vary

anymore. Nanoledge S.A. (Montpellier, France), for instance, had a current production that reached several tens of kilograms per year (raw **SWNTs**, in other words unpurified), with a market price of ≈ 65 Euros/g in 2005, which was much cheaper than any other production method. It is however likely that the drop of prices for raw **SWNTs** down to 2–5 Euros/g which was anticipated for 2007 will not be possible. Actually, Bucky USA (Houston, Texas, USA) are still supplying raw **SWNTs** derived from electric arcs at a market price of 250 \$/g in 2006 (which is, however, a 75% decrease in two years), which is barely lower than the ≈ 350 \$/g pro-

posed for 70–90%-purified SWNTs from Nanocarlab (Moscow, Russia).

Three-Phase AC Arc Plasma

An original semi-industrial three-phase AC plasma technology has been developed for the processing of carbon nanomaterials [3.52, 53]. The technology has been specially developed for the treatment of liquid, gaseous or dispersed materials. An electric arc is established between three graphite electrodes. The system is powered

by a three-phase AC power supply operated at 600 Hz and at arc currents of 250–400 A. Carbon precursors, gaseous, liquid or solid, are injected at the desired (variable) position into the plasma zone. The reactive mixture can be extracted from the reaction chamber at different predetermined positions. After cooling down to room temperature, the aerosol passes through a filtering system. The main operating parameters, which are freely adjustable, include the arc current, the flow rate and the nature of the plasma gas (N_2 , Ar, H_2 , He, and so on), the carbon precursor (gaseous, liquid, solid, up to 3 kg/h), the injection and extraction positions, and the quenching rate. This plasma technology has shown very high versatility and it has been demonstrated that it can be

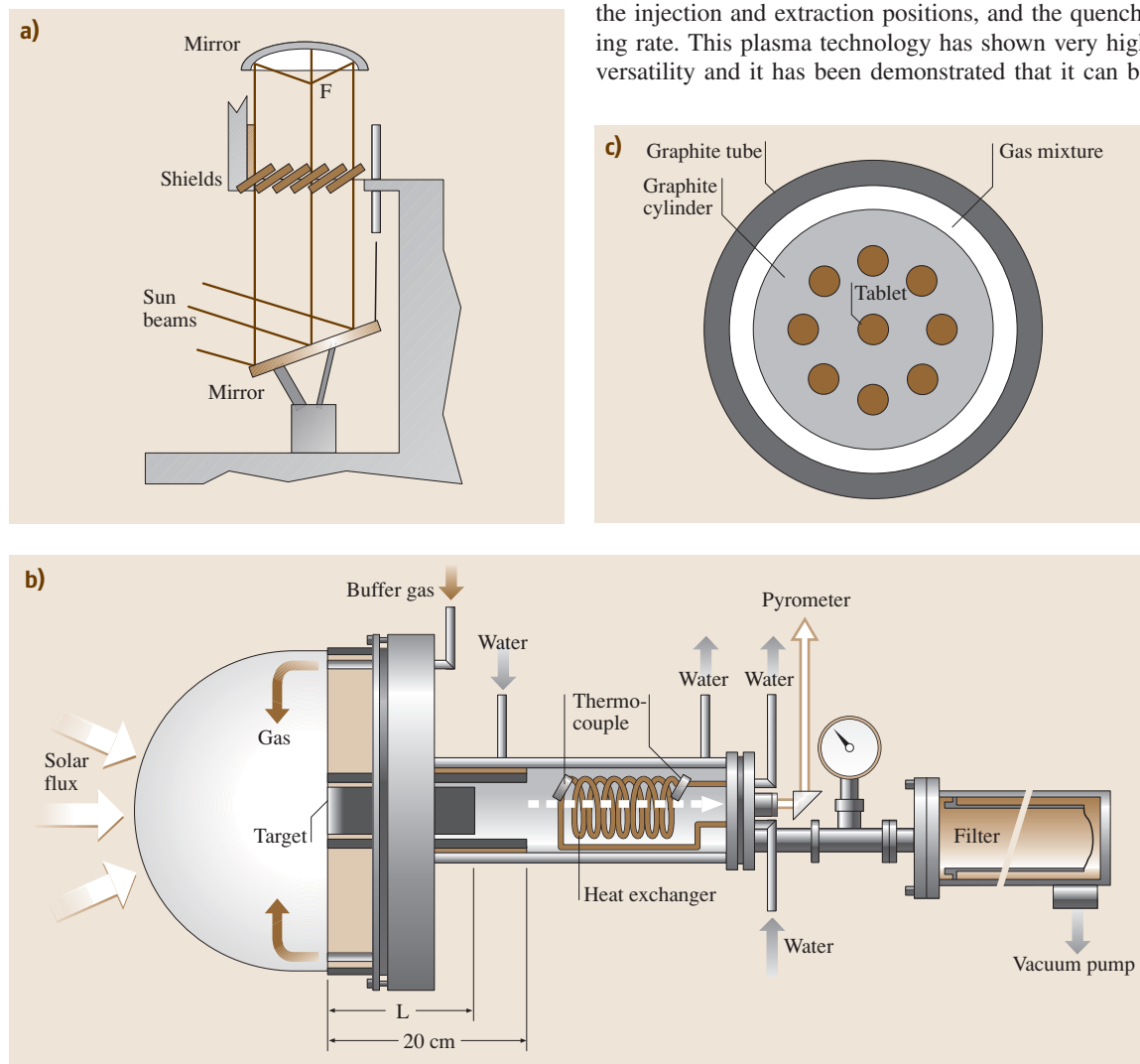


Fig. 3.14a–c Sketch of a solar energy reactor in use in the PROMES-CNRS Laboratory, Odeillo (France). **(a)** Gathering of sun rays, focused at F; **(b)** Side view of the experimental set-up at the focus of the 1 MW solar furnace; **(c)** top view of the target graphite rod. (Adapted from [3.51])

used to produce a wide range of carbon nanostructures ranging from carbon blacks to carbon nanotubes over fullerenes with a high product selectivity.

Solar Furnace

Solar furnace devices were originally utilized by several groups to produce fullerenes [3.54–56]. *Heben et al.* [3.57] and *Laplaze et al.* [3.58] later modified their original devices to achieve carbon nanotube production. This modification consisted mainly of using more powerful ovens [3.59, 60].

Solar Furnace – Experimental Devices

The principle of this technique is again based on the sublimation of a mixture of graphite powder and catalysts placed in a crucible in an inert gas. An example of such a device is shown in Fig. 3.14. The solar rays are collected by a plain mirror and reflected toward a parabolic mirror that focuses them directly onto a graphite pellet in a controlled atmosphere (Fig. 3.14a). The high temperature of about 4000 K causes both the carbon and the catalysts to vaporize. The vapors are then dragged by the neutral gas and condense onto the cold walls of the thermal screen. The reactor consists of a brass support cooled by water circulation, upon which Pyrex chambers of various shapes can be fixed (Fig. 3.14b). This support contains a watertight passage permitting the introduction of the neutral gas and a copper rod onto which the target is mounted. The target is a graphite rod that includes pellets containing the catalysts, which is surrounded by a graphite tube (Fig. 3.14c) that acts as both a thermal screen to reduce radiation losses (very important in the case of graphite) and a duct to lead carbon vapors to a filter, which stops soot from being deposited on the Pyrex chamber wall. The graphite rod target replaces the graphite crucible filled with powdered graphite (for fullerene synthesis) or the mixture of graphite and catalysts (for nanotube synthesis) that were used in the techniques we have discussed previously.

These studies primarily investigated the target composition, the type and concentration of catalyst, the flow-rate, the composition and pressure of the plasma-genic gas inside the chamber, and the oven power. The objectives were similar to those of the works associated with the other solid carbon source-based processes. When possible, specific *in situ* diagnostics (pyrometry, optical emission spectroscopy, and so on) are also performed in order to investigate the roles of various parameters (temperature measurements at the crucible surface, along the graphite tube acting as thermal screen,

C_2 radical concentration in the immediate vicinity of the crucible).

Solar Furnace – Results

Some of the results obtained by different groups concerning the influence of the catalyst can be summarized as follows. With Ni/Co, and at low pressure, the sample collected contains mainly MWNTs with bamboo texture, carbon shells, and some bundles of SWNTs [3.59]. At higher pressures, only bundles of SWNTs are obtained, with fewer carbon shells. Relatively long bundles of SWNTs are observed with Ni/Y and at a high pressure. Bundles of SWNTs are obtained in the soot with Co; the diameters of the SWNTs range from 1 to 2 nm. *Laplaze et al.* [3.59] observed very few nanotubes but a large quantity of carbon shells.

In order to proceed to large-scale synthesis of single-wall carbon nanotubes, which is still a challenge for chemical engineers, *Flamant et al.* [3.51] and *Luxembourg et al.* [3.61] recently demonstrated that solar energy-based synthesis is a versatile method for obtaining SWNTs that can be scaled up from 0.1–0.2 g/h to 10 g/h and then to 100 g/h productivity using existing solar furnaces. Experiments performed on a medium scale produced about 10 g/h of SWNT-rich material using various mixtures of catalysts (Ni/Co, Ni/Y, Ni/Ce). A numerical reactor simulation was performed in order to improve the quality of the product, which was subsequently observed to reach 40% SWNT in the soot [3.62].

3.2.2 Gaseous Carbon Source-Based Production Techniques for Carbon Nanotubes

As mentioned in the *Introduction*, the catalysis-enhanced thermal cracking of a gaseous carbon source (hydrocarbons, CO) – commonly referred to as catalytic chemical vapor deposition (CCVD) – has long been known to produce carbon nanofilaments [3.3], so reporting on all of the works published in the field since the beginning of the century is almost impossible. Until the 1990s, however, carbon nanofilaments were mainly produced to act as a core substrate for the subsequent growth of larger (micrometric) carbon fibers – so-called vapor-grown carbon fibers – via thickening in catalyst-free CVD processes [3.63, 64]. We are therefore going to focus instead on more recent attempts to prepare genuine carbon nanotubes.

The synthesis of carbon nanotubes (either single- or multiwalled) by CCVD methods involves the cat-

alytic decomposition of a carbon-containing source on small metallic particles or clusters. This technique involves either an heterogeneous process if a solid substrate is involved or an homogeneous process if everything takes place in the gas phase. The metals generally used for these reactions are transition metals, such as Fe, Co and Ni. It is a rather low-temperature process compared to arc discharge and laser ablation methods, with the formation of carbon nanotubes typically occurring between 600 °C and 1000 °C. Because of the low temperature, the selectivity of the **CCVD** method is generally better for the production of **MWNTs** with respect to graphitic particles and amorphous-like carbon, which remain an important part of the raw arc discharge **SWNT** samples, for example. Both homogeneous and heterogeneous processes appear very sensitive to the nature and the structure of the catalyst used, as well as to the operating conditions. Carbon nanotubes prepared by **CCVD** methods are generally much longer (a few tens to hundreds of micrometers) than those obtained by arc discharge (a few micrometers). Depending on the experimental conditions, it is possible to grow dense arrays of nanotubes. It is a general statement that **MWNTs** from **CCVD** contain more structural defects (exhibit a lower nanotexture) than **MWNTs** from arc discharge, due to the lower temperature of the reaction, which does not allow any structural rearrangements. These defects can be removed by subsequently applying heat treatments in vacuum or inert atmosphere to the products. Whether such a discrepancy is also true for **SWNTs** remains questionable. **CCVD SWNTs** are generally gathered into bundles that are generally of smaller diameter (a few tens of nm) than their arc discharge and laser ablation counterparts (around 100 nm in diameter). **CCVD**

provides reasonably good perspectives on large-scale and low-cost processes for the mass production of carbon nanotubes, a key point for their application at the industrial scale.

A final word concerns the nomenclature. Because work in the field started more than a century ago, the names of the carbon objects prepared by this method have changed with time with the authors, research areas, and fashions. These same objects have been called vapor-grown carbon fibers, nanofilaments, nanofibers and nanotubes. For multilayered fibrous morphologies (since single-layered fibrous morphologies can only be **SWNT** anyway), the exact name should be vapor-grown carbon nanofilaments (**VGCNF**). Whether or not the filaments are tubular is a matter of textural description, which should go with other textural features such as bamboo, herringbone and concentric (see Sect. 3.1.2). In the following, we will therefore use **MWNTs** for any hollowed nanofilament, whether they contain graphene walls oriented transversally or not. Any other nanofilament will be termed a “nanofiber.”

Heterogeneous Processes

Heterogeneous **CCVD** processes simply involve passing a gaseous flow containing a given proportion of a hydrocarbon (mainly CH_4 , C_2H_2 , C_2H_4 , or C_6H_6 , usually as a mixture with either H_2 or an inert gas such as Ar) over small transition metal particles (Fe, Co, Ni) in a furnace. The particles are deposited onto an inert substrate, by spraying a suspension of the metal particles on it or by another method. The reaction is chemically defined as catalysis-enhanced thermal cracking

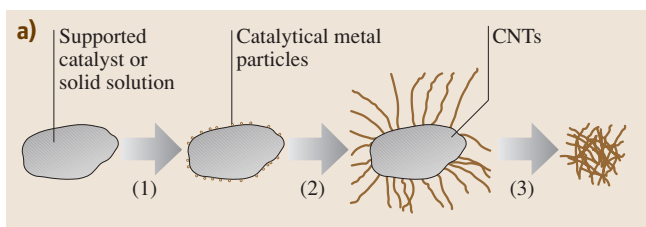
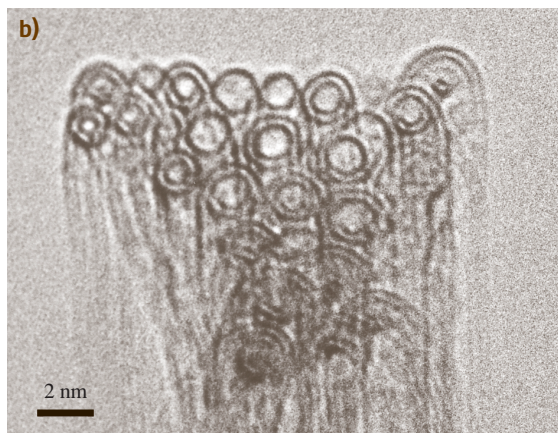


Fig. 3.15 (a) Formation of nanotubes via the **CCVD**-based impregnation technique. (1) Formation of catalytic metal particles by reduction of a precursor; (2) Catalytic decomposition of a carbon-containing gas, leading to the growth of carbon nanotubes; (3) Removal of the catalyst to recover the nanotubes (from [3.65]). **(b)** Example of a bundle of double-wall nanotubes (**DWNTs**) prepared this way (from [3.66])



Catalysis-enhanced thermal cracking was used as long ago as the late nineteenth century. Extensive works on this topic published before the 1990s include those by *Baker et al.* [3.5, 67], or *Endo et al.* [3.68, 69]. Several review papers have been published since then, such as [3.70], in addition to many regular papers.

CO can be used instead of hydrocarbons; the reaction is then chemically defined as catalysis-enhanced disproportionation (the so-called the Boudouard equilibrium)



Heterogeneous Processes – Experimental Devices

The ability of catalysis-enhanced CO disproportionation to make carbon nanofilaments was reported by *Davis et al.* [3.71] as early as 1953, probably for the first time. Extensive follow-up work was performed by *Boehm* [3.72], *Audier et al.* [3.17, 73–75], and *Gadelle et al.* [3.76–79].

Although formation mechanisms for **SWNTs** and **MWNTs** can be quite different (see Sect. 3.3, or refer to a review article such as [3.80]), many of the catalytic process parameters play similar and important roles in the type of nanotubes formed: the temperature, the duration of the treatment, the gas composition and flow rate, and of course the catalyst nature and size. At a given temperature, depending mainly on the nature of both the catalyst and the carbon-containing gas, the catalytic decomposition will take place at the surfaces of the metal particles, followed by mass transport of the freshly produced carbon by surface or volume diffusion until the carbon concentration reaches the solubility limit, and the precipitation starts.

It is now agreed that **CCVD** carbon nanotubes form on very small metal particles, typically in the nanometer range [3.80]. These catalytic metal particles are prepared mainly by reducing transition metal compounds (salts, oxides) by H_2 prior to the nanotube formation step (where the carbon containing gas is required). It is possible, however, to produce these catalytic metal particles in situ in the presence of the carbon source, allowing for a one-step process [3.81]. Because controlling the metal particle size is the key issue (they have to be nanosized), coalescence is generally avoided by placing them on an inert support such as an oxide (Al_2O_3 , SiO_2 , zeolites, MgAl_2O_4 , MgO) or more rarely on graphite. A low concentration of the catalytic metal precursor is required to limit the coalescence of the metal particles, which can happen during the reduction step. The supported cata-

lysts can be used as a static phase placed within the gas flow, but can also be used as a fine powder suspended into and by the gas phase, in a so-called fluidised bed process. In the latter, the reactor has to be vertical so that to compensate the effect of gravity by the suspending effect of the gas flow.

There are two main ways to prepare the catalyst: (a) the impregnation of a substrate with a solution of a salt of the desired transition metal catalyst, and (b) the preparation of a solid solution of an oxide of the chosen catalytic metal in a chemically inert and thermally stable host oxide. The catalyst is then reduced to form the metal particles on which the catalytic decomposition of the carbon source will lead to carbon nanotube growth. In most cases, the nanotubes can then be separated from the catalyst (Fig. 3.15).

Heterogeneous Processes – Results with CCVD Involving Impregnated Catalysts

A lot of work had been done in this area even before the discovery of fullerenes and carbon nanotubes, but although the formation of tubular carbon structures by catalytic processes involving small metal particles was clearly identified, the authors did not focus on the preparation of **SWNTs** or **MWNTs** with respect to the other carbon species. Some examples will be given here to illustrate the most striking improvements obtained.

With the impregnation method, the process generally involves four different and successive steps: (1) impregnation of the support by a solution of a salt (nitrate, chloride) of the chosen metal catalyst; (2) drying and calcination of the supported catalyst to get the oxide of the catalytic metal; (3) reduction in a H_2 -containing atmosphere to make the catalytic metal particles, and lastly (4) the decomposition of a carbon-containing gas over the freshly prepared metal particles that leads to nanotube growth. For example, *Ivanov et al.* [3.82] prepared nanotubes through the decomposition of C_2H_2 (pure or mixed with H_2) on well-dispersed transition metal particles (Fe, Co, Ni, Cu) supported on graphite or SiO_2 . Co- SiO_2 was found to be the best catalyst/support combination for the preparation of **MWNTs**, but most of the other combinations led to carbon filaments, sometimes covered with amorphous-like carbon. The same authors have developed a precipitation-ion-exchange method that provides a better dispersion of metals on silica compared to the classical impregnation technique. The same group then proposed the use of a zeolite-supported Co catalyst [3.83, 84], resulting in very finely dispersed metal particles (from 1 to 50 nm in diameter). They observed **MWNTs** with a diameter around 4 nm and only

two or three walls only on this catalyst. *Dai et al.* [3.85] have prepared **SWNTs** by CO disproportionation on nanosized Mo particles. The diameters of the nanotubes obtained are closely related to those of the original particles and range from 1 to 5 nm. The nanotubes obtained by this method are free of an amorphous carbon coating. They also found that a synergetic effect occurs for the alloy instead of the components alone, and one of the most striking examples is the addition of Mo to Fe [3.86] or Co [3.87].

Heterogeneous Processes – Results with CCVD Involving Solid Solution–Based Catalysts

A solid solution of two metal oxides is formed when ions of one metal mix with ions of the other metal. For example, Fe_2O_3 can be prepared in solid solution in Al_2O_3 to give a $\text{Al}_{2-2x}\text{Fe}_{2x}\text{O}_3$ solid solution. The use of a solid solution allows a perfectly homogeneous dispersion of one oxide in the other to be obtained. These solid solutions can be prepared in different ways, but coprecipitation of mixed oxalates and combustion synthesis are the most common methods used to prepare nanotubes. The synthesis of nanotubes by the catalytic decomposition of CH_4 over an $\text{Al}_{2-2x}\text{Fe}_{2x}\text{O}_3$ solid solution was originated by *Peigney et al.* [3.81] and then studied extensively by the same group using different oxides such as spinel-based solid solutions ($\text{Mg}_{1-x}\text{M}_x\text{Al}_2\text{O}_4$ with $\text{M} = \text{Fe}, \text{Co}, \text{Ni}$, or a binary alloy [3.65, 88]) or magnesia-based solid solutions [3.65, 89] ($\text{Mg}_{1-x}\text{M}_x\text{O}$, with $\text{M} = \text{Fe}, \text{Co}$ or Ni). Because of the very homogeneous dispersion of the catalytic oxide, it is possible to produce very small catalytic metal particles at the high temperature required for the decomposition of CH_4 (which was chosen for its greater thermal stability compared to other hydrocarbons). The method proposed by these authors involves the heating of the solid solution from room temperature to a temperature of between 850 °C and 1050 °C in a mixture of H_2 and CH_4 , typically containing 18 mol.% of CH_4 . The nanotubes obtained clearly depend upon the nature of both the transition metal (or alloy) used and the inert oxide (matrix); the latter because the Lewis acidity seems to play an important role [3.90]. For example, in the case of solid solutions containing around 10 wt% of Fe, the amount of carbon nanotubes obtained decreases in the following order depending on the matrix oxide: $\text{MgO} > \text{Al}_2\text{O}_3 > \text{MgAl}_2\text{O}_4$ [3.65]. In the case of MgO-based solid solutions, the nanotubes can be very easily separated from the catalyst by dissolving it (in diluted HCl for example) [3.89]. The nanotubes obtained are typically gathered into small-diameter bundles (less

than 15 nm) with lengths of up to 100 μm . The nanotubes are mainly **SWNTs** and **DWNTs**, with diameters of between 1 and 3 nm.

Obtaining pure nanotubes by the **CCVD** method requires, as for all the other techniques, the removal of the catalyst. When a catalyst supported (impregnated) in a solid solution is used, the supporting – and catalytically inactive – oxide is the main impurity, both in weight and volume. When oxides such as Al_2O_3 or SiO_2 (or even combinations) are used, aggressive treatments involving hot caustic solutions (KOH , NaOH) for Al_2O_3 or the use of **HF** for SiO_2 are required. These treatments have no effect, however, on other impurities such as other forms of carbon (amorphous-like carbon, graphitized carbon particles and shells, and so on). Oxidizing treatments (air oxidation, use of strong oxidants such as HNO_3 , KMnO_4 , H_2O_2) are thus required and permit the removal of most unwanted forms of carbon, but they result in a low final yield of carbon nanotubes, which are often quite damaged. *Flahaut et al.* [3.89] were the first to use a MgCoO solid solution to prepare **SWNTs** and **DWNTs** that could be easily separated without incurring any damage via fast and safe washing with an aqueous HCl solution.

In most cases, only very small quantities of catalyst (typically less than 500 mg) are used, and most claims of “high-yield” productions of nanotubes are based on laboratory experimental data, without taking into account all of the technical problems related to scaling up to a laboratory-scale **CCVD** reactor. At the present time, although the production of **MWNTs** is possible on an industrial scale, the production of affordable **SWNTs** is still a challenge, and controlling the arrangement of and the number of walls in the nanotubes is also problematic. For example, adding small amounts of molybdenum to the catalyst [3.91] can lead to drastic modifications of the nanotube type (from regular nanotubes to carbon nanofibers—see Sect. 3.1). *Flahaut et al.* have recently shown that the method used to prepare a particular catalyst can play a very important role [3.92]. Double-walled carbon nanotubes (**DWNTs**) represent a special case: they are at the frontier between single- (**SWNTs**) and multiwalled nanotubes (**MWNTs**). Because they are the **MWNTs** with the lowest possible number of walls, their structures and properties are very similar to those of **SWNTs**. Any subsequent functionalization, which is often required to improve the compatibility of nanotubes with their external environment (composites) or to give them new properties (solubility, sensors), will partially damage the external wall, resulting in drastic modifications in terms of both electrical and mechani-

cal properties. This is a serious drawback for *SWNTs*. In the case of *DWNTs*, the outer wall can be modified (functionalized) while retaining the structure of the inner tube. *DWNTs* have been recently synthesised on a gram-scale by *CCVD* [3.66], with a high purity and a high selectivity (around 80% *DWNTs*) (Fig. 3.15b).

Homogeneous Processes

The homogenous route, also called the “floating catalyst method,” differs from the other *CCVD*-based methods because it uses only gaseous species and does not require the presence of any solid phase in the reactor. The basic principle of this technique, similar to the other *CCVD* processes, is to decompose a carbon source (ethylene, xylene, benzene, carbon monoxide, and so on) on nanosized transition metal (generally Fe, Co, or Ni) particles in order to obtain carbon nanotubes. The catalytic particles are formed directly in the reactor, however, and are not introduced before the reaction, as occurs in supported *CCVD* for instance.

Homogeneous Processes – Experimental Devices

The typical reactor used in this technique is a quartz tube placed in an oven into which the gaseous feedstock, containing the metal precursor, the carbon source, some hydrogen and a vector gas (N_2 , Ar, or He), is passed. The first zone of the reactor is kept at a lower temperature, and the second zone, where the formation of tubes occurs, is heated to 700–1200 °C. The metal precursor is generally a metal-organic compound, such as a zero-valent carbonyl compound like $[Fe(CO)_5]$ [3.93], or a metallocene [3.94–96] such as ferrocene, nickelocene or cobaltocene. The use of metal salts, such as cobalt nitrate, has also been reported [3.97]. It may be advantageous to make the reactor vertical, so that gravity acts symmetrically on the gaseous volume inside the furnace.

Homogeneous Processes – Results

The metal-organic compound decomposes in the first zone of the reactor, generating nanosized metallic particles that can catalyze nanotube formation. In the second part of the reactor, the carbon source is decomposed to atomic carbon, which is then responsible for the formation of nanotubes.

This technique is quite flexible and *SWNTs* [3.98], *DWNTs* [3.99] and *MWNTs* [3.100] have been obtained, in proportions depending on the carbon feedstock gas. The technique has also been exploited for some time in the production of vapor-grown carbon nanofibers [3.101].

The main drawback of this type of process is again that it is difficult to control the size of the metal nanoparticles, and thus nanotube formation is often accompanied by the production of undesired carbon forms (amorphous carbon or polyaromatic carbon phases found as various phases or as coatings). In particular, encapsulated forms have been often found as the result of the formation of metal particles that are too large to promote nanotube growth (and so they can end up being totally covered with graphene layers instead).

The same kind of parameters have to be controlled as for heterogeneous processes in order to finely tune this process and selectively obtain the desired morphology and structure of the nanotubes formed, such as: the choice of the carbon source; the reaction temperature; the residence time; the composition of the incoming gaseous feedstock, with particular attention paid to the role played by the proportion of hydrogen, which can influence the orientation of the graphene with respect to the nanotube axis, thus switching from *c-MWNT* to *h-MWNT* [3.77]; and the ratio of the metallorganic precursor to the carbon source [3.94]. In an independent study [3.102], it was shown that the general tendency is: (i) to synthesize *SWNTs* when the ferrocene/benzene molar ratio is high, typically $\approx 15\%$; (ii) to produce *MWNTs* when the ferrocene/benzene molar ratio is between $\approx 4\%$ and $\approx 9\%$, and; (iii) to synthesize carbon nanofibers when the ferrocene/benzene molar ratio is below $\approx 4\%$.

As recently demonstrated, the overall process can be improved by adding other compounds such as ammonia or sulfur-containing species to the reactive gas phase. The former allows aligned nanotubes and mixed C–N nanotubes [3.103] to be obtained, while the latter results in a significant increase in productivity [3.101, 104]. An interesting result is the increase in yield and purity brought about by a small input of oxygen, as achieved by using alcohol vapors instead of hydrocarbons as feedstock [3.105]. It is assumed that the oxygen preferably burns the poorly organized carbon out into CO_2 , thereby enhancing the purity, and prevents the catalyst particles from being encapsulated in the carbon shells too early, making them inactive, thereby enhancing the nanotube yield. Moreover, it was found to promote the formation of *SWNTs* over *MWNTs*, since suppressing carbon shell formation suppresses *MWNT* formation too.

It should be emphasized that only small amounts have been produced so far, and scale-up to industrial levels seems quite difficult due to the large number of parameters that must be considered. A critical one is to

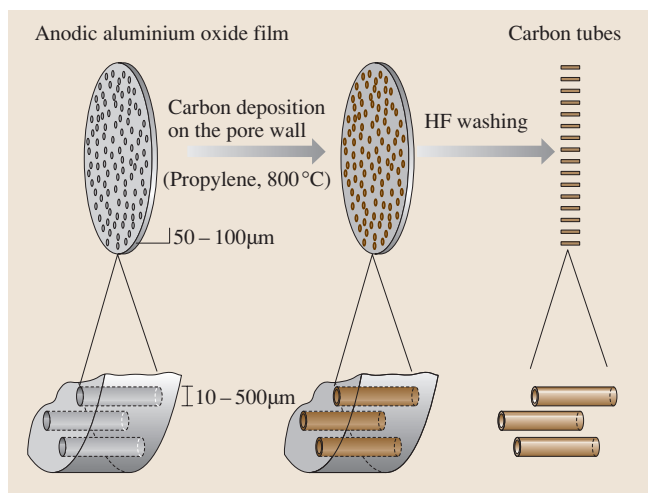


Fig. 3.16 Principle of the templating technique used in the catalyst-free formation of single-walled or concentric-type multiwalled carbon nanotubes (from [3.106])

be able to increase the quantity of metallorganic compound that is used in the reactor, in order to increase production, without obtaining particles that are too big. This problem has not yet been solved. An additional problem inherent in the process is the possibility of clogging the reactor due to the deposition of metallic nanoparticles on the reactor walls followed by carbon deposition.

A significant breakthrough concerning this technique could be the HiPCo process developed at Rice University, which produces SWNTs of very high purity [3.107, 108]. This gas phase catalytic reaction uses carbon monoxide to produce, from $[\text{Fe}(\text{CO})_5]$, a SWNT material that is claimed to be relatively free of by-products. The temperature and pressure conditions required are applicable to industrial plants. Upon heating, the $[\text{Fe}(\text{CO})_5]$ decomposes into atoms which condense into larger clusters, and SWNT nucleate and grow on these particles in the gas phase via CO disproportionation (the Boudouard reaction, see *Heterogeneous Processes* in Sect. 3.1.2):

The company Carbon Nanotechnologies Inc. (Houston, TX, USA) currently sells raw SWNT materials prepared in this way, at a market price of 375 \$/g, or 500 \$/g if purified (2005 data). Other companies that specialize in MWNTs include Applied Sciences Inc. (Cedarville, OH, USA), currently has a production facility of ≈ 40 tons/year of ≈ 100 nm large MWNTs (Pyrograf-III), and Hyperion Catalysis (Cambridge, MA, USA), which makes MWNT-based materials.

Though prepared in a similar way by CCVD-related processes, MWNTs remain far less expensive than SWNTs, reaching prices as low as 0.055 \$/g (current ASI fares for Pyrograf-III grade).

Templating

Another interesting technique, although one that is definitely not suitable for mass production (and so we only touch on it briefly here), is the templating technique. It is the only other method aside from the electric arc technique that is able to synthesize carbon nanotubes without any catalyst. Any other work reporting the catalyst-free formation of nanotubes is actually likely to have involved the presence of catalytic metallic impurities in the reactor or some other factors that caused a chemical gradient in the system. Another useful aspect of this approach is that it allows aligned nanotubes to be obtained naturally, without the help of any subsequent alignment procedure. However, the template must be removed (dissolved) to recover the nanotubes, in which case the alignment of the nanotubes is lost.

Templating – Experimental Devices

The principle of this technique is to deposit the solid carbon coating obtained from the CVD method onto the walls of a porous substrate whose pores are arranged in parallel channels. The feedstock is again a hydrocarbon, such as a common source of carbon. The substrate can be alumina or zeolite for instance, which present natural channel pores, while the whole system is heated to a temperature that cracks the hydrocarbon selected as the carbon source (Fig. 3.16).

Templating – Results

Provided the chemical vapor deposition mechanism (which is actually better described as a chemical vapor infiltration mechanism) is well controlled, synthesis results in the channel pore walls being coated with a variable number of graphenes. Both MWNTs (exclusively concentric type) and SWNTs can be obtained. The smallest SWNTs (diameters ≈ 0.4 nm) ever obtained (mentioned in Sect. 3.1) were actually been synthesized using this technique [3.10]. The nanotube lengths are directly determined by the channel lengths; in other words by the thickness of the substrate plate. One main advantage of the technique is the purity of the tubes (no catalyst remnants, and few other carbon phases). On the other hand, the nanotube structure is not closed at both ends, which can be an advantage or a drawback depend-

ing on the application. For instance, the porous matrix must be dissolved using one of the chemical treatments previously cited in order to recover the tubes. The fact that the tubes are open makes them even more sensitive to attack from acids.

3.2.3 Miscellaneous Techniques

In addition to the major techniques described in Sects. 3.2.1 and 3.2.2, many attempts to produce nanotubes in various ways, often with a specific goal in mind, such as looking for a low-cost or a catalyst-free production process, can be found in the literature. As yet, none has been convincing enough to be presented as a serious alternative to the major processes described previously. Some examples are provided in the following.

Hsu et al. [3.109] have succeeded in preparing **MWNTs** (including coiled **MWNTs**, a peculiar morphology resembling a spring) by a catalyst-free (although Li was present) electrolytic method, by running a 3–5 A current between two graphite electrodes (the anode was a graphite crucible and the cathode a graphite rod). The graphite crucible was filled with lithium chloride, while the whole system was heated in air or argon at $\approx 600^\circ\text{C}$. As with many other techniques, by-products such as encapsulated metal particles, carbon shells, amorphous carbon, and so on, are formed.

Cho et al. [3.110] have proposed a pure chemistry route to nanotubes, using the polyesterification of citric acid onto ethylene glycol at 50°C , followed by polymerization at 135°C and then carbonization at 300°C under argon, followed by oxidation at 400°C in air. Despite the latter oxidation step, the solid product contains short **MWNTs**, although they obviously have poor nanotextures. By-products such as carbon shells and amorphous carbon are also formed.

Li et al. [3.111] have also obtained short **MWNTs** through a catalyst-free (although Si is present) pyrolytic method which involves heating silicon carbonitride nanograins in a BN crucible to $1200\text{--}1900^\circ\text{C}$ in nitrogen within a graphite furnace. No details are given about the possible occurrence of by-products, but they are likely considering the complexity of the chemical system (Si-C-B-N) and the high temperatures involved.

Terranova et al. [3.112] have investigated the catalyzed reaction between a solid carbon source and atomic hydrogen. Graphite nanoparticles ($\approx 20\text{ nm}$) are sent with a stream of H_2 onto a Ta filament heated at 2200°C . The species produced, whatever they are, then hit a Si polished plate warmed to 900°C that supports transition metal particles. The whole chamber is kept in a dynamic

vacuum of 40 torr. **SWNTs** are supposed to form according to the authors, although their images are not very convincing. One major drawback of the method, besides its complexity compared to the others, is that it is difficult to recover the “nanotubes” from the Si substrates to which they seem to be firmly bonded.

The final example is an attempt to prepare nanotubes by diffusion flame synthesis [3.113]. A regular gaseous hydrocarbon source (ethylene, . . .) along with ferrocene vapor is passed into a laminar diffusion flame derived from air and CH_4 of temperature $500\text{--}1200^\circ\text{C}$. **SWNTs** are formed, together with encapsulated metal particles, soot, and so on. In addition to a low yield, the **SWNT** structure is quite poor.

3.2.4 Synthesis of Carbon Nanotubes with Controlled Orientation

Several applications (such as field emission-based displays, see Sect. 3.6) require that carbon nanotubes grow as highly aligned bunches, in highly ordered arrays, or that they are located at specific positions. In this case, the purpose of the process is not mass production but controlled growth and purity, with subsequent control of nanotube morphology, texture and structure. Generally speaking, the more promising methods for the synthesis of aligned nanotubes are based on **CCVD** processes, which involve the use of molecular precursors as carbon sources, and the method of thermal cracking assisted by the catalytic activity of transition metal (Co, Ni, Fe) nanoparticles deposited onto solid supports. Although this approach mainly produces **MWNT**, some attempts have been made to obtain arrays of **SWNTs**. Generally speaking, **SWNTs** and **DWNTs** nucleate at higher temperatures than **MWNTs** [3.114].

However, the catalyst-free templating methods related to those described in Sect. 3.2.2 are not considered here, due to the lack of support after the template is removed, which means that the previous alignment is not maintained.

During the **CCVD** growth, nanotubes can self-assemble into nanotube bunches aligned perpendicular to the substrate if the catalyst film on the substrate has a critical thickness [3.115, 116]. The driving forces for this alignment are the van der Waals interactions between the nanotubes, which allow them to grow perpendicularly to the substrates. If the catalyst nanoparticles are deposited onto a mesoporous substrate, the mesoscopic pores may also have an effect on the alignment when the growth starts, thus controlling the growth direction of the nanotubes. Two kinds of substrates

have been used so far for this purpose: mesoporous silica [3.117, 118] and anodic alumina [3.119].

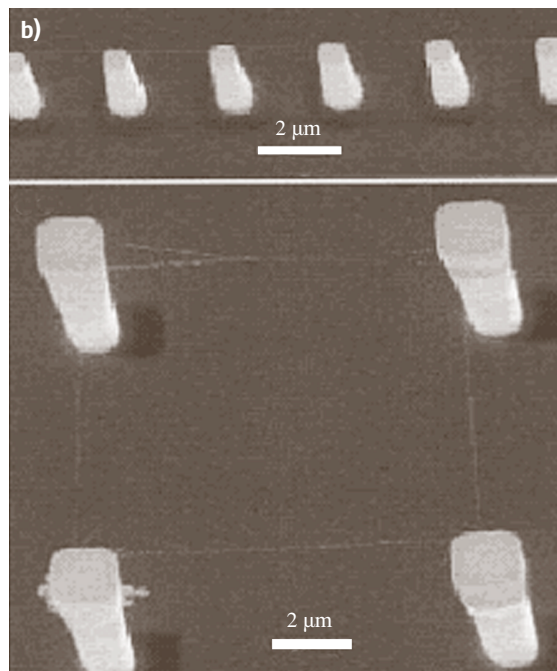
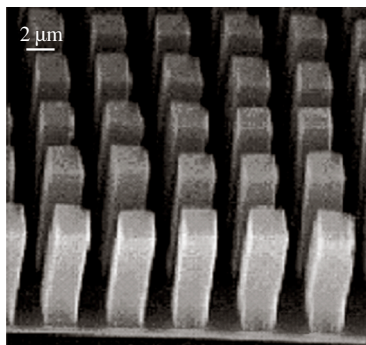
Different methods of depositing metal particles onto substrates have been reported in the literature: (i) deposition of a thin film on alumina substrates using metallic salt precursor impregnation followed by oxidation/reduction steps [3.122]; (ii) embedding catalyst particles in mesoporous silica by sol-gel processes [3.117]; (iii) thermal evaporation of Fe, Co, Ni or Co-Ni metal alloys on SiO₂ or quartz substrates under high vacuum [3.123, 124]; (iv) photolithographic patterning of metal-containing photoresist polymer using conventional black and white films as a mask [3.125] or photolithography and the inductive plasma deep etching technique [3.126]; (v) electrochemical deposition into pores in anodic aluminium oxide templates [3.119], (vi) deposition of colloidal suspensions of catalyst particles with tailored diameters on a support [3.127–131], by spin-coating for instance; (vii) stamping a catalyst precursor over a patterned silicon wafer is also possible and has been used to grow networks of nanotubes parallel to the substrate (Fig. 3.17a), or more generally to localize the growth of individual CNTs [3.132]. A technique that combines the advantages of electron beam lithography and template methods has also been reported for the large-scale production of ordered MWNTs [3.133] or AFM tips [3.134].

Depositing the catalyst nanoparticles onto a prepatterned substrate allows one to control the frequency of local occurrence and the arrangement of the nanotube bunches formed. The materials produced mainly consist of arrayed, densely packed, freestanding, aligned MWNTs (Fig. 3.17b), which are quite suitable for field emission-based applications for instance [3.121]. SWNTs have also been produced, and it was reported that the introduction of water vapor during the CVD

process allows impurity-free SWNTs to be synthesized [3.135], due to a mechanism related to that previously proposed for the effect of using alcohol instead of hydrocarbon feedstock [3.115].

When a densely packed coating of vertically aligned MWNTs is desired (Fig. 3.18c), another route is the pyrolysis of hydrocarbons in the presence of organometallic precursor molecules like metallocene or iron pentacarbonyl, operating in a dual furnace system (Fig. 3.18a,b). The organo-metallic precursor (such as ferrocene) is first sublimed at low temperature in the first furnace or injected as a solution along with the hydrocarbon feedstock, and then the whole system is pyrolyzed at higher temperature in the second furnace [3.98, 136–139]. The important parameters here are the heating or feeding rate of ferrocene, the flow rates of the vector gas (Ar or N₂) and the gaseous hydrocarbon, and the temperature of pyrolysis (650–1050 °C). Generally speaking, the codeposition process using [Fe(CO)₅] as the catalyst source results in thermal decomposition at elevated temperatures, producing atomic iron that deposits on the substrates in the hot zone of the reactor. Since nanotube growth occurs at the same time as the introduction of [Fe(CO)₅], the temperatures chosen for the growth depend on the carbon feedstock utilized; for example, they can vary from 750 °C for acetylene to 1100 °C for methane. Mixtures of [FeCp₂] and xylene

Fig. 3.17 (a) Example of a controlled network of nanotubes grown parallel to the substrate [3.120]; (b) Example of a freestanding MWNT array obtained from the pyrolysis of a gaseous carbon source over catalyst nanoparticles previously deposited onto a patterned substrate. Each square-base rod is a bunch of MWNTs aligned perpendicular to the surface (from [3.121])



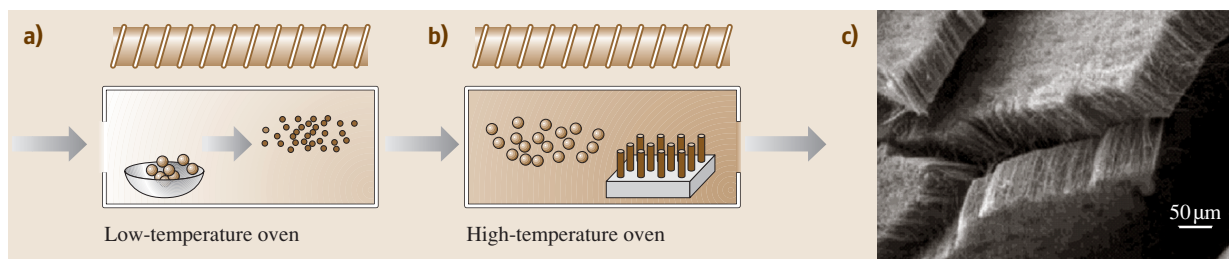


Fig. 3.18a–c Sketch of a double-furnace CCVD device used in the organometallic/hydrocarbon copolyolysis process. (a) Sublimation of the precursor. (b) Decomposition of the precursor and MWNT growth onto the substrate. (c) Example of the densely packed and aligned MWNT material obtained (from [3.137])

or $[\text{FeCp}_2]$ and acetylene have also been successfully used to produce freestanding MWNTs.

The nanotube yield and quality are directly linked to the amount and size of the catalyst particles, and since the planar substrates used do not exhibit high surface areas, the dispersion of the metal can be a key step in the process. It has been observed that an etching pretreatment of the surface of the deposited catalyst thin film with NH_3 may be critical to efficient nanotube growth of nanotubes since it provides the appropriate metal particle size distribution. It may also favor the alignment of

MWNTs and prevent the formation of amorphous carbon due to the thermal cracking of acetylene [3.140]. The application of phthalocyanines of Co, Fe and Ni has also been reported, and in this case the pyrolysis of the organometallic precursors also produces the carbon for the vertically aligned MWNTs [3.141].

Densely packed coatings of vertically aligned MWNTs may also be produced over metal-containing deposits, such as iron oxides on aluminium [3.142], in which case MWNT synthesis takes place on small particles that are formed from the iron oxide deposit.

3.3 Growth Mechanisms of Carbon Nanotubes

The growth mechanisms of carbon nanotubes are still the source of much debate. However, researchers have been impressively imaginative, and have come up with a number of hypotheses. One reason for the debate is that the conditions that allow carbon nanofilaments to grow are very diverse, which means that there are many related growth mechanisms. For a given set of conditions, the true mechanism is probably a combination of or a compromise between some of the proposals. Another reason is that the phenomena that occur during growth are pretty rapid and difficult to observe in situ. It is generally agreed, however, that growth occurs such that the number of dangling bonds is minimized, for energetic reasons.

3.3.1 Catalyst-Free Growth

As already mentioned, in addition to the templating technique, which is merely a chemical vapor infiltration mechanism for pyrolytic carbon, the growth of c-MWNT as a deposit on the cathode in the electric arc method is a rare example of catalyst-free carbon nanofilament growth. The driving force is obviously related to the

electric field; in other words to charge transfer from one electrode to the other via the particles contained in the plasma. It is not clear how the MWNT nucleus is formed, but once it has, it may include the direct incorporation of C_2 species into the primary graphene structure, as it was previously proposed for fullerenes [3.143]. This is supported by recent C_2 radical concentration measurements that reveal an increasing concentration of C_2 from the anode being consumed at the growing cathode (Fig. 3.13). This indicates that C_2 are only secondary species and that the C_2 species may actually actively participate in the growth of c-MWNTs in the arc method.

3.3.2 Catalytically Activated Growth

Growth mechanisms involving catalysts are more difficult to ascertain, since they are more diverse. Although it involves a more or less extensive contribution from a VLS (vapor-liquid-solid [3.144]) mechanism, it is quite difficult to find comprehensive and plausible explanations that are able to account for both the various conditions used and the various morphologies observed. What follows is an attempt to provide overall expla-

nations of most of the phenomena, while remaining consistent with the experimental data. We do not consider any hypothesis for which there is a lack of experimental evidence, such as the moving nanocatalyst mechanism, which proposes that dangling bonds from a growing SWNT may be temporarily stabilized by a nanosized catalyst located at the SWNT tip [3.25], or the scooter mechanism, which proposes that dangling bonds are temporarily stabilized by a single catalyst atom which moves around the edge of the SWNT, allowing subsequent C atom addition [3.145].

From various results, it appears that the most important parameters are probably the thermodynamic ones (only temperature will be considered here), the catalyst particle size, and the presence of a substrate. Temperature is critical and basically corresponds to the discrepancy between CCVD methods and solid carbon source-based methods.

Low-Temperature Conditions

Low-temperature conditions are typical used in CCVD, where nanotubes are frequently found to grow far below 1000 °C. If the conditions are such that the catalyst is a crystallized solid, the nanofilament is probably formed via a mechanism similar to a VLS mechanism, in which three steps are defined: (i) adsorption then decomposition of C-containing gaseous moieties at the catalyst surface; (ii) dissolution then diffusion of the C species through the catalyst, thus forming a solid solution; (iii) back-precipitation of solid carbon as nanotube walls. The texture is then determined by the orientation of the crystal faces relative to the filament axis (Fig. 3.19), as demonstrated beyond doubt by transmission electron microscopy images such as those in Rodriguez et al. [3.16]. This mechanism can therefore provide either c-MWNT, h-MWNT, or platelet nanofibers. The latter, however, are mainly formed in large particle sizes (> 100 nm for example). Platelet nanofibers with low diameters (below 40 nm) have never been observed. The reasons for this are related to graphene energetics, such as the need to reach the optimal ratio between the amount of edge carbon atoms (with dangling bonds) and inner carbon atoms (where all of the σ and π orbitals are satisfied).

If conditions are such that the catalyst is a liquid droplet, due to the use of high temperatures or because a catalyst that melts at a low temperature is employed, a mechanism similar to that described above can still occur, which is really VLS (vapor = gaseous C species, liquid = molten catalyst, S = graphenes), but there are obviously no crystal faces

to orient preferentially with the rejected graphenes. Energy minimization requirements will therefore tend to make them concentric and parallel to the filament axis.

With large catalyst particles (or in the absence of any substrate), the mechanisms above will generally follow a “tip growth” scheme: the catalyst will move forward while the rejected carbon will form the nanotube behind, whether there is a substrate or not. In this case, there is a good chance that one end will be open. On the other hand, when the catalyst particles deposited onto the substrate are small enough (nanoparticles) to be held in place by interaction forces with the substrate, the growth mechanism will follow a “base growth” scheme, where the carbon nanofilament grows away from the substrate, leaving the catalyst nanoparticle attached to the substrate (Fig. 3.20).

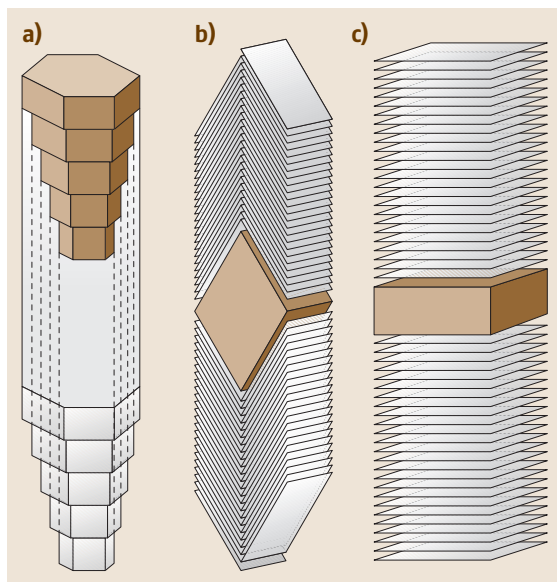


Fig. 3.19a–c Illustration of the possible relationships between the outer morphology of the catalyst crystal and the inner texture of the subsequent carbon nanofilament (adapted from [3.16]). Crystals are drawn with the projected plane perpendicular to the electron beam in a transmission electron microscope; the crystal morphologies and the subsequent graphene arrangements in the out-of-plane dimension are not intended to be accurate representations in these sketches (for example, the graphenes in the herringbone-type nanotubes or nanofibers in (b) cannot be arranged like a pile of open books, as sketched here, because it would leave too many dangling bonds)

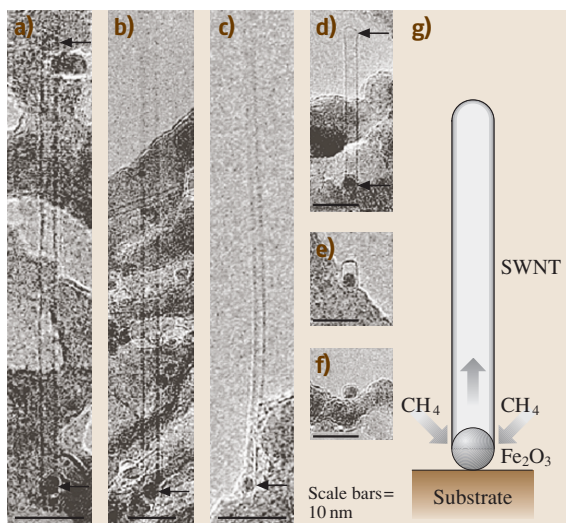


Fig. 3.20 High-resolution transmission electron microscopy images of several SWNTs grown from iron-based nanoparticles using the CCVD method, showing that particle sizes determine SWNT diameters in this case (adapted from [3.147])

The bamboo texture that affects both the herringbone and the concentric texture may reveal a distinguishing aspect of the dissolution-rejection mechanism: the periodic, discontinuous dynamics of the phenomenon. Once the catalyst has reached the saturation threshold in terms of its carbon content, it expels it quite suddenly. Then it becomes able to incorporate a given amount of carbon again without having any catalytic activity for a little while. Then over-saturation is reached again, and so on. An exhaustive study of this phenomenon has been carried out by *Jourdain et al.* [3.146].

Therefore, it is clear that 1 catalyst particle = 1 nanofilament in any of the mechanisms above. This explains why, although it is possible to make SWNTs by CCVD methods, controlling the catalyst particle size is critical, since it influences the nanofilament that grows from it. Achieving a really narrow size distribution in CCVD is quite challenging, particularly when nanosizes are required for the growth of SWNTs. Only particles < 2 nm are useful for this (Fig. 3.20), since larger SWNTs are not favored energetically [3.9]. Another distinguishing aspect of the CCVD method and its related growth mechanisms is that the process can occur all along the isothermal zone of the reactor furnace since it is continuously fed with a carbon-rich feedstock, which is generally in excess, with a constant composition at a given species time of flight. Roughly

speaking, the longer the isothermal zone (in gaseous carbon excess conditions), the longer the nanotubes. This is why the lengths of the nanotubes can be much longer than those obtained using solid carbon source-based methods.

Table 3.2 provides an overview of the relationship between general synthesis conditions and some features of nanotube grown.

High-Temperature Conditions

High-temperature conditions are typical used in solid carbon source-based methods such as the electric arc method, laser vaporization, and the solar furnace method (see Sect. 3.2). The huge temperatures involved (several thousands of °C) atomize both the carbon source and the catalyst. Of course, catalyst-based SWNTs do not form in the areas with the highest temperatures (contrary to c-MWNTs in the electric arc method); medium is a mixture of atoms and radicals, some of which are likely to condense back into the same droplet (since the medium is liquid at the beginning). At some distance from the atomization zone, the medium is therefore made of carbon metal alloy droplets and of secondary carbon species that range from C₂ to higher order molecules such as corannulene, which is made of a central pentagon surrounded by five hexagons. The preferred formation of such a molecule can be explained by the previous association of carbon atoms into a pentagon, because it is the fastest way to limit dangling bonds at low energetic cost, thereby providing a fixation site for other carbon atoms (or C₂) which also will tend to close into a ring, again to limit dangling bonds. Since adjacent pentagons are not energetically favored, these cycles will be hexagons. Such a molecule is thought to be a probable precursor for fullerenes. Fullerenes are actually always produced, even in conditions that produce SWNTs. The same saturation in C described in Sect. 3.3.2 occurs for the carbon-metal alloy droplet as well, resulting in the precipitation of excess C outside the particle due to the effect of the decreasing thermal gradient in the reactor, which decreases the solubility threshold of C in the metal [3.148]. Once the “inner” carbon atoms reach the surface of the catalyst particle, they meet the “outer” carbon species, including corannulene, that will contribute to capping the merging nanotubes. Once formed and capped, nanotubes can grow both from the inner carbon atoms (Fig. 3.21a), according to the VLS mechanism proposed by *Saito et al.* [3.148], and from the outer carbon atoms, according the adatom mechanism proposed by *Bernholc et al.* [3.149]. In the latter, carbon atoms from the surrounding medium in the reactor are

Table 3.2 Guidelines indicating the relationships between possible carbon nanoflament morphologies and some basic synthesis conditions. Columns (1) and (2) mainly relate to CCVD-based methods; column (3) mainly relates to plasma-based methods

		Increasing temperature and physical state of catalyst			Substrate		Thermal gradient	
		solid (crystallized) (1)	liquid from melting (2)	liquid from condensing atoms (3)	yes	no	low	high
Catalyst particle size	< ~ 3 nm	SWNT	SWNT	?	base- growth			
	> ~ 3 nm	MWNT (c,h,b) platelet nanofiber	c-MWNT	SWNT	tip- growth	tip- growth	long length	short length
Nanotube diameter		(heterogeneous related to catalyst particle size)		homogeneous (independent from particle size)	(except for SWNTs growing from case (3) catalyst)			
Nanotube/particle		one nanotube/particle		several SWNTs/particle				

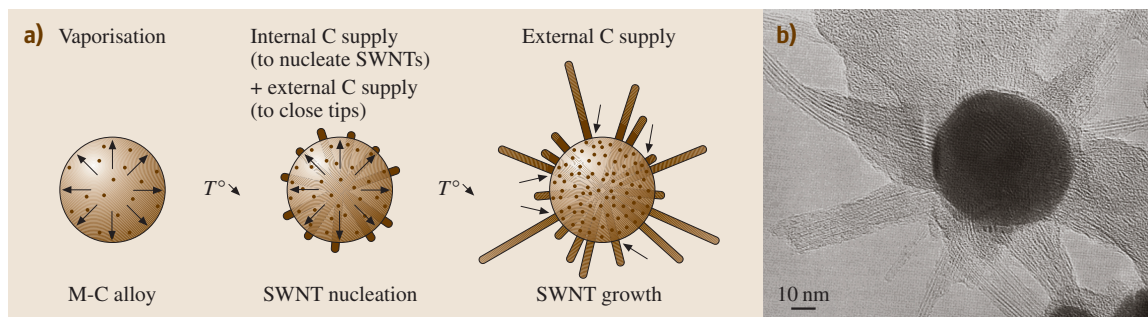


Fig. 3.21 (a) Mechanism proposed for SWNT growth (see text). (b) Transmission electron microscopy image of SWNT growing radially from the surface of a large Ni catalyst particle in an electric arc experiment. (Modified from [3.18])

attracted then stabilized by the carbon/catalyst interface at the nanotube/catalyst surface contact, promoting their subsequent incorporation at the tube base. The growth mechanism therefore mainly follows the base growth scheme. However, once the nanotubes are capped, any C_2 species that still remains in the medium that meets the growing nanotubes far from the nanotube/catalyst interface may still incorporate the nanotubes from both the side wall or the tip, thereby giving rise to some proportion of Stone–Wales defects [3.42]. The occurrence

of a nanometer-thick surface layer of yttrium carbide (onto the main Ni-containing catalyst core), the lattice distance of which is commensurable with that of the C–C distance in graphene (as recently revealed by *Gavillet et al.* [3.50]), could possibly play a beneficial role in stabilizing the nanotube/catalyst interface, which could explain why the SWNT yield is enhanced by bimetallic alloys (as opposed to single metal catalysts).

A major difference from the low-temperature mechanisms described for CCVD methods is that many

nanotubes are formed from a single, relatively large ($\approx 10\text{--}50\text{ nm}$) catalyst particle (Fig. 3.21b), whose size distribution is therefore not as critical as it is for the low-temperature mechanisms (particles that are too large, however, induce polyaromatic shells instead of nanotubes). This is why the diameters of **SWNTs** grown at high temperature are much more homogeneous than those associated with **CCVD** methods. The reason that the most frequent diameter is $\approx 1.4\text{ nm}$ is again a matter of energy balance. Single-wall nanotubes larger than $\approx 2.5\text{ nm}$ are not stable [3.9]. On the other hand, the strain on the C–C bond increases as the radius of curvature decreases. The optimal diameter (1.4 nm) should therefore correspond to the best energetic compromise. Another difference from the low-temperature mechanism for **CCVD** is that temperature gradients in high temperature

methods are huge, and the gas phase composition surrounding the catalysts droplets is also subjected to rapid changes (as opposed to what could happen in a laminar flow of a gaseous feedstock whose carbon source is in excess). This explains why nanotubes from arcs are generally shorter than nanotubes from **CCVD**, and why mass production by **CCVD** is favored. In the latter, the metallic particle can act as a catalyst repeatedly as long as the conditions are maintained. In the former, the surrounding conditions change continuously, and the window for efficient catalysis can be very narrow. Decreasing the temperature gradients that occur in solid carbon source-based methods of producing **SWNT**, such as the electric arc reactor, should therefore increase the **SWNT** yield and length [3.150]. Amazingly, this is in opposition to what is observed during arc-based fullerene production.

3.4 Properties of Carbon Nanotubes

In previous sections, we noted that the normal planar configuration of graphene can, under certain growth conditions (see Sect. 3.3), be changed into a tubular geometry. In this section, we take a closer look at the properties of these carbon nanotubes, which can depend on whether they are arranged as **SWNTs** or as **MWNTs** (see Sect. 3.1).

3.4.1 Overview

The properties of **MWNTs** are generally similar to those of regular polyaromatic solids (which may exhibit graphitic, turbostratic or intermediate crystallographic structure). Variations are mainly due to different textural types of the **MWNTs** considered (concentric, herringbone, bamboo) and the quality of the nanotexture (see Sect. 3.1), both of which control the extent of anisotropy. Actually, for polyaromatic solids that consist of stacked graphenes, the bond strength varies significantly depending on whether the in-plane direction is considered (characterized by very strong covalent and therefore very short – 0.142 nm – bonds) or the direction perpendicular to it (characterized by very weak van der Waals and therefore very loose – $\approx 0.34\text{ nm}$ – bonds). Such heterogeneity is not found in single (isolated) **SWNTs**. However, the heterogeneity returns, along with the related consequences, when **SWNTs** associate into bundles. Therefore, the properties – and applicability – of **SWNTs** may also change dramatically depending on whether single **SWNT** or **SWNT** ropes are involved.

In the following, we will emphasize the properties of **SWNTs**, since their unique structures often lead to different properties to regular polyaromatic solids. However, we will also sometimes discuss the properties of **MWNTs** for comparison.

3.4.2 General Properties of SWNTs

The diameters of **SWNT**-type carbon nanotubes fall in the nanometer regime, but **SWNTs** can be hundreds of micrometers long. **SWNTs** are narrower in diameter than the thinnest line that can be obtained in electron beam lithography. **SWNTs** are stable up to $750\text{ }^\circ\text{C}$ in air (but they are usually damaged before this temperature is reached due to oxidation mechanisms, as demonstrated by the fact that they can be filled with molecules (see Sect. 3.5). They are stable up to $\approx 1500\text{--}1800\text{ }^\circ\text{C}$ in inert atmosphere, beyond which they transform into regular, polyaromatic solids (phases built with stacked graphenes instead of single graphenes) [3.151]. They have half the mass density of aluminium. The properties of a **SWNT**, like any molecule, are heavily influenced by the way that its atoms are arranged. The physical and chemical behavior of a **SWNT** is therefore related to its unique structural features [3.152].

3.4.3 Adsorption Properties of SWNTs

An interesting feature of a **SWNT** is that it has the highest surface area of any molecule due to the fact that a graphene sheet is probably the only example of a sheet-

like molecule that is energetically stable under normal conditions. If we consider an isolated **SWNT** with one open end (achieved through oxidation treatment for instance), the surface area is equal to that of a single, flat graphene sheet: $\approx 2700 \text{ m}^2/\text{g}$ (accounting for both sides).

In reality, nanotubes – specifically **SWNTs** – are usually associated with other nanotubes in bundles, fibers, films, papers, and so on, rather than as a single entity. Each of these associations has a specific range of porosities that determines its adsorption properties (this topic is also covered in Sect. 3.6.2 on applications). It is therefore more appropriate to discuss adsorption onto the outer or the inner surface of a bundle of **SWNTs**.

Furthermore, theoretical calculations have predicted that the adsorption of molecules onto the surface or inside of a nanotube bundle is stronger than that onto an individual tube. A similar situation exists for **MWNTs**, where adsorption can occur on or inside the tubes or between aggregated **MWNTs**. It has also been shown that the curvature of the graphene sheets constituting the nanotube walls results in a lower heat of adsorption compared to planar graphene (see Sect. 3.1.1).

Accessible SWNT Surface Area

Various studies dealing with the adsorption of nitrogen onto **MWNTs** [3.154–156] and **SWNTs** [3.157] have highlighted the porous nature of these two materials. The pores in **MWNTs** can be divided mainly into hollow inner cavities with small diameters (with narrow size distributions, mainly 3–10 nm) and aggregated pores (with wide size distributions, 20–40 nm), formed by interactions between isolated **MWNTs**. It is also worth noting that the ultra-strong nitrogen capillarity in the aggregated pores dominates the total adsorption, indicating that the aggregated pores are much more important than the inner cavities of the **MWNTs** during adsorption. Adsorption of N_2 has been studied on as-prepared and acid-treated **SWNTs**, and the results obtained highlight the microporous nature of **SWNT** materials, as

opposed to the mesoporous nature of **MWNT** materials. Also, as opposed to isolated **SWNTs** (see above), surface areas that are well above $400 \text{ m}^2 \text{ g}^{-1}$ have been measured for **SWNT**-bundle-containing materials, with internal surface areas of $300 \text{ m}^2 \text{ g}^{-1}$ or higher.

The theoretical surface area of a carbon nanotube has a broad range, from 50 to $1315 \text{ m}^2 \text{ g}^{-1}$ depending on the number of walls, the diameter, and the number of nanotubes in a bundle of **SWNTs** [3.158]. Experimentally, the surface area of a **SWNT** is often larger than that of a **MWNT**. The total surface area of as-grown **SWNTs** is typically between 400 and $900 \text{ m}^2 \text{ g}^{-1}$ (micropore volume, 0.15 – $0.3 \text{ cm}^3 \text{ g}^{-1}$), whereas values of 200 and $400 \text{ m}^2 \text{ g}^{-1}$ for as-produced **MWNTs** are often reported. In the case of **SWNTs**, the diameters of the tubes and the number of tubes in the bundle will have the most effect on the BET value. It is worth noting that opening or closing the central canal significantly influences the adsorption properties of nanotubes. In the case of **MWNTs**, chemical treatments such as KOH or NaOH activation are useful for promoting microporosity, and surface areas as high as $1050 \text{ m}^2 \text{ g}^{-1}$ have been reported [3.159, 160]. An efficient two-step treatment (acid + CO_2 activation) has been reported to open both ends of **MWNTs** [3.161]. Therefore, it appears that opening or cutting carbon nanotubes, as well as chemically treating them (using purification steps for example) can considerably affect their surface area and pore structure.

Adsorption Sites and Binding Energy of the Adsorbates

An important problem to solve when considering adsorption onto nanotubes is to identify the adsorption sites. The adsorption of gases into a **SWNT** bundle can occur inside the tubes (pore), in the interstitial triangular channels between the tubes, on the outer surface of the bundle, or in the grooves formed at the contacts between adjacent tubes on the outside of the bundle (Fig. 3.22). Modeling studies have pointed out that the convex surface of the **SWNT** is more reactive than the concave one and that this difference in reactivity increases as the tube diameter decreases [3.162]. Compared to the highly bent region in fullerenes, **SWNTs** are only moderately curved and are expected to be much less reactive towards dissociative chemisorption. Models have also predicted enhanced reactivity at the kink sites of bent **SWNTs** [3.163]. Additionally, it is worth noting that unavoidable imperfections, such as vacancies, Stone–Wales defects, pentagons, heptagons and dopants, are believed to play a role in tailoring the adsorption properties [3.164].

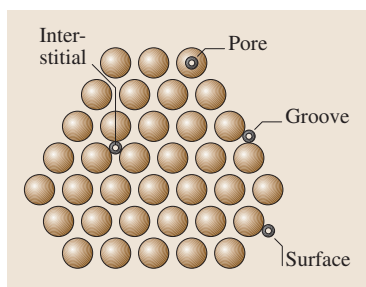


Fig. 3.22 Sketch of a **SWNT** bundle, illustrating the four different adsorption sites (adapted from [3.153])

Considering closed-end **SWNTs** first, simple molecules can be adsorbed onto the walls of the outer nanotubes of the bundle and preferably on the external grooves. In the first stages of adsorption (corresponding to the most attractive sites for adsorption), it seems that adsorption or condensation in the interstitial channels of the **SWNT** bundles depends on the size of the molecule (or on the **SWNT** diameters) and on their interaction energies [3.165, 166]. Opening the tubes favors gas adsorption (including O₂, N₂ within the inner walls [3.167, 168]). It was found that the adsorption of nitrogen on open-ended **SWNT** bundles is three times larger than that on closed-ended **SWNT** bundles [3.169]. The significant influence that the external surface area of the nanotube bundle has on the character of the surface adsorption isotherm of nitrogen (type I, II or even IV of the IUPAC classification) has been demonstrated from theoretical calculations [3.170]. For hydrogen and other small molecules like CO, computational methods have shown that, for open **SWNTs**, the pore, interstitial and groove sites are energetically more favorable than surface sites [3.171, 172]. In the case of carbon monoxide, aside from physisorbed CO, CO hydrogen bonds to hydroxyl functionalities created on the **SWNTs** by acid purification have been identified [3.172]. FTIR and temperature-programmed desorption (TPD) experiments have shown that NH₃ or NO₂ adsorb molecularly and that NO₂ is slightly more strongly bound than NH₃ [3.173]. For NO₂, the formation of nitrito (O-bonded) complexes is preferred to nitro (N-bonded) ones. For ozone, a strong oxidizing agent, theoretical calculations have shown that physisorption occurs on ideal, defect-free **SWNT**, whereas strong chemisorption occurs on Stone–Wales defects, highlighting the key role of defec-

tive sites in adsorption properties [3.174]. Finally, for acetone, TPD experiments have shown that this molecule chemisorbs on **SWNT** while physisorption occurs on graphite [3.175].

For **MWNTs**, adsorption can occur in the aggregated pores, inside the tube or on the external walls. In the latter case, the presence of defects, as incomplete graphene layers, must be taken into consideration. Although adsorption between the graphenes (intercalation) has been proposed in the case of hydrogen adsorption in **h-MWNTs** or platelet nanofibers [3.176], it is unlikely to occur for many molecules due to steric effects and should not prevail for small molecules due to the long diffusion paths involved. In the case of inorganic fluorides (BF₃, TiF₄, NbF₅ and WF₆), accommodation of the fluorinated species into the carbon lattice has been shown to result from intercalation and adsorption/condensation phenomena. In this case, doping-induced charge transfer has been demonstrated [3.177].

Only a few studies deal with adsorption sites in **MWNTs**, but it has been shown that butane adsorbs more onto **MWNTs** with smaller outside diameters, which is consistent with another statement that the strain on curved graphene surfaces affects sorption. Most of the butane adsorbs to the external surface of the **MWNTs** while only a small fraction of the gas condenses in the pores [3.178]. Comparative adsorption of krypton or of ethylene onto **MWNTs** or onto graphite has allowed scientists to determine the dependence of the adsorption and wetting properties of the nanotubes on their specific morphologies. Nanotubes were found to have higher condensation pressures and lower heats of adsorption than graphite [3.179]. These differences are mainly due

Table 3.3 Adsorption properties and sites of **SWNTs** and **MWNTs**. The letters in the *Absorption sites* column refer to Fig. 3.22. The data in the last two columns are from [3.153]

Type of nanotube	Porosity (cm ³ g ⁻¹)	Surface area (m ² /g)	Binding energy of the adsorbate	Adsorption sites	Attractive potential per site (eV)	Surface area per site (m ² /g)
SWNT (bundle)	Microporous V _{micro} : 0.15–0.3	400–900	Low, mainly physisorption 25–75 % > graphite	Surface (A)	0.049	483
				Groove (B)	0.089	22
				Pore (C)	0.062	783
				Interstitial (D)	0.119	45
MWNT	Mesoporous	200–400	Physisorption	Surface Pore Aggregated pores	—	—

to decreased lateral interactions between the adsorbed molecules, related to the curvature of the graphene sheets.

A limited number of theoretical as well as experimental studies on the binding energies of gases onto carbon nanotubes exist. While most of these studies report low binding energies on SWNTs, consistent with physisorption, some experimental results, in particular for hydrogen, are still controversial (see Sect. 3.6.2). For platelet nanofibers, the initial dissociation of hydrogen on graphite edge sites, which constitute most of the nanofiber surface, has been proposed [3.180]. For carbon nanotubes, a mechanism that involves H₂ dissociation on the residual metal catalyst followed by H spillover and adsorption on the most reactive nanotube sites was envisaged [3.181]. Similarly, simply mixing carbon nanotubes with supported palladium catalysts increased the hydrogen uptake of the carbon by a factor of three, due to hydrogen spillover from the supported catalyst [3.182]. Doping nanotubes with alkali may enhance hydrogen adsorption, due to charge transfer from the alkali metal to the nanotube, which polarizes the H₂ molecule and induces dipole interactions [3.183].

Generally speaking, the adsorbates can be either charge donors or acceptors to the nanotubes. Trends in the binding energies of gases with different van der Waals radii suggest that the groove sites of SWNTs are the preferred low coverage adsorption sites due to their higher binding energies. Finally, several studies have shown that, at low coverage, the binding energy of the adsorbate on SWNT is between 25% and 75% higher than the binding energy on a single graphene. This discrepancy can be attributed to an increase of effective coordination at the binding sites, such as the groove sites, in SWNTs bundles [3.184, 185]. Representative results on the adsorption properties of SWNTs and MWNTs are summarized in Table 3.3.

3.4.4 Electronic and Optical Properties

The electronic states in SWNTs are strongly influenced by their one-dimensional cylindrical structures. One-dimensional sub-bands are formed that have strong singularities in the density of states (Van Hove singularities). By rolling the graphene sheet to form a tube, new periodic boundary conditions are imposed on the electronic wavefunctions, which give rise to one-dimensional sub-bands: $C_n K = 2q$ where q is an integer. C_n is the roll-up vector $na_1 + ma_2$ which defines the

helicity (chirality) and the diameter of the tube (see Sect. 3.1). Much of the electronic band structure of CNTs can be derived from the electronic band structure of graphene by applying the periodic boundary conditions of the tube under consideration. The conduction and the valence bands of the graphene only touch at six corners (K points) of the Brillouin zone [3.186]. If one of these sub-bands passes through the K point, the nanotube is metallic; otherwise it is semiconducting. This is a unique property that is not found in any other one-dimensional system, which means that for certain orientations of the honeycomb lattice with respect to the tube axis (chirality), some nanotubes are semiconducting and others are metallic. The band gap for semiconducting tubes is found to be inversely proportional to the tube diameter. As pointed out in Sect. 3.1, knowing (n, m) allows us, in principle, to predict whether the tube is metallic or not. The energy gap decreases for larger tube diameters and MWNTs with larger diameter are found to have properties similar to other forms of regular, polyaromatic solids. It has been shown that electronic conduction mostly occurs through the external tube for MWNTs; even so, interactions with internal tubes often cannot be neglected and they depend upon the helicity of the neighboring tubes [3.187]. The electronic and optical properties of the tubes are considerably influenced by the environment [3.188]. Under externally applied pressure, the small interaction between the tube walls results in the internal tubes experiencing reduced pressure [3.189]. The electronic transition energies are in the infrared and visible spectral range. The one-dimensional Van Hove singularities have a large influence on the optical properties of CNTs. Visible light is selectively and strongly absorbed. It has been observed that a broad band flash in the visible spectral range can lead to the spontaneous burning of agglomerated SWNTs in air at room temperature [3.190]. The exact energy band positions and the existence and formation of excitons in CNTs are not yet well known and/or understood, and are currently being explored [3.191]. Photoluminescence can be observed in individual SWNT aqueous suspensions stabilized by the addition of surfactants. Detailed photoexcitation maps provide information about the helicity (chirality)-dependent transition energies and the electronic band structures of CNTs [3.192]. Agglomeration of tubes into ropes or bundles influences the electronic states of CNTs. Photoluminescence signals are quenched for agglomerated tubes.

CNTs are model systems for the study of one-dimensional transport in materials. Apart from the

singularities in the density of states, electron–electron interactions are expected to show drastic changes at the Fermi edge; the electrons in CNTs are not described by a Fermi liquid, but instead by a Luttinger liquid model [3.193] that describes electronic transport in one-dimensional systems. It is expected that the variation of electronic conductance vs. temperature follows a power law, with zero conductance at low temperatures. Depending on how L_ϕ (the coherence length) on the one hand and L_m (the electronic mean free path) on the other compare to L (the length of the sample), different conduction modes are observed: ballistic if $L \ll L_\phi$, $L \ll L_m$, diffusive if $L_\phi \ll L_m < L$ and localization if $L_m \ll L_\phi \ll L$. Fluctuations in the conductance can be seen when $L \approx L_\phi$. For ballistic conduction (a small number of defects) [3.194–196], the predicted electronic conductance is independent of the tube length. The conductance value is twice the fundamental conductance unit $G_0 = 4e/h$ due to the existence of two propagating modes. Due to the reduced electron scattering observed for metallic CNTs and their stability at high temperatures, CNTs can support high current densities (max 10^9 A/cm²): about three orders of magnitude higher than Cu. Structural defects can, however, lead to quantum interference of the electronic wave function, which localizes the charge carriers in one-dimensional systems and increases resistivity [3.193, 197, 198]. Localization and quantum interference can be strongly influenced by applying a magnetic field [3.199]. At low temperatures, the discrete energy spectrum leads to a Coulomb blockade resulting in oscillations in the conductance as the gate voltage is increased [3.198]. In order to observe the different conduction regimes, it is important to consider the influence of the electrodes where Schottky barriers are formed. Recently it was shown [3.200] that palladium electrodes form excellent junctions with tubes. The influence of superconducting electrodes or ferromagnetic electrodes on electronic transport in CNTs due to spin polarization has also been explored [3.201, 202].

As a probable consequence of both the small number of defects (at least the kind of defects that oppose phonon transport) and the cylindrical topography, SWNTs exhibit a large phonon mean free path, which results in a high thermal conductivity. The thermal conductivity of SWNTs is comparable to that of a single, isolated graphene layer or high purity diamond [3.203], or possibly higher (≈ 6000 W/mK).

Finally, carbon nanotubes may also exhibit positive or negative magnetoresistance depending on the current, the temperature, and the field, whether they are MWNTs [3.204] or SWNTs [3.198].

3.4.5 Mechanical Properties

While tubular nanomorphology is also observed for many two-dimensional solids, carbon nanotubes are unique due to the particularly strong bonding between the carbons (sp^2 hybridization of the atomic orbitals) of the curved graphene sheet, which is stronger than in diamond (sp^3 hybridization), as revealed by the difference in C–C bond lengths (0.142 vs. 0.154 nm for graphene and diamond respectively). This makes carbon nanotubes – SWNTs or c-MWNTs – particularly stable against deformations. The tensile strength of SWNTs can be 20 times that of steel [3.205] and has actually been measured as ≈ 45 GPa [3.206]. Very high tensile strength values are also expected for ideal (defect-free) c-MWNTs, since combining perfect tubes concentrically is not supposed to be detrimental to the overall tube strength, provided the tube ends are well capped (otherwise, concentric tubes could glide relative to each other, inducing high strain). Tensile strength values as high as ≈ 150 GPa have actually been measured for perfect MWNTs from an electric arc [3.207], although the reason for such a high value compared to that measured for SWNTs is not clear. It probably reveals the difficulties involved in carrying out such measurements in a reliable manner. The flexural modulus of perfect MWNTs should logically be higher than that for SWNTs [3.205], with a flexibility that decreases as the

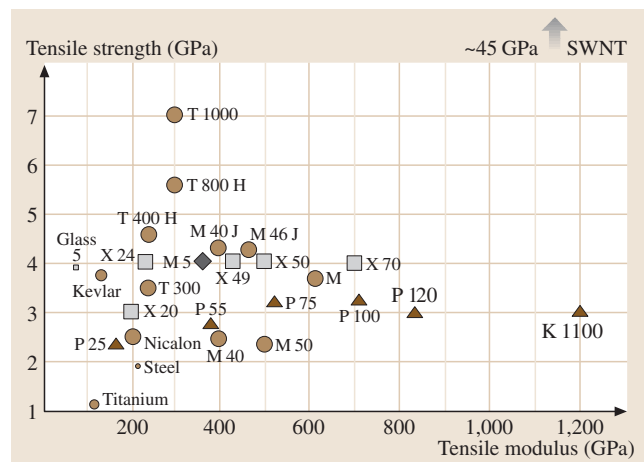


Fig. 3.23 Plot of the tensile strength versus the tensile modulus for various fibrous materials and SWNTs. *Large circles* are PAN-based carbon fibers, which include the fiber with the highest tensile strength available on the market (T1000 from Torayca); *Triangles* are pitch-based carbon fibers, which include the fiber with the highest tensile modulus on the market (K1100 from Amoco)

number of walls increases. On the other hand, measurements performed on defective MWNTs obtained from CCVD exhibit a range of 3–30 GPa [3.208]. Values of tensile modulus are also the highest values known, 1 TPa for MWNTs [3.209], and possibly even higher for SWNTs, up to 1.3 TPa [3.210, 211]. Figure 3.23 illustrates how defect-free carbon nanotubes could spectacularly revolutionize the field of high performance fibrous materials.

3.4.6 Reactivity

The chemical reactivities of graphite, fullerenes, and carbon nanotubes are similar in many ways. Like any small object, carbon nanotubes have a large surface to interact with their environment (see Sect. 3.4.1). It is worth noting, however, that nanotube chemistry differs from that observed for regular polyaromatic carbon materials due to the unique shape of the nanotube, its small diameter, and its structural properties. Unlike graphite, perfect SWNTs have no (chemically active) dangling bonds (the reactions of polyaromatic solids is known to occur mainly at graphene edges). Unlike fullerenes, the ratio of “weak” sites (C–C bonds involved in heterocycles) to strong sites (C–C bonds between regular hexagons) is only deviates slightly from 0 for ideal tubes. For C_{60} fullerenes this ratio is 1 – C_{60} molecules have 12 pentagons (therefore accounting for $5 \times 12 = 30$ C–C bonds) and 20 hexagons, each of them with three C–C bonds not involved in an adjacent pentagon but shared with a neighboring hexagon (so $20 \times 3 \times 1/2 = 30$ C–C bonds are involved in hexagons only). Although graphene faces are chemically relatively inert, the radius of curvature imposed on the graphene in nanotubes causes the three normally planar C–C bonds caused by sp^2 hybridization to undergo distortions, resulting in bond angles that are closer to three of the four C–C bonds in diamond (characteristic of genuine sp^3 hy-

bridization), as the radius of curvature decreases. Even though it is not enough to make the carbon atoms chemically reactive, one consequence of this is that either nesting sites are created at the concave surface, or strong physisorption sites are created above each carbon atom of the convex surface, both with a bonding efficiency that increases as the nanotube diameter decreases.

As already pointed out in Sect. 3.1, the chemical reactivities of SWNTs (and c-MNWTs) are believed to derive mainly from the caps, since they contain six pentagons each, as opposed to the tube body, which supposedly only contains hexagons. Indeed, applying oxidizing treatments to carbon nanotubes (air oxidation, wet-chemistry oxidation) selectively opens the nanotube tips [3.212]. However, that SWNTs can be opened by oxidation methods and then filled with foreign molecules such as fullerenes (see Sect. 3.5) suggests the occurrence of side defects [3.14], whose identity and occurrence were discussed and then proposed to be an average of one Stone–Wales defect every 5 nm along the tube length, involving about 2% of the carbon atoms in a regular (10,10) SWNT [3.213]. A Stone–Wales defect is formed from four adjacent heterocycles, two pentagons and two heptagons, arranged in pairs opposite each other. Such a defect allows localized double bonds to form between the carbon atoms involved in the defect (instead of these electrons participating in the delocalized electron cloud above the graphene as usual, enhancing the chemical reactivity, for example toward chlorocarbenes [3.213]). This means that the overall chemical reactivity of carbon nanotubes should depend strongly on how they are synthesized. For example, SWNTs prepared by the arc-discharge method are believed to contain fewer structural defects than CCVD-synthesized SWNTs, which are more chemically reactive. Of course, the reactivity of h-MWNT-type nanotubes is intrinsically higher, due to the occurrence of accessible graphene edges at the nanotube surface.

3.5 Carbon Nanotube-Based Nano-Objects

3.5.1 Heteronanotubes

It is possible to replace some or all of the carbon atoms in a nanotube with atoms of other elements without damaging the overall honeycomb lattice-based graphene structure. Nanotubes modified in this way are termed here “heteronanotubes”.

The elements used to replace carbon in this case are boron and/or nitrogen. Replacing carbon atoms

in this way can result in new behavior (for example, BN nanotubes are electrical insulators), improved properties (resistance to oxidation for instance), or better control over such properties. For instance, one current challenge in carbon SWNT synthesis is to control the processing so that the desired SWNT structure (metallic or semiconductor) is formed selectively. In this regard, it was demonstrated that replacing some C atoms with N or B atoms leads to

SWNTs with systematically metallic electrical behavior [3.214, 215].

Some examples of heteronanotubes – mainly **MWNTs** – can be found in the literature. The heteroatom usually involved is nitrogen, due to the ease with which gaseous or solid nitrogen- and/or boron-containing species (such as N_2 , NH_3 , BN , HfB_2) can be passed into existing equipment for synthesizing **MWNTs** [3.214, 216] until complete substitution of carbon occurs [3.217, 218]. An amazing result of such attempts to synthesize hetero-**MWNTs** is the subsequent formation of “multilayered” c-**MWNTs**: **MWNTs** made up of coaxial alternate carbon graphene tubes and boron nitride graphene tubes [3.219]. On the other hand, there are only a few examples of hetero-**SWNTs**. Syntheses of B- or N-containing **SWNTs** have recently been reported [3.215, 220], while just one successful synthesis of genuine **BN-SWNTs** has been reported so far [3.221].

3.5.2 Hybrid Carbon Nanotubes

Hybrid carbon nanotubes are defined here as carbon nanotubes, **SWNTs** or **MWNTs** that have inner cavities filled (partially or entirely) with foreign atoms, molecules, compounds or crystals. The terminology **X@SWNT** (or **X@MWNT**, if appropriate, where X is the atom, molecule and so on involved) is used for such structures [3.222].

Motivation

But why should we want to fill the cavities of carbon nanotubes [3.213]? The very small inner cavity of nanotubes is an amazing tool for preparing and studying the properties of confined nanostructures of any type, such as salts, metals, oxides, gases, or even discrete molecules like C_{60} , for example. Due to the almost one-dimensional structure of carbon nanotubes (particularly for **SWNTs**), we might expect that encapsulated material might have different physical and/or chemical properties to the unencapsulated material, and that the hybrid nanotube itself may behave differently to a “pure” nanotube. Indeed, if the volume available inside a carbon nanotube is small enough, the foreign material is largely “surface atoms” of reduced coordination. The original motivation to create such hybrids was to obtain metal nanowires that are likely to be of interest in electronics (as quantum wires). In this case, the nanotubes were considered to be nanomolds for the metal filler, and it was probably intended that the nanomold was to be removed afterwards. However, it is likely that this removal of the **SWNT** “container” to liberate the one-dimensional structure inside it

may destroy or at least transform this structure due to the stabilizing effect of interactions with the nanotube wall.

Filling nanotubes while they grow (in situ filling) was one of the pioneering methods of nanotechnology. In most cases, however, the filling step is separate from nanotube synthesis. Three filling methods can then be distinguished: (a) wet chemistry procedures; capillarity-based physical procedures involving (b) a molten material or (c) a sublimated material.

Generally speaking, it is difficult to estimate the filling rate, and this is usually achieved through **TEM** observation, without obtaining any statistics on the number of tubes observed. Moreover, as far as **SWNTs** are concerned, the fact that the nanotubes are gathered into bundles makes it difficult to observe the exact number of filled tubes, as well as to estimate the filled length for each tube. It however seems that estimation of filling rates can now be reliably obtained from X-ray studies and Raman spectroscopy.

It is also possible to fill carbon nanotubes with materials that could not have been introduced directly. This is done by first filling the nanotubes with an appropriate precursor (one that is able to sublime, or melt or solubilize) that will later be transformed into the required material by chemical reaction or by a physical interaction, such as electron beam irradiation for example [3.223]. For secondary chemical transformation, reduction by H_2 is often used to obtain nanotubes filled with metals [3.224]. Sulfides can also be obtained if H_2S is used as a reducing agent [3.224].

Because the inner diameters of **SWNTs** are generally smaller than those of **MWNTs**, it is more difficult to fill them, and the driving forces involved in this phenomenon are not yet totally understood (see the review paper by *Monthieux* [3.213]). This field is therefore growing fairly rapidly, and so we have chosen to cite the pioneering works and then to focus on more recent works dealing with the more challenging topic of filling **SWNTs**.

In Situ Filling Method

Initially, most hybrid carbon nanotubes synthesized were based on **MWNTs** prepared using the electric arc method, and were obtained directly during processing. The filling materials were easily introduced in the system by drilling a central hole in the anode and filling it with the heteroelement. The first hybrid products obtained using this approach were all reported the same year [3.225–229] for heteroelements such as Pb, Bi, YC_2 and TiC. Later on, *Loiseau et al.* [3.230] showed that **MWNTs** could also be filled to several

μm in length by elements such as Se, Sb, S, and Ge, but only with nanoparticles of elements such as Bi, B, Al and Te. Sulfur was suggested to play an important role during the in situ formation of filled MWNTs using arc discharge [3.231]. This technique is no longer the preferred one because it is difficult to control the filling ratio and yield and to achieve mass production.

Wet Chemistry Filling Method

The wet chemistry method requires that the nanotube tips are opened by chemical oxidation prior to the filling step. This is generally achieved by refluxing the nanotubes in dilute nitric acid [3.233–235], although other oxidizing liquid media may work as well, such as $[\text{HCl} + \text{CrO}_3]$ [3.236] or chlorocarbenes formed from the photolytic dissociation of CHCl_3 [3.213], a rare example of a nonacidic liquid route to opening SWNT tips. If a dissolved form (such as a salt or oxide) of the desired metal is introduced during the opening step, some of it will get inside the nanotubes. An annealing treatment (after washing and drying the treated nanotubes) may then lead to the oxide or to the metal, depending on the annealing atmosphere [3.212]. Although the wet chemistry method initially looked promising because a wide variety of materials can be introduced into nanotubes in this way and it operates at temperatures that are not much different from room temperature; however, close attention must be paid to the oxidation method that is used. The damage caused to nanotubes by severe treatments (such by using nitric acid) make them unsuitable

for use with SWNTs. Moreover, the filling yield is not very good, probably due to the solvent molecules that also enter the tube cavity: the filled lengths rarely exceed 100 nm. Mittal et al. [3.236] have recently filled SWNTs with CrO_3 using wet chemistry with an average yield of $\approx 20\%$.

Molten State Filling Method

The physical filling method involving a liquid (molten) phase is more restrictive, firstly because some materials can decompose when they melt, and secondly because the melting point must be compatible with the nanotubes, so the thermal treatment temperature should remain below the temperature of transformation or the nanotubes will be damaged. Because the filling occurs due to capillarity, the surface tension threshold of the molten material is $100\text{--}200\text{ N/cm}^2$ [3.237], although this threshold was proposed for MWNTs, whose inner diameters (5–10 nm) are generally larger than those of SWNTs (1–2 nm). In a typical filling experiment, the MWNTs are closely mixed with the desired amount of filler by gentle grinding, and the mixture is then vacuum-sealed in a silica ampoule. The ampoule is then slowly heated to a temperature above the melting point of the filler and slowly cooled. This method does not require that the nanotubes are opened prior to the heat treatment. The mechanism of nanotube opening is yet to be clearly established, but it is certainly related to the chemical reactivities of the molten materials toward carbon, and more precisely toward defects in the tube structure (see Sect. 3.4.4).

Most of the works involving the application of this method to SWNTs come from Oxford University [3.232, 238–241], although other groups have followed the same procedure [3.233, 235, 242]. The precursors used to fill the nanotubes were mainly metal halides. Although little is known about the physical properties of halides crystallized within carbon nanotubes, the crystallization of molten salts within small-diameter SWNTs has been studied in detail, and the one-dimensional crystals have been shown to interact strongly with the surrounding graphene wall. For example, Sloan et al. [3.239] described two-layer 4:4 coordinated KI crystals that formed within SWNTs that were approximately 1.4 nm in diameter. These two-layer crystals were “all surface” and had no “internal” atoms. Significant lattice distortions occurred compared to the bulk structure of KI, where the normal coordination is 6:6 (meaning that each ion is surrounded by six identical close neighbors). Indeed, the distance between two ions across the SWNT capillary is 1.4 times as much as the same distance along

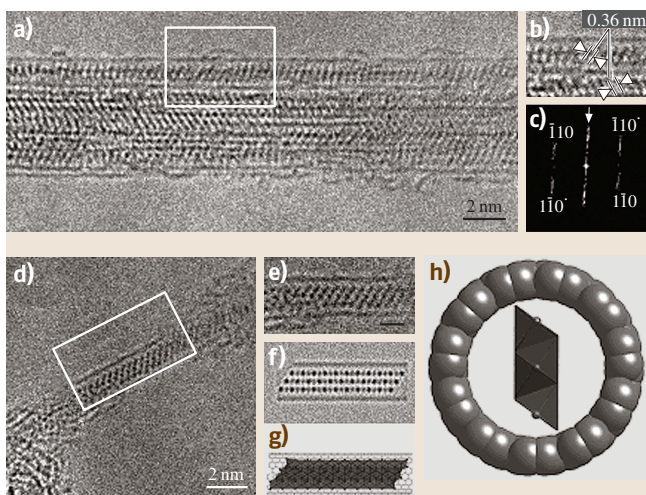


Fig. 3.24 HRTEM images and corresponding structural model for Pb_2 filled SWNTs (from [3.232])

the tube axis. This suggests an accommodation of the KI crystal into the confined space provided by the inner nanotube cavity in the constrained crystal direction (across the tube axis). This implies that the interactions between the ions and the surrounding carbon atoms are strong. The volume available within the nanotubes thus somehow controls the crystal structures of inserted materials. For instance, the structures and orientations of encapsulated PbI_2 crystals inside their capillaries were found to differ for SWNTs and DWNTs, depending on the diameter of the confining nanotubes [3.232]. For SWNTs, most of the encapsulated one-dimensional PbI_2 crystals obtained exhibited a strong preferred orientation, with their (110) planes aligning at an angle of around 60° to the SWNT axes, as shown in Fig. 3.24a and 3.24b. Due to the extremely small diameters of the nanotube capillaries, individual crystallites are often only a few polyhedral layers thick, as outlined in Fig. 3.24d to 3.24h. Due to lattice terminations enforced by capillary confinement, the edging polyhedra must be of reduced coordination, as indicated in Fig. 3.24g and 3.24h. Similar crystal growth behavior was generally observed to occur for PbI_2 formed inside DWNTs in narrow nanotubes with diameters comparable to those of SWNTs. As the diameter of the encapsulating capillary increases, however, different preferred orientations are frequently observed (Fig. 3.25). In this example, the PbI_2 crystal is oriented with the [121] direction parallel to the direction of the electron beam (Fig. 3.25a to 3.25d). If the PbI_2 @DWNT hybrid is viewed “side-on” (as indicated by the arrow in Fig. 3.25e), polyhedral slabs are seen to arrange along the capillary, oriented at an angle of around 45° with respect to the tubule axis. High-yield filling of CNTs by the capillary method is generally difficult but fillings of more than 60% have been reported for different halides, with filling lengths of up to a couple of hundreds of nm [3.243]. Results from the imaging and characterization of individual molecules and atomically thin, effectively one-dimensional crystals of rock salt and other halides encapsulated within single-walled carbon nanotubes have recently been reviewed by Sloan et al. [3.244].

Sublimation Filling Method

This method is even more restrictive than the previous one, since it is only applicable to a very limited number of compounds due to the need for the filling material to sublime within the temperature range of thermal stability of the nanotubes. Examples are therefore scarce. Actually, except for a few attempts to fill SWNTs with ZrCl_4 [3.240] or selenium [3.245], the first and most

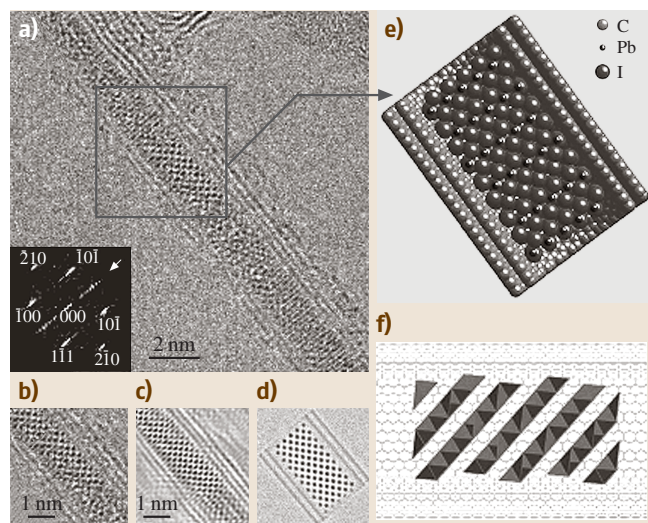


Fig. 3.25a–f HRTEM images (experimental and simulated) and corresponding structural model for a PbI_2 -filled double-wall carbon nanotube (from [3.232])

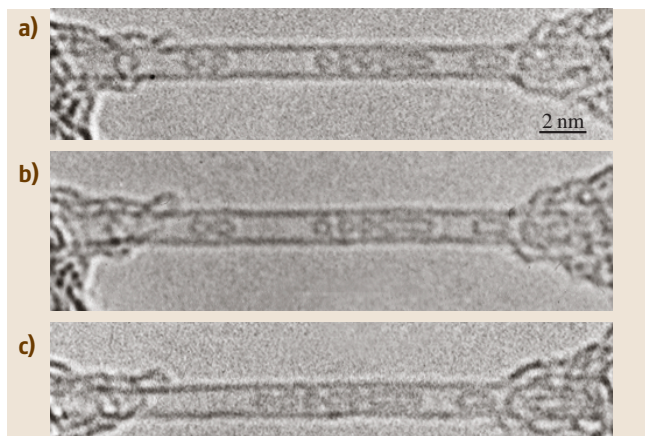


Fig. 3.26a–c HRTEM images of (a) an example of five regular C_{60} molecules encapsulated together with two higher fullerenes (C_{120} and C_{180}) as distorted capsules (on the right) within a regular 1.4 nm-diameter SWNT. (a)–(c) Example of the diffusion of the C_{60} -molecules along the SWNT cavity. The time between each image in the sequence is about 10 s. The fact that nothing occurs between (a) and (b) illustrates the randomness of the ionization events generated by the electron beam that are assumed to be responsible for the molecular displacement

successful example published so far is the formation of C_{60} @SWNT (nicknamed “peapods”), reported for the first time in 1998 [3.246], where regular ≈ 1.4 nm-large SWNTs are filled with C_{60} fullerene molecule

chains (Fig. 3.26a). Of course, the process requires that the SWNTs are opened by some method, as discussed previously; typically either acid attack [3.247] or heat treatment in air [3.248]. The opened SWNTs are then inserted into a glass tube together with fullerene powder, which is sealed and placed into a furnace heated above the sublimation temperature for fullerite ($> \approx 350^\circ\text{C}$). Since there are no filling limitations related to Laplace's law or the presence of solvent (only gaseous molecules are involved), filling efficiencies may actually reach $\approx 100\%$ for this technique [3.248].

$\text{C}_{60}@SWNT$ has since been shown to possess remarkable behavior traits, such as the ability of the C_{60} molecules to move freely within the SWNT cavity (Fig. 3.26b and 3.26c) upon random ionization effects from electron irradiation [3.249], to coalesce into 0.7 nm-wide elongated capsules upon electron irradiation [3.250], or into a 0.7 nm-wide nanotube upon subsequent thermal treatment above 1200°C under vacuum [3.249, 251]. Annealing $\text{C}_{60}@SWNT$ material could therefore be an efficient way to produce DWNTs with constant inner (≈ 0.7 nm) and outer (≈ 1.4 nm) diameters. Using the coalescence of encapsulated fullerenes through both electron irradiation and thermal treatment, it appears to be possible to control subsequent DWNT features (inner tube diameter, intertube distance) by varying the electron energy, flow and dose conditions, the temperature, and the outer tube diameter [3.252]. The smallest MWNTs have been obtained in this way.

By synthesizing “endofullerenes” [3.12], it has been possible to use this process to synthesize more complex nanotube-based hybrid materials such as $\text{La}_2@\text{C}_{80}@SWNTs$ [3.253], $\text{Gd}@\text{C}_{82}@SWNTs$ [3.254], and $\text{Er}_x\text{Sc}_{3-x}\text{N}@\text{C}_{80}@SWNT$ [3.255], among other examples. This suggests even more potential applications for peapods, although they are still speculative since the related properties are still being investigated [3.256–258].

The last example discussed here is the successful attempt to produce peapods by a related method, using accelerated fullerene ions (instead of neutral gaseous molecules) to force the fullerenes to enter the SWNT structure [3.259].

3.5.3 Functionalized Nanotubes

Noting the reactivity of carbon nanotubes (discussed in Sect. 3.4.6), nanotube functionalization reactions can be divided into two main groups. One is based on the chemical oxidation of the nanotubes (tips, structural defects) leading to carboxylic, carbonyl and/or hydroxyl

functions. These functions are then used for additional reactions, to attach oligomeric or polymeric functional entities. The second group is based on direct addition to the graphitic-like surface of the nanotubes (without any intermediate step). Examples of the latter reactions include oxidation or fluorination (an important first step for further functionalization with other organic groups). The properties and applications of functionalized nanotubes have been reviewed in [3.260].

Oxidation of Carbon Nanotubes

Carbon nanotubes are often oxidized and therefore opened before chemical functionalization in order to increase their chemical reactivity (to create dangling bonds). The chemical oxidation of nanotubes is mainly performed using either wet chemistry or gaseous oxidants such as oxygen (typically air) or CO_2 . Depending on the synthesis used, the oxidation resistance of nanotubes can vary. When oxidation is achieved using a gas phase, thermogravimetric analysis (TGA) is of great use for determining at which temperature the treatment should be applied. It is important to note that TGA accuracy increases as the heating rate diminishes, while the literature often provides TGA analyses obtained in unoptimized conditions, leading to overestimated oxidation temperatures. Differences in the presence of catalyst remnants (metals or, more rarely, oxides), the type of nanotubes used (SWNTs, c-MWNTs, h-MWNTs), the oxidizing agent used (air, O_2 is an inert gas, CO_2 , and so on), as well as the flow rate used make it difficult to compare published results. It is generally agreed, however, that amorphous carbon burns first, followed by SWNTs and then multiwall materials (shells, MWNTs), even if TGA is often unable to separate the different oxidation steps clearly. Air oxidation (static or dynamic conditions) can however be used to prepare samples of very high purity – although the yield is generally low – as monitored by in situ Raman spectroscopy [3.261]. Aqueous solutions of oxidizing reagents are often used for nanotube oxidation. The main reagent is nitric acid, either concentrated or diluted (around 3 moles per liter in most cases), but oxidants such as potassium dichromate ($\text{K}_2\text{Cr}_2\text{O}_7$), hydrogen peroxide (H_2O_2) or potassium permanganate (KMnO_4) are often used as well. HCl, like HF, does not damage nanotubes because it is not oxidizing.

Functionalization of Oxidized Carbon Nanotubes

The carboxylic groups located at the nanotube tips can be coupled to different chemical groups. Oxidized nano-

tubes are usually reacted with thionyl chloride (SOCl_2) to generate the acyl chloride, even if a direct reaction is theoretically possible with alcohols or amines, for example. The reaction of **SWNTs** with octadecylamine (ODA) was reported by *Chen et al.* [3.262] after reacting oxidized **SWNTs** with SOCl_2 . The functionalized **SWNTs** are soluble in chloroform (CHCl_3), dichloromethane (CH_2Cl_2), aromatic solvents, and carbon bisulfide (CS_2). Many other reactions between functionalized nanotubes (after reaction with SOCl_2) and amines have been reported in the literature and will not be reviewed here. Noncovalent reactions between the carboxylic groups of oxidized nanotubes and octadecylammonium ions are possible [3.263], providing solubility in tetrahydrofuran (THF) and CH_2Cl_2 . Functionalization by glucosamine using similar procedures [3.264] produced water soluble **SWNTs**, which is of special interest when considering biological applications of functionalized nanotubes. Functionalization with lipophilic and hydrophilic dendra (with long alkyl chains and oligomeric poly(ethyleneglycol) groups) has been achieved via amination and esterification reactions [3.265], leading to solubility of the functionalized nanotubes in hexane, chloroform, and water. It is interesting to note that, in the latter case, the functional groups could be removed simply by modifying the pH of the solution (base- and acid-catalyzed hydrolysis reaction conditions, [3.266]). One last example is the possible interconnection of nanotubes via chemical functionalization. This has been recently achieved by *Chiu et al.* [3.267] using the acyl chloride method and a bifunctionalized amine to link the nanotubes through the formation of amide bonds.

Sidewall Functionalization of Carbon Nanotubes

Covalent functionalization of nanotube walls is possible through fluorination reactions. It was first reported by *Mickelson et al.* [3.268], based on F_2 gas (the nanotubes can then be defluorinated, if required, with anhydrous hydrazine). As recently reviewed by *Khabashesku et al.* [3.269], it is then possible to use these fluorinated nanotubes to carry out subsequent derivatization reactions. Thus, sidewall-alkylated nanotubes can be prepared by nucleophilic substitution (Grignard synthesis or reaction with alkyllithium precursors [3.270]).

These alkyl sidewall groups can be removed by air oxidation. Electrochemical addition of aryl radicals (from the reduction of aryl diazonium salts) to nanotubes has also been reported by *Bahr et al.* [3.271]. Functionalizations of the external wall of the nanotube by cycloaddition of nitrenes, addition of nucleophilic carbenes or addition of radicals have been described by *Holzinger et al.* [3.272]. Electrophilic addition of dichlorocarbene to **SWNTs** occurs via a reaction with the deactivated double bonds in the nanotube wall [3.273]. Silanization reactions are another way to functionalize nanotubes, although only tested with **MWNTs**. *Velasco-Santos et al.* [3.274] have reacted oxidized **MWNTs** with an organosilane (RsiR_3 , where R is an organo functional group attached to silicon) and obtained nanotubes with organo functional groups attached via silanol groups.

The noncovalent sidewall functionalization of nanotubes is important because the covalent bonds are associated with changes from sp^2 hybridization to sp^3 carbon hybridization, which corresponds to loss of the graphite-like character. The physical properties of functionalized nanotubes, specifically **SWNTs**, can therefore be modified. One way to achieve the noncovalent functionalization of nanotubes is to wrap the nanotubes in a polymer [3.275], which permits solubilization (enhancing processing possibilities) while preserving the physical properties of the nanotubes. One reason to functionalize **SWNTs** is to make them soluble in regular solvents. A promising method to do this was found by *Pénicaud et al.*, who made water-soluble by adding charges to **SWNTs** via the transient and reversible formation of a nanotube salt [3.276].

Finally, it is worth bearing in mind that none of these chemical reactions are specific to nanotubes and so they can affect most of the carbonaceous impurities present in the raw materials as well, making it difficult to characterize the functionalized samples. The experiments must therefore be performed with very pure carbon nanotube samples, which is unfortunately not always the case for the results reported in the literature. On the other hand, purifying the nanotubes to start with may also bias the functionalization experiments, since purification involves chemical treatment. However a demand for such products already exists, and purified then fluorinated **SWNTs** can be bought for \$900/g (Carbon Nanotechnologies Inc., 2005).

3.6 Applications of Carbon Nanotubes

A carbon nanotube is inert, has a high aspect ratio and a high tensile strength, has low mass density, high heat conductivity, a large surface area, and a versatile electronic behavior, including high electron conductivity. However, while these are the main characteristics of individual nanotubes, many of them can form secondary structures such as ropes, fibers, papers and thin films with aligned tubes, all with their own specific properties. These properties make them ideal candidates for a large number of applications provided their cost is sufficiently low. The cost of carbon nanotubes depends strongly on both the quality and the production process. High-quality single-shell carbon nanotubes can cost 50–100 times more than gold. However, carbon nanotube synthesis is constantly improving, and sale prices are falling rapidly. The application of carbon nanotubes is therefore a very fast moving field, with new potential applications found every year, even several times per year. Therefore, creating an exhaustive list of these applications is not the aim of this section. Instead, we will cover the most important applications, and divide them up according to whether they are “current” (Sect. 3.6.1) – they are already on the market, the application is possible in the near future, or because prototypes are currently being developed by profit-based companies – or “expected” applications (Sect. 3.6.2).

3.6.1 Current Applications

Near-Field Microscope Probes

The high mechanical strength of carbon nanotubes makes them almost ideal candidates for use as force sensors in scanning probe microscopy (SPM). They provide higher durability and the ability to image surfaces with a high lateral resolution, the latter being a typical limitation of conventional force sensors (based on ceramic tips). The idea was first proposed and tested by *Dai et al.* [3.85] using c-MWNTs. It was extended to SWNTs by *Hafner et al.* [3.278], since small-diameter SWNTs were believed to give higher resolution than MWNTs due to the extremely short radius of curvature of the tube end. However, commercial nanotube-based tips (such as those made by Piezomax, Middleton, WI, USA) use MWNTs for processing convenience. It is also likely that the flexural modulus of a SWNT is too low, resulting in artifacts that affect the lateral resolution when scanning a rough surface. On the other hand, the flexural modulus of a c-MWNT is believed to increase with the number of walls, although the radius of curvature

of the tip increases at the same time. Whether based on SWNT or MWNT, such SPM tips also offer the potential to be functionalized, leading to the prospect of selective imaging based on chemical discrimination in “chemical force microscopy” (CFM). Chemical function imaging using functionalized nanotubes represents a huge step forward in CFM because the tip can be functionalized very specifically (ideally only at the very tip of the nanotube, where the reactivity is the highest), increasing the spatial resolution. The interaction between the chemical species present at the end of the nanotube tip and the surface containing chemical functions can be recorded with great sensitivity, allowing the chemical mapping of molecules [3.279, 280].

Current nanotube-based SPM tips are quite expensive; typically \approx \$450 /tip (Nanoscience Co., 2005). This high cost is due to processing difficulties (it is necessary to grow or mount a single MWNT in the appropriate direction at the tip of a regular SPM probe; Fig. 3.27), and the need to individually control the tip quality. The market for nanotube SPM tips has been estimated at \approx \$ 20 M/year.

Field Emission-Based Devices

In a pioneering work by *de Heer et al.* [3.281], carbon nanotubes were shown to be efficient field emitters and this property is currently being used several applications, including flat panel displays for television sets and computers (the first prototype of such a display was exhibited by Samsung in 1999), and devices

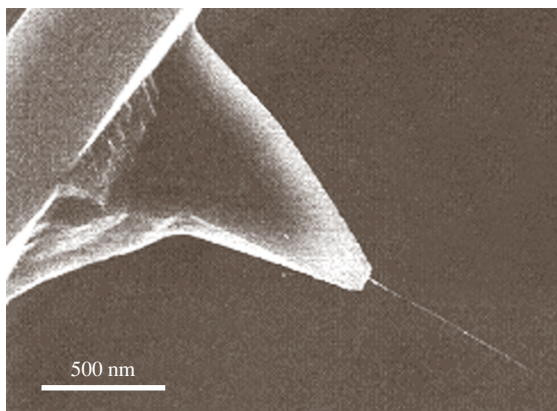


Fig. 3.27 Scanning electron microscopy image of a carbon nanotube (MWNT) mounted onto a regular ceramic tip as a probe for atomic force microscopy (modified from [3.277])

requiring an electron-producing cathode, such as X-ray sources. The principle of a field emission-based screen is demonstrated in Fig. 3.28a. Briefly, a potential difference is set up between the emitting tips and an extraction grid so that electrons are pulled from the tips onto an electron-sensitive screen layer. Replacing the glass support and protecting the screen using a polymer-based material should even permit the development of flexible screens. Unlike regular (metallic) electron-emitting tips, the structural perfection of carbon nanotubes allows higher electron emission stability, higher mechanical resistance, and longer lifetimes. Most importantly, using them saves energy since the tips operate at a lower heating temperature and require much lower threshold voltage than in other set-ups. For example, it is possible to produce a current density of 1 mA/cm^2 for a threshold voltage of $3 \text{ V}/\mu\text{m}$ with nanotubes, while it requires $20 \text{ V}/\mu\text{m}$ for graphite powder and $100 \text{ V}/\mu\text{m}$ for regular Mo or Si tips. The subsequent reductions in cost and energy consumption are estimated at 1/3 and 1/10 respectively. Generally speaking, the maximum current density that can be obtained ranges from 10^6 A/cm^2 to 10^8 A/cm^2 depending on the nanotubes involved (SWNT or MWNT, opened or capped, aligned or not, and so on) [3.282–284]. Although the side walls of the nanotubes seem to emit as well as the tips, many works have investigated the growth of nanotubes perpendicular to the substrate surface as regular arrays (Fig. 3.28b). Besides, it does not appear necessary to use SWNTs instead of MWNTs for many of these applications when they are used as bunches. On the other hand, when considering single, isolated nanotubes, SWNTs are generally less preferable since they permit much lower electron doses than MWNTs, although they often provide a more coherent source (an useful feature for devices such as electron microscopes or X-ray generators).

The market associated with this application is huge. With major companies involved, such as Motorola, NEC, NKK, Samsung, Thales and Toshiba, the first flat TV sets and computers using nanotube-based screens should enter the market in 2007 (Samsung data), once a problem with product lifetime (still only about half that required) is fixed. On the other hand, companies such as Oxford Instruments and Medirad are now commercializing miniature X-ray generators for medical applications that use nanotube-based cold cathodes developed by Applied Nanotech Inc.

Chemical Sensors

The electrical conductance of semiconductor SWNTs was recently demonstrated to be highly sensitive to

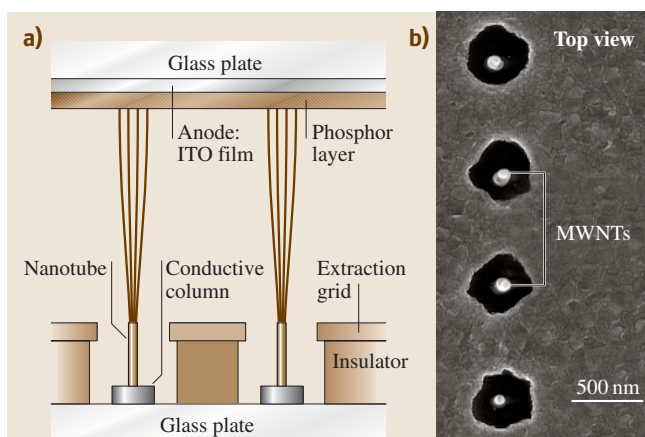


Fig. 3.28 (a) Principle of a field emitter-based screen. (b) Scanning electron microscope image of a nanotube-based emitter system (*top view*). Round dots are MWNT tips seen through the holes corresponding to the extraction grid. Courtesy of P. Legagneux (Thales Research & Technology, Orsay, France)

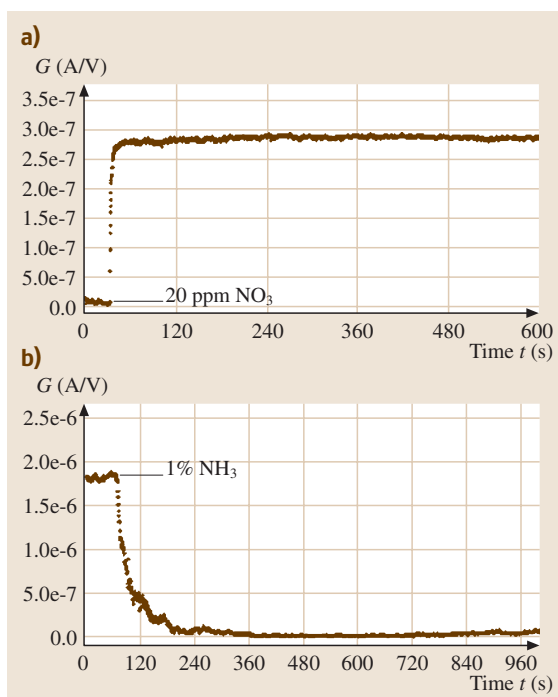


Fig. 3.29a,b Demonstration of the ability of SWNTs to detect trace molecules in inert gases. (a) Increase in the conductance of a single SWNT when 20 ppm of NO_2 are added to an argon gas flow. (b) Same, but with 1% NH_3 added to the argon gas flow (from [3.285])

changes in the chemical composition of the surrounding atmosphere at room temperature, due to charge transfer between the nanotubes and the molecules from the gases adsorbed onto **SWNT** surfaces. It has also been shown that there is a linear dependence between the concentration of the adsorbed gas and the change in electrical properties, and that the adsorption is reversible. First tries involved NO_2 or NH_3 [3.285] and O_2 [3.286]. **SWNT**-based chemical NO_2 and NH_3 sensors are characterized by extremely short response times (Fig. 3.29), unlike conventional sensors [3.285, 287]. The electrical response has been measured by exposing **MWNT** films to sub-ppm NO_2 concentrations (10–100 ppb in dry air) at different operating temperatures ranging between 25 and 215 °C [3.288]. For **SWNTs**, the sensor responses are linear for similar concentrations, with detection limits of 44 ppb for NO_2 and 262 ppb for nitrotoluene [3.289]. High sensitivity to water or ammonia vapor has been demonstrated on a **SWNT**- SiO_2 composite [3.290]. This study indicated the presence of p-type **SWNTs** dispersed among the predominantly metallic **SWNTs**, and that the chemisorption of gases on the surface of the semiconductor **SWNTs** is responsible for the sensing action. Determinations of CO_2 and O_2 concentrations on a **SWNT**- SiO_2 composite have also been reported [3.291]. By doping nanotubes with palladium nanoparticles, Kong et al. [3.292] have also shown that the modified material can reveal the presence of hydrogen at levels of up to 400 ppm, whereas the as-grown material was totally ineffective. Miniaturized gas ionization sensors, which work by fingerprinting the ionization characteristics of distinct gases, have also been reported, with detection limits of 25 ppm for NH_3 [3.293].

Generally speaking, the sensitivities of these new nanotube-based sensors are three orders of magnitude higher than those of standard solid state devices. Another reason for using nanotubes instead of current sensors is their simplicity, the facts that they can be placed in very small systems and that they can operate at room temperature, as well as their selectivity. These advantages allow a limited number of sensor device architectures to be built for a variety of industrial purposes, while the current technology requires a large variety of devices based on mixed metal oxides, optomechanics, catalytic beads, electrochemistry, and so on. The market for such devices is expected to be \$ 1.6 billion by 2006, including sensing applications in biological fields and the chemical industry. Nanotube-based sensors are currently being developed by large and small companies, such as Nanomix (Emeryville, CA, USA), for example.

Catalyst Support

Carbon-based materials make good supports in heterogeneous catalytic processes due to their ability to be tailored to a specific need: indeed, activated carbons are already currently employed as catalyst supports due to their high surface areas, their stability at high temperatures (under nonoxidizing atmospheres), and the possibility of controlling both their porous structure and the chemical nature of their surfaces [3.294, 295]. Attention has focused on nanosized fibrous morphologies of carbon have appeared over the last decade, that show great potential for use as supports [3.296]. Carbon nanofibers (also incorrectly called graphite nanofibers) and carbon nanotubes have been successfully used in this area, and have been shown to provide, as catalyst-supporting materials, properties superior to those of such other regular catalyst-supports, such as activated carbon, soot or graphite [3.297–299]. Various reactions have been studied [3.297–299]; hydrogenation reactions, hydrocarbon decomposition and use as fuel cell electrocatalysts are among the most popular domains. The application of graphite nanofibers as direct catalysts for oxidative dehydrogenation [3.300, 301] or methane decomposition [3.302] has also been reported.

The morphology and size of the carbon nanotubes (particularly their aspect ratios), can play a significant role in catalytic applications due to their ability to disperse catalytically active metal particles. Their electronic properties are also of primary importance [3.303], since the conductive support may cause electronic perturbations as well as constraining the geometries of the dispersed metal particles. A recent comparison between the interactions of transition metal atoms with carbon nanotube walls and their interactions with graphite has shown major differences in bonding sites, magnetic moments, and charge transfer direction [3.304]. Thus the possibility of a strong metal–support interaction must be taken into account. Their mechanical strength is also important, and this makes them resistant to attrition when recycled. Their external and internal surfaces are strongly hydrophobic and adsorb organic molecules strongly. For **MWNT**-based catalyst-supports, the relatively high surface area and the absence of microporosity (pores < 2 nm), associated with a high meso- and macropore volume (see Sect. 3.4.3), result in significant improvements in catalytic activity for liquid phase reactions when compared to catalysts supported on activated carbon. With nanotube supports, the mass transfer of the reactants to the active sites is unlimited, due to the absence of microporosity, and the apparent contact time of the products with the catalyst is dimin-

Table 3.4 Preparation and catalytic performances of some nanotube-supported catalysts

Catalyst	Preparation route	Catalytic reaction	Comments
Ru/MWNT+SWNT [3.296]	Liquid phase impregnation, no pretreatment of the tubes	Liquid phase cinnamaldehyde hydrogenation	A different kind of metal support interaction compared to activated carbon
Pt/MWNT electrodes [3.305]	Electrodeless plating with prefunctionalization of MWNT	Oxygen reduction for fuel cell applications	High electrocatalytic activity
Rh/MWNT [3.306]	Surface-mediated organometallic synthesis, prefunctionalization of MWNT	Liquid phase hydroformylation and hydrogenation	Higher activity of Rh/MWNT compared to Rh/activated carbon
Ru-alkali/MWNT [3.307]	Liquid phase impregnation, no pretreatment of the tubes	Ammonia synthesis, gas phase reaction	Higher activity with MWNT than with graphite
Rh-phosphine/MWNT [3.308]	Liquid phase grafting from [RhH(CO)(PPh ₃) ₃]	Liquid phase hydroformylation	Highly active and regioselective catalyst

ished, leading to more active and more selective catalytic effects. Finally, as for activated carbon, catalyst-forming is possible and porous granules of carbon nanotubes or electrodes based on carbon nanotubes can be obtained for catalysis or electrocatalysis respectively.



Fig. 3.30 Transmission electron microscopy image showing rhodium nanoparticles supported on the surface of an MWNT (from [3.306])

The technique usually used to prepare carbon nanotube-supported catalysts is incipient wetness impregnation, in which the purified support is impregnated with a solution of the metal precursor and then dried, calcinated and/or reduced in order to obtain metal particles dispersed on the support. Chemical treatment and/or modification of the carbon nanotube surface were found to be useful ways of controlling its hydrophobic or hydrophilic character [3.309]. A strong metal/support interaction can thus be expected from the occurrence of functionalized groups created by the oxidation of the support surface, resulting in smaller particle sizes [3.310]. A more sophisticated technique for achieving the grafting of metal particles onto carbon nanotubes consists of functionalizing the outer surface of the tubes and then performing a chemical reaction with a metal complex, resulting in a good dispersion of the metallic particles (Fig. 3.30) [3.306]. The functionalization of noncovalent carbon nanotubes with polymer multilayers followed by the attachment of gold nanoparticles has also been reported [3.311].

Selected examples of some carbon nanotube-based catalysts together with related preparation routes and catalytic activities are listed in Table 3.4.

The market is important for this application, since it often concerns the heavy chemical industry. It implies and requires mass production of low-cost nanotubes, processed by methods other than those based on solid carbon as the source (see Sect. 3.2.1). Such an application also requires some surface reactivity, making the h-MWNT-type nanotubes, with poor nanotextures (see Sect. 3.1.2), the most suitable starting material for preparing such catalyst supports. Catalysis-enhanced

thermal cracking of gaseous carbon precursors is therefore preferred, and pilot plants are already being built by major chemical industrial companies (such as Arkema in France).

3.6.2 Expected Applications Related to Adsorption

Adsorptions of various gases, liquids or metals onto carbon nanotubes, and interactions between them, have attracted much attention recently. The applications resulting from the adsorptive properties of carbon nanotubes can be arbitrarily divided into two groups. The first group is based on the consequences of molecular adsorption on the electronic properties of nanotubes; the main application of this is chemical sensing (see Sect. 3.6.1). The second group includes gas storage, gas separation, the use of carbon nanotubes as adsorbants, and results from morphological investigations of carbon nanotubes (surface areas, aspect ratios, and so forth). Among these latter potential applications, the possibility of storing gases – particularly hydrogen – on carbon nanotubes has received most attention.

Gas Storage – Hydrogen

The development of a lightweight and safe system for hydrogen storage is necessary for the widespread use of highly efficient H₂-air fuel cells in transportation vehicles. The U.S. Department of Energy Hydrogen Plan has provided a commercially significant benchmark for the amount of reversible hydrogen adsorption required. This benchmark requires a system weight efficiency (the ratio of H₂ weight to system weight) of 6.5 wt% hydrogen, and a volumetric density of 63 kg H₂/m³.

The failure to produce a practical storage system for hydrogen has prevented hydrogen from becoming one of the most important transportation fuels. The ideal hydrogen storage system needs to be light, compact, relatively inexpensive, safe, easy to use, and reusable without the need for regeneration. While research and development are continuing into such technologies as liquid hydrogen systems, compressed hydrogen systems, metal hydride systems, and superactivated carbon systems, all have serious disadvantages. For example, liquid hydrogen systems are very expensive, primarily because the hydrogen must be cooled to about -252 °C. This means that a liquid hydrogen system costs about four times as much as an equivalent amount of gasoline. Also, liquid hydrogen must be kept cooled to prevent it from boiling away, even when the vehicle is parked. Compressed hydrogen is

much cheaper than liquid hydrogen, but also much bulkier.

Metal hydride systems store hydrogen as a solid in combination with other materials. For example, metal hydrides are produced by bathing a metal, such as palladium or magnesium, in hydrogen. The metal splits the dihydrogen gas molecules and binds the hydrogen atoms to the metal until released by heating. The disadvantages of a metal hydride system are its weight (typically about eight times more than an equivalent amount of liquid hydrogen or gasoline) and the need to warm it up to release the hydrogen.

Superactivated carbon provides the basis of another system for storing hydrogen that initially showed commercial potential. Superactivated carbon is a material similar to the highly porous activated carbon used in water filters but that can gently adsorb hydrogen molecules through physisorption at subzero temperatures. The colder the carbon, the less heat is needed to disturb the weak forces holding the carbon and hydrogen together. Therefore, again, a major disadvantage of such a system is that it must constantly remain at very low temperatures to stop the hydrogen from escaping, even when the vehicle is parked.

Therefore, there is still a great need for a material that can store hydrogen but is also light, compact, relatively inexpensive, safe, easy to use, and reusable without regeneration. Some recent articles and patents on the very high, reversible adsorption of hydrogen in carbon nanotubes or platelet nanofibers have aroused tremendous interest in the research community, stimulating much experimental and theoretical work. Most of the work done on hydrogen adsorption on carbon nanotubes have been recently reviewed [3.312–317].

A group from Northeastern University [3.176, 318] was the first to report the supposedly successful storage of hydrogen in carbon layered nanostructures possessing some crystallinity. The authors claimed that up to 75 wt % of hydrogen (a C/H ratio of 1/9) can be stored in platelet nanofibers (3–50 nm in width). Complete hydrogen desorption occurs only at very high temperature. However, the same authors recently pointed out the need for the carbon nanofibers to be thermally treated prior to H₂ adsorption [3.318]. This thermal treatment, although simple (1000 °C in an inert gas), is critical for removing chemisorbed gases from the edge and step regions of the carbon structures. Failure to perform this treatment results in a dramatic decrease in the hydrogen adsorption of the material. The authors also performed the experiments at room temperature, and hydrogen uptakes of 20 to 40 wt % were recorded for 100 bar of H₂. The au-

thors also demonstrated (by XRD) that the material was structurally perturbed following hydrogen treatment, as demonstrated by an expansion of the graphitic interplane distance (from 0.34 before H₂ adsorption to 0.347 after H₂ uptake). Another study also underlined the key role played by the structure (tubular or herringbone) and the in situ pretreatment of the material in oxidizing, reducing or neutral environments [3.319]. The presence of residual catalyst in the sample also needs to be taken into account, as it can produce hydrogen spillover [3.320].

Hydrogen adsorption and desorption measurements on nanofibers similar to those used by *Rodriguez et al.* [3.16] were also performed by *Ahn et al.* [3.321]. The authors measured a hydrogen uptake of 2.4 wt %. In fact, in their study, none of the graphite nanofiber material tested gave hydrogen storage abilities above the values already reported for activated carbons.

The adsorption of H₂ onto platelet nanofibers was computed via Monte Carlo simulations [3.322]. The graphene spacing was optimized to maximize the weight fraction of H₂ adsorbed. Given the results of their calculations, the authors concluded that no physically realistic graphite–hydrogen potential can account for the tremendous adsorption ability reported by the group from Penn State.

Rzepka et al. [3.323] have also used theoretical Monte Carlo calculations to calculate the amount of physically adsorbed hydrogen molecules in carbon slit pores with dimensions similar to those used by the Penn State group (an interplanar distance between the graphenes in the nanofibers of 0.34 nm). They reached the conclusion that no hydrogen could be adsorbed at all. Even if the interplanar distance is assumed to expand during the adsorption process, the maximum calculated adsorption is 1 wt % for $d = 0.7$ nm. These authors concluded that the Penn State experimental results could not be attributed to some “abnormal capillary condensation effect” as initially claimed. Since then, nobody has been able to duplicate the results from those first experiments.

Meanwhile, hydrogen storage experiments were also attempted on SWNTs. The first work was reported by *Dillon et al.* [3.324], who used temperature-programmed desorption measurements. A major drawback of their experimental procedure was that they used only 1 mg of *unpurified* soot containing 0.1% of SWNTs. They attributed the reversible hydrogen capacity of 0.01 wt % observed to the SWNTs alone, giving a presumed capacity of 5–10 wt % for a pure sample of nanotubes. TPD experiments indicated that H₂ desorption occurred between –170 and +100 °C. Despite the weakness of the demonstration, the paper, which was not published

not long before that of *Chambers et al.* [3.176], induced worldwide excitement in the field. Hydrogen adsorption studies based on ¹H and ²H NMR spectroscopy have revealed that adsorption is fast and reversible and must be described as physisorption [3.325].

Hydrogen adsorption measurements were also performed on SWNT samples of high purity [3.326]. At –193 °C, 160 bar of H₂ were admitted and the hydrogen adsorption was found to exceed 8 wt %. In this case, the authors proposed that hydrogen is initially adsorbed on the outer surfaces of the crystalline material. However, no data on H₂ desorption were given.

In other reports, *Dresselhaus* and coworkers [3.312, 327] reported hydrogen storage in SWNTs (average diameter 1.85 nm) at room temperature. A hydrogen storage capacity of 4.2 wt % was achieved reproducibly at 100 bar for about 0.5 g of a SWNT-containing material that had been previously soaked in hydrochloric acid and then heat-treated (500 °C) in vacuum. The purity of the sample was estimated from TGA and TEM observations to be about 50 to 60%. Moreover, 78% of the adsorbed hydrogen could be released under ambient pressure at room temperature, while releasing the residual stored hydrogen required some heating at 200 °C.

Valuable input to the topic was provided by *Hirscher et al.* [3.328], who demonstrated that several of the supposedly successful experiments regarding the storage of H₂ in SWNTs were actually misled by the hydrogen storage capacity of Ti nanoparticles originating from the sonoprobe frequently used at one step or another of the procedure, specifically when the SWNT material is purified beforehand. Since then, studies on hydrogen adsorption in SWNTs have reported regularly lower values, ranging between 0.5 and 1.2 wt % at 77 K and atmospheric pressure [3.329–331]. Furthermore, no significant difference has been found by neutron scattering between the hydrogen molecules adsorbed in nanotubes, fibers and coals [3.329]. Hydrogen adsorption has been measured at 0.3 wt % for MWNTs samples as large as 85 g at 300 K and 10 MPa, while 2.27 wt % hydrogen was released at 77 K by nitric acid treated MWNTs [3.332].

Density functional theory (DFT) was used [3.333] to estimate H₂ adsorption in SWNTs. From their calculations, within the regime of operating conditions where adsorptive storage seems attractive, the storage properties of H₂ in a SWNT system appear to fall far short of the DOE target. In their model, rolling graphite into a cylindrical sheet does not significantly alter the nature of the carbon–H₂ interaction, contradicting the

latest calculations, which indicate that the physisorption increases as the radius of curvature of the SWNT decreases [3.334].

However, Lee et al. [3.335–337] have also used DFT calculations to search for hydrogen adsorption sites and to predict the maximum storage capacity of SWNTs. They found two chemisorption sites: at the exterior and the interior of the tube wall. Thus, they predict that the maximum hydrogen storage capacity could exceed 14 wt % (160 kg H₂/m³). The authors have also considered H₂ adsorption in multiwall carbon nanotubes and have predicted lower storage capacities for the latter. At 77 K and 4 MPa, DFT calculations predict a total excess gravimetric storage capacity of hydrogen of 7.1 wt % for open 2.719 nm nanotube arrays and 9.5 wt % for open isolated 2.719 nm nanotubes [3.338]. However, at 300 K, the total excess adsorption of hydrogen on both carbon nanotube arrays and isolated nanotubes does not exceed 1 wt %.

These calculations are constrained, however, by the starting hypotheses. While considering the same (10,10) SWNT, calculations based on DFT predict between 14.3% and 1 wt % storage [3.336, 338], calculations based on a geometrical model predict 3.3% [3.312], and calculations based on a quantum mechanical molecular dynamics model predict 0.47% [3.339].

In conclusion, neither experimental results, obviously biased by some problem in the procedures, nor theoretical results are yet able to demonstrate that an efficient storage of H₂ is possible for carbon nanotubes, whatever the type. However, a definitive statement of failure cannot yet be claimed. Further efforts have to be made to enhance the quality of these materials, in particular (i) by adjusting the surface properties, which can be modified by chemical or mechanical treatments, and (ii) by adjusting the structure of the material, such as the pore size [3.340] and possibly the curvature. Whether the best carbon material for H₂ adsorption will then be nanotube-based is another story.

Gas Storage – Gases Other than Hydrogen

Encouraged by the potential applications related to hydrogen adsorption, several research groups have tried to use carbon nanotubes as a means of stocking and transporting other gases such as oxygen, nitrogen, noble gases (argon and xenon) and hydrocarbons (methane, ethane, and ethylene). These studies have shown that carbon nanotubes could become the world's smallest gas cylinders, combining low weight, easy transportability and safe use with acceptable adsorbed quantities. Nanotubes may also be used in medicine, where it would

be extremely useful to physically confine special gases (¹³³Xe for instance) prior to injection.

Kusnetzova et al. [3.341] conducted experiments with xenon and found that the storage capacities of nanotubes can be enhanced by a tremendous amount (a factor of 280, up to a molar ratio of $N_{\text{Xe}}/N_{\text{C}} = 0.045$) by opening the SWNT bundles via thermal activation at 800 °C. The gas can be adsorbed inside the nanotubes and the rates of adsorption are also increased using this treatment.

The possibility of storing argon in carbon nanotubes has been studied, with encouraging results, by Gadd et al. [3.342]. Their experiments show that large amounts of argon can be trapped in catalytically grown MWNTs (20–150 nm) by hot isostatic pressing (HIP-ing) for 48 hours at 650 °C under an argon pressure of 1700 bar. Energy-dispersive X-ray spectroscopy was used to determine that the gas was located inside the tubes and not on the tube walls. Further studies determined the argon pressure inside the tubes at room temperature. The authors estimated this to be around 600 bars, indicating that equilibrium pressure was attained in the tubes during the HIP-ing and that MWNTs would be a convenient material for storing the gas.

Gas Separation

As SWNTs or MWNTs have regular geometries that can, to some extent, be controlled, they could be used to develop precise separation tools. If the sorption mechanisms are known, it should be possible to control sorption of various gases through particular combinations of temperature, pressure and nanotube morphology. Since the large-scale production of nanotubes is gradually progressing, and this should ultimately result in low costs, accurate separation methods based on carbon nanotubes are now being investigated.

A theoretical study has aimed to determine the effects of different factors such as tube diameter, density and type of the gas used on the flow of molecules inside nanotubes. An atomistic simulation with methane, ethane and ethylene [3.343] has shown that the molecular mobility decreases with decreasing tube for each of the three gases. Ethane and ethylene have smaller mobilities due to the stronger interactions they seem to have with the nanotube walls. In another theoretical study into the possibility of hydrocarbon mixture separation on SWNT bundles, the authors conclude that carbon nanotubes can be used to separate methane/*n*-butane and methane/isobutene mixtures [3.344] with an efficiency that increases as the average tube diameter decreases. Experimental work was also performed by the same

group on the sorption of butane on MWNTs [3.178]. It has been also reported that the Fickian diffusivities of CH₄/H₂ mixtures in SWNT, like their pure component counterparts, are extraordinarily large when compared with adsorbed gases in other nanoporous materials [3.345].

Grand canonical Monte Carlo simulations of the separation of hydrogen and carbon monoxide by adsorption on SWNTs have also been reported [3.346]. In most of the situations studied, SWNTs were found to adsorb more CO than H₂, and excellent separation could again probably be obtained by varying the SWNT average diameter.

Adsorbents

Carbon nanotubes were found to be able to adsorb some toxic gases such as dioxins [3.347], fluoride [3.348], lead [3.349] and alcohols [3.350] better than adsorbent materials in common use, such as activated carbon. These pioneering works opened a new field of applications as cleaning filters for many industrial processes with hazardous by-products. The adsorption of dioxins, which are very common and persistent carcinogenic by-products of many industrial processes, is a good example of the potential of nanotubes in this field. Growing ecological awareness has resulted in the imposition of emission limits on dioxin-generating sources in many countries, but it is difficult to find materials that can act as effective filters, even at extremely low concentrations. Long et al. [3.347] found that nanotubes can attract and trap more dioxins than activated carbons or other polyaromatic materials that are currently used as filters. This improvement is probably due to the stronger interaction forces that exist between dioxin molecules and the curved surfaces of nanotubes compared to those for flat graphene sheets.

The capacity of Al₂O₃/MWNT to adsorb fluoride from water has been reported to be 13.5 times that of activated carbon and four times that of Al₂O₃ [3.348]. The same group has also reported a capacity of MWNTs to adsorb lead from water that is higher than that for activated carbon [3.349]. The possibility of using graphite nanofibers to purify water from alcohols has also been explored [3.350]. MWNTs were found to be good adsorbents for the removal of dichlorobenzene from wastewaters over a wide range of pH. Typically, the nanotubes adsorb 30 mg of the organic molecule per gram of MWNTs from a 20 mg/l solution [3.351]. It has also been shown that SWNTs act as molecular sponges for molecules such as CCl₄; the nanotubes were in contact with a support sur-

face which also adsorbs molecules, although more weakly than the nanotubes [3.352]. These experimental results suggest that carbon nanotubes may be promising adsorbents for removing polluting agents from water.

Biosensors

Attaching molecules of biological interest to carbon nanotubes is an excellent way to produce nanometer-sized biosensors. The electrical conductivities of these functionalized nanotubes would depend on the interaction of the probe with the medium being studied, which would be affected by chemical changes or interactions with the target species. The science of attaching biomolecules to nanotubes is rather recent and was inspired by similar research in the fullerene area. Some results have already been patented, and so such systems may become available in the near future. Using the internal cavities of nanotubes to deliver drugs would be another amazing application, but little work has been carried out so far to investigate the toxicity of nanotubes in the human body. Comparison between the effects of nanotubes and asbestos was investigated by Huczko et al. [3.353] and they concluded that the tested samples were innocuous. However, a more recent work has shown that contact with nanotubes may lead to dermal toxicity [3.354] or induce lung lesions characterized by the presence of granulomas [3.355]. Pantarotto et al. [3.356] reported the translocation of water-soluble SWNT derivatives across cell membranes and have shown that cell death can be induced by functionalised nanotubes (bioactive peptides), depending upon their concentration in the media. Recent results also indicate that nanotubes may lead to an inflammatory response of the immune system by activating the complement system [3.357].

MWNTs have been used by Mattson et al. [3.358] as a substrate for neuronal growth. They have compared the activity of untreated MWNTs with that of MWNTs coated with a bioactive molecule (4-hydroxynonenal) and observed that neurons elaborated multiple neurites on these latter functionalized nanotubes. This is an important result that illustrates the feasibility of using nanotubes as a substrate for nerve cell growth.

Davis et al. [3.359] immobilized different proteins (metallothionein, cytochrome c and c₃, β-lactamase I) in MWNTs and checked whether these molecules were still catalytically active compared to the free ones. They have shown that confining a protein within a nanotube provides some protection for the external environment. Protein immobilization via noncovalent sidewall func-

tionalization was proposed by *Chen et al.* [3.360] using a bifunctional molecule (1-pyrenebutanoic acid, succinimidyl ester). This molecule is tied to the nanotube wall by the pyrenyl group, and amine groups or biological molecules can react with the ester function to form amide bonds. This method was also used to immobilize ferritin and streptavidin onto SWNTs. Its main advantages are that it does not modify the SWNT wall and that it does not perturb the sp^2 structure, so the physical properties of the nanotubes are maintained. *Shim et al.* [3.361] have functionalized SWNTs with biotin and observed specific binding with streptavidin, suggesting biomolecular recognition possibilities. *Dwyer et al.* [3.362] have functionalized SWNTs by covalently coupling DNA strands to them using EDC(1-ethyl-3-(3-dimethylaminopropyl) carbodiimide hydrochloride) but did not test biomolecular recognition; other proteins such as bovine serum albumin (BSA) [3.363] have been attached to nanotubes using the same process (diimide-activated amidation with EDC) and most of the attached proteins remained bioactive. Instead of working with individual nanotubes (or more likely nanotube bundles in the case of SWNTs), *Nguyen et al.* [3.364] have functionalized nanotubes arrayed with a nucleic acid, still using EDC as the coupling agent, in order to realize biosensors based on protein-functionalized nanotubes. *Azamian et al.* [3.365] have immobilized a series of biomolecules (cytochrome c, ferritin, and glucose oxidase) on SWNTs, and they observed that the use of EDC was not always necessary, indicating that the binding was predominantly noncovalent. In the case of glucose oxidase, they tested the catalytic activity of functionalized nanotubes immobilized on a glassy carbon electrode and observed a tenfold greater catalytic response compared to that seen in the absence of modified SWNTs.

Functionalization of nanotubes with biomolecules is still in its infancy, and their use as biosensors may lead to practical applications earlier than expected. For example, functionalized nanotubes can be used as AFM tips (see Sect. 3.6.1), allowing single-molecule measurements to be taken using “chemical force microscopy” (CFM). Important improvements in the characterization of biomolecules have even been achieved with unfunctionalized nanotube-based tips (see the review by [3.278]). Nanotube-based biosensors have now been developed. They are based on either field effect transistors [3.366] involving functionalized CNTs (biomolecules) or on electrochemical detection [3.367].

3.6.3 Expected Applications Related to Composite Systems

Because of their exceptional morphological, electrical, thermal, and mechanical characteristics, carbon nanotubes make particularly promising reinforcement materials in composites with metals, ceramics or polymer matrices. Key issues to address include the good dispersion of the nanotubes, the control of the nanotube/matrix bonding, the densification of bulk composites and thin films, and the possibility of aligning the nanotubes. In addition, the nanotube type (SWNT, c-MWNT, h-MWNT, etc.) and origin (arc, laser, CCVD, etc.) are also important variables that help determine the structural perfection, surface reactivity and aspect ratio of the reinforcement.

The application of carbon nanotubes in this field is expected to lead to major advances in composites. The following sections will give overviews of current work on metal-, ceramic- and polymer-matrix composites containing nanotubes. Nanotubes coated with another material are not considered here. Filled nanotubes are discussed in Sect. 3.5.2.

Metal Matrix Composites

Nanotube-metal matrix composites are still rarely studied. Matrices include Al-, Cu-, Mg-, Ni-, Ni-P-, Ti-, WC-Co- and Zr-based bulk metallic glasses. The materials are generally prepared by standard powder metallurgy techniques, but in this case the nanotube dispersion is not optimal. Other techniques such as plasma spray forming [3.368], the so-called nanoscale-dispersion method [3.369] and the rapid solidification technique [3.370] have also been developed. The spark plasma sintering (SPS) technique is sometimes used to densify the composites whilst avoiding matrix-grain growth [3.371, 372]. The room-temperature electrical resistivity of hot-pressed CCVD MWNT-Al composites increases slightly upon increasing the MWNT volume fraction [3.373]. The tensile strengths and elongations of unpurified arc discharge MWNT-Al composites are only slightly affected by annealing at 873 K in contrast to those of pure Al [3.374]. The Young’s modulus of nonpurified arc discharge MWNTs-Ti composite is about 1.7 times that of pure Ti [3.375]. The formation of TiC, probably resulting from a reaction between amorphous carbon and the matrix, was observed, but the MWNTs themselves were not damaged. An increase in the Vickers hardness by a factor of 5.5 over that of pure Ti was associated with the suppression of coarsening of the Ti grains, TiC formation, and

the addition of MWNTs. Purified nanotube-WC-Co nanocomposites exhibit better hardness-to-toughness relationships than pure nanocrystalline WC-Co [3.372]. MWNT-Mg composites show a higher tensile strength (+150%) and elongation ratio (+30%) than Mg [3.376]. Ni-plated MWNTs give better results than unplated MWNTs in strength tests. Indeed, nanotube coating is a promising way to improve the strength of bonding with the matrix [3.377]. Compressive testing of carbon nanotube-reinforced Zr-based bulk metallic glass composites [3.378] shows that the composites display a high fracture strength. In addition, the composites have strong ultrasonic attenuation characteristics and excellent ability to absorb waves. This implies that such composites may also be useful for shielding acoustic sound or environmental noise. CCVD MWNTs-Cu composites [3.379] also show a higher hardness and a lower friction coefficient and wear loss. Fifty to sixty percent deformation of the composites was observed. Carbon nanotube-Cu composite electrodes have been applied to the amperometric detection of carbohydrates, where they show an enhanced sensitivity compared to detectors based on Cu or nanotubes alone [3.380]. Composite films and coatings on various substrates have also been studied. The addition of up to 15 vol % purified SWNTs to nanocrystalline Al films reduces the coefficient of thermal expansion by as much as 65% and the resulting material could be a promising electronic packaging material [3.381]. Ni-carbon nanotube coatings deposited on carbon steel show significantly increased resistance to corrosion [3.382]. Ni-carbon nanotube coatings with a Zn-Ni interlayer electrodeposited on an Al substrate show an improved wear resistance at lower applied loads. The friction coefficient of the composite coatings decreases with increasing volume fraction of nanotubes due to the reinforcement and self-lubrication of the nanotubes [3.383]. Ni-P-SWNT coatings prepared by electroless plating show not only higher wear resistance but also a lower friction coefficient and a higher corrosion resistance compared to Ni-P coatings [3.384].

Ceramic Matrix Composites

Carbon nanotube-containing ceramic matrix composites have been studied more frequently than their metal matrix equivalents. Much of the effort has focused on obtaining tougher ceramics [3.385]. Composites can be processed using the regular processing route, where the nanotubes are usually mechanically dry- or wet-mixed with the matrix (or a matrix precursor) and then densified using hot-pressing sintering. Zhan et al. [3.386]

ball-milled SWNT bundles (from the HiPCo technique) and nanometric alumina powders, producing a fairly homogeneous dispersion, supposedly without damaging the SWNTs. Like Sun et al. [3.387], they used the SPS technique to prepare fully dense composites without damaging the SWNTs. Ning et al. succeeded in improving the homogeneity of the dispersion of MWNTs in the SiO₂ matrix using surfactants [3.388]. Other original composite processing techniques include the sol-gel route by which bulk and thin film composites were prepared [3.389], and in situ SWNT growth in ceramic foams, using procedures closely related to those described in Sect. 3.2.2 [3.390].

Ma et al. [3.391] prepared MWNT-SiC composites by hot-pressing mixtures of CCVD MWNTs and nano-SiC powders, but the dispersion of the MWNTs looked poor. They claimed that the presence of the MWNTs produces an increase of about 10% in both the bending strength and fracture toughness. Siegel et al. [3.392] claimed that the fracture toughness of 10 vol % MWNT-alumina hot-pressed composites is increased by 24% (to 4.2 MPa m^{1/2}) over that of pure alumina. However, the density and grain size are not reported, so it is difficult to consider this result to be evidence for the beneficial role of the MWNTs themselves. A confirmation can be found in the work by Sun et al. [3.387], who developed a colloidal route to coating the nanotubes with alumina particles prior to another mixing step with alumina particles and then densification by SPS. A gain in fracture toughness (calculated from Vickers indentation) is reported (from 3.7 MPa m^{1/2} for pure Al₂O₃ to 4.9 MPa m^{1/2} for an addition of 0.1 wt % of SWNT nanotubes, but it is possible that the beneficial input of the nanotubes is due to the previous coating of the nanotubes before sintering, resulting in improved bonding with the matrix. Zhan et al. [3.386] also used Vickers indentations to determine that the fracture toughness of SWNT-Al₂O₃ composites would be enhanced from 3.3 MPa m^{1/2} for Al₂O₃ to 9.7 MPa m^{1/2} (for 10 vol % CNTs). However, these results were refuted by Wang et al. [3.393] who reported that CNT-alumina composites are highly contact damage-resistant and showed that the fracture toughness of such composites can be strongly overestimated when measured by the standard indentation method [3.386]. Several detailed studies [3.89, 394–397] have dealt with the preparation of nanotube-Fe-Al₂O₃, nanotube-Co-MgO, and nanotube-Fe/Co-MgAl₂O₄ composites by hot-pressing the corresponding composite powders. The nanotubes were grown in situ in the starting powders by a CCVD method [3.65, 81, 398–402] and are

therefore very homogeneously dispersed between the metal oxide grains, in a way that may be impossible to achieve by mechanical mixing. The nanotubes (mostly SWNTs and DWNTs) gather in long, branched bundles smaller than 50 nm in diameter, which appear to be very flexible. Depending on the matrix and hot-pressing temperature, a fraction of the nanotubes seems to be destroyed during hot-pressing in a primary vacuum. Increasing the quantity of nanotubes (of approximately 2–12 wt %) leads to a refinement of the microstructure but also to a strong decrease in relative density (70–93%). Peigney et al. [3.403] showed that, during hot-pressing of nanotube-Fe/Co-MgAl₂O₄ composites, nanotubes do influence the rearrangement step, being favorable to this process at low contents, but detrimental at higher contents because they form a web structure that is too rigid. Moreover, nanotubes are detrimental to the plastic flow controlled by a Nabarro–Herring dislocation creep. Probably because of the insufficient densification, the fracture strength and the toughness of the nanotube-containing composites are generally lower than those of the nanotube-free metal-oxide composites and only marginally higher than those of the corresponding ceramics. SEM observations revealed both the trapping of some of the nanotubes within the matrix grains or at grain boundaries and a relatively good wetting in the case of alumina. Most nanotubes are cut near the fracture surface after some pull-out and could contribute to mechanical reinforcement. Xia et al. [3.404] reported microstructural investigations on MWNTs well-aligned in the pores of an alumina membrane. Different possible reinforcement mechanisms induced by the MWNTs have been evidenced, such as crack deflection, crack bridging, MWNT pullout, and MWNT collapse in shear bands. Indeed, although neither the SENB nor the SEVNB results have shown that nanotubes can significantly reinforce alumina ceramics so far, this could be obtained with ceramic-matrix composites in which the nanotubes have been properly organized.

Bulk properties other than mechanical properties are also being investigated. Interestingly, the presence of well-dispersed nanotubes confers an electrical conductivity to the otherwise insulating ceramic-matrix composites. Rul et al. [3.405] showed that the percolation threshold of SWNT in an MgAl₂O₄ matrix was very low ($p_c = 0.64$ vol %) due to the very high aspect ratio of the nanotubes, and that the DC electrical conductivity was well fitted by the scaling law of percolation theory $\sigma = \sigma_0(p - p_c)^t$ with $t = 1.73$, close to the theoretical value ($t = 1.94$) characteristic of a three-

dimensional network. This work also showed that the electrical conductivities of such composites can be tailored over a wide scale (10^{-2} – 10 S.cm⁻¹) using the nanotube content.

Moreover, extrusion at high temperatures in vacuum allows the nanotubes to be aligned in the matrix, thus inducing an anisotropy in the electrical conductivity [3.406]. Zhan et al. [3.407] measured DC electrical conductivities of up to 33.45 S.cm⁻¹ in Al₂O₃-based composites containing ropes of SWNTs. Huang et al. [3.408] densified MWNT-BaTiO₃ composites and showed that their electrical conductivities decreased when the nanotube content was increased. This phenomenon has been attributed to a Schottky barrier constructed at the nanotube–matrix contact, which could be used in the fabrication of new ferroelectric and thermoelectric devices.

One of the early works involved MWNTs in a superconducting Bi₂Sr₂CaCu₂O_{8+ δ} matrix [3.409]. The very high thermal conduction of nanotubes suggests that they could be used to manage the thermal properties of ceramics. Seeger et al. [3.410] incorporated MWNTs into SiO₂ by partial matrix melting, and they reported that the presence of nanotubes was crucial to the heat absorption and melting of the matrix, showing that the thermal transport of SiO₂ was probably greatly enhanced by the nanotubes. Zhan et al. [3.411] reported that SWNT-Al₂O₃ composites exhibit anisotropic thermal diffusivity, with a decrease in the direction transverse to SPS pressing. However, no increase in thermal conductivity due to nanotubes in ceramic-matrix composites has been reported so far and further work is required to investigate the heat transport mechanisms involved. The application of MWNT-lanthanum cobaltate composites in an oxygen electrode used in zinc/air [3.412] was also reported. The friction coefficient was also shown to increase and the wear loss to decrease when the nanotube volume fraction was increased in carbon/carbon composites [3.413].

The latter is one of the few examples where carbon has been considered as the matrix. Another one is the work reported by Andrews et al. [3.414], who introduced 5 wt % of SWNTs into a pitch material before spinning it into a SWNT-reinforced pitch-fiber. Subsequent carbonization transformed it into a SWNT-reinforced carbon fiber. Due to the contribution of the SWNTs, which were aligned by the spinning stresses, the resulting gains in tensile strength, modulus, and electrical conductivity with respect to the unreinforced carbon fiber was claimed to be 90, 150 and 340%, respectively.

Polymer Matrix Composites

Nanotube-polymer composites, first reported by *Ajayan et al.* [3.415], have now been intensively studied; especially epoxy- and polymethylmethacrylate (PMMA)-matrix composites. In terms of mechanical characteristics, the three key issues that affect the performance of a fiber-polymer composite are the strength and toughness of the fibrous reinforcement, its orientation, and good interfacial bonding, which is crucial to load transfer [3.416]. The ability of the polymer to form large-diameter helices around individual nanotubes favors the formation of a strong bond with the matrix [3.416]. Isolated SWNTs may be more desirable than MWNTs or bundles for dispersion in a matrix because of the weak frictional interactions between layers of MWNTs and between SWNTs in bundles [3.416]. The main mechanisms of load transfer are micromechanical interlocking, chemical bonding and van der Waals bonding between the nanotubes and the matrix. A high interfacial shear stress between the fiber and the matrix will transfer the applied load to the fiber over a short distance [3.417]. SWNTs longer than 10–100 μm would be needed for significant load-bearing ability in the case of nonbonded SWNT-matrix interactions, whereas the critical length for SWNTs cross-linked to the matrix is only 1 μm [3.418]. Defects are likely to limit the working length of SWNTs, however [3.419].

The load transfer to MWNTs dispersed in an epoxy resin was much higher in compression than in tension [3.417]. It was proposed that all of the walls of the MWNTs are stressed in compression, whereas only the outer walls are stressed in tension because all of the inner tubes are sliding within the outer tube. Mechanical tests performed on 5 wt% SWNT-epoxy composites [3.420] showed that SWNT bundles were pulled out of the matrix during the deformation of the material. The influence of the interfacial nanotube/matrix interaction was demonstrated by *Gong et al.* [3.421]. It was also reported that coating regular carbon fiber with MWNTs prior to their dispersion into an epoxy matrix improves the interfacial load transfer, possibly via local stiffening of the matrix near interface [3.422].

As for ceramic matrix composites, the electrical characteristics of SWNT- and MWNT-epoxy composites are described by the percolation theory. Very low percolation thresholds (below 1 wt%) are often reported [3.423–425]. Industrial epoxy loaded with 1 wt% unpurified CCVD-prepared SWNTs showed an increase in thermal conductivity of 70% and 125% at 40 K and at room temperature, respectively [3.426]. Also, the Vickers hardness rose with the SWNT loading up

to a factor of 3.5 at 2 wt%. Increasing the amount of MWNTs increased the glass transition temperatures of the MWNT-epoxy composites. The effect is stronger when using samples containing functionalized MWNTs [3.427]. Nanocomposites consisting of double-wall carbon nanotubes in an epoxy matrix were produced by a standard calendaring technique with a very good dispersion [3.428]. Increased strength, Young's modulus and strain to failure for a nanotube content of only 0.1 wt% was reported. A significantly improved fracture toughness was also observed for the nanocomposites. *Pecastaings et al.* [3.429] have investigated the role of interfacial effects in carbon nanotube-epoxy nanocomposite behavior. The conductivity of laser-prepared SWNT-PMMA composites increases with the SWNT loading (1–8 wt% SWNTs) [3.416]. Thermogravimetric analysis shows that, compared to pure PMMA, the thermal degradation of PMMA films occurs at a slightly higher temperature when 26 wt% of MWNTs are added [3.430]. Improving the wetting between the MWNTs and the PMMA by coating the MWNTs with poly(vinylidene fluoride) prior to melt-blending with PMMA resulted in an increased storage modulus [3.431]. The impact strength in aligned SWNT-PMMA composites increased significantly with only 0.1 wt% of SWNTs, possibly because of weak interfacial adhesion and/or of the high flexibility of the SWNTs and/or the pullout and sliding effects of individual SWNTs within bundles [3.432]. The transport properties of arc discharge SWNT-PMMA composite films (10 μm -thick) were studied in great detail [3.433, 434]. The electrical conductivity increases by nine orders of magnitude from 0.1 to 8 wt% SWNTs. The room-temperature conductivity is again well described by the standard percolation theory, confirming the good dispersion of the SWNTs in the matrix. The rheological threshold of SWNT-PMMA composites is about 0.12 wt%, smaller than the percolation threshold of electrical conductivity, about 0.39 wt% [3.435]. This is understood in terms of the smaller nanotube–nanotube distance required for electrical conductivity compared to that required to impede polymer mobility. Furthermore, decreased SWNT alignment, improved SWNT dispersion and/or longer polymer chains increase the elastic response of the nanocomposite. The effects of small quantities of SWNTs (up to 1 wt%) in PMMA on its flammability properties were studied [3.436]. The formation of a continuous SWNTs network layer covering the entire surface without any cracks is critical for obtaining the lowest mass-loss rate of the nanocomposites.

Polymer composites with other matrices include CCVD-prepared MWNT-polyvinyl alcohol [3.437], arc-prepared MWNT-polyhydroxyaminoether [3.438], arc-prepared MWNT-polyurethane acrylate [3.439, 440], SWNT-polyurethane acrylate [3.441], SWNT-polycarbonate [3.442], MWNT-polyaniline [3.443], MWNT-polystyrene [3.444], CCVD double-walled nanotubes-polystyrene-polymethylacrylate [3.445], MWNT-polypropylene [3.446, 447], SWNT-polyethylene [3.448–450], SWNT-poly(vinyl acetate) [3.449, 450], CCVD-prepared MWNT-polyacrylonitrile [3.451], SWNT-polyacrylonitrile [3.452], MWNT-oxotitanium phthalocyanine [3.453], arc-prepared MWNT-poly(3-octylthiophene) [3.454], SWNT-poly(3-octylthiophene) [3.455] and CCVD MWNT-poly(3-hexylthiophene) [3.456]. These works

deal mainly with films 100–200 micrometer thick, and aim to study the glass transition of the polymer, its mechanical and electrical characteristics, as well as the photoconductivity.

A great deal of work has also been devoted to the applications of nanotube-polymer composites as materials for molecular optoelectronics, using primarily poly(m-phenylenevinylene-co-2,5-dioctoxy-p-phenylenevinylene) (PmPV) as the matrix. This conjugated polymer tends to coil, forming a helical structure. The electrical conductivity of the composite films ([–w%t]436 MWNTs) is increased by eight orders of magnitude compared to that of PmPV [3.458]. Using the MWNT-PmPV composites as the electron transport layer in light-emitting diodes results in a significant increase in bright-

Table 3.5 Applications of nanotube-based multifunctional materials (from [3.457]), courtesy of *B. Maruyama* (WPAFB, Dayton, Ohio)

Fiber fraction	Applications	Mechanical			Electrical			Thermal		Thermo-mechanical	
		Strength/stiffness	Specific strength	Through-thickness strength	Static dissipation	Surface conduction ^a	EMI shielding	Service ^b temperature	Conduction/dissipation ^c	Dimensional stability ^d	CTE reduction ^e
Low volume fraction (fillers)											
Elastomers	Tires	×			×				×		
Thermoplastics	Chip package				×				×		
	Electronics/Housing	×					×	×	×		
Thermosets	Epoxy products	×	×	×		×				×	×
	Composites			×						×	
High Volume Fraction											
Structural composites	Space/aircraft components		×	×							
High conduction composites	Radiators	×							×	×	
	Heat exchangers	×						×	×		×
	EMI shield	×					×				
^a For electrostatic painting, to mitigate lightning strikes on aircraft, etc. ^b To increase service temperature rating of product ^c To reduce operating temperatures of electronic packages ^d Reduces warping ^e Reduces microcracking damage in composites											

ness [3.459]. The SWNTs act as a hole-trapping material that blocks the holes in the composites; this is probably induced through long-range interactions within the matrix [3.460]. Similar investigations were carried out on arc discharge SWNT-polyethylene dioxythiophene (PEDOT) composite layers [3.461] and MWNT-polyphenylenevinylene composites [3.462].

To conclude, two critical issues must be considered when using nanotubes as components for advanced composites. One is to choose between SWNTs and MWNTs. The former seem more beneficial to mechanical strengthening, provided that they are isolated or arranged into cohesive yarns so that the load can be conveniently transferred from one SWNT to another. Unfortunately, despite many advances [3.463–468], this is still a technical challenge. The other issue is to tailor the nanotube/matrix interface with respect to the matrix; this is the current focus of many laboratories involved in the field.

Multifunctional Materials

One of the major benefits expected from incorporating carbon nanotubes into other solid or liquid materials is that they endow the material with some electrical conductivity while leaving other properties or behaviors unaffected. As already mentioned in the previous section, the percolation threshold is reached at very low nanotube loadings. Tailoring the electrical conductivity of a bulk material is then achieved by adjusting the nanotube volume fraction in the formerly insulating material while making sure that this fraction is not too large. As demonstrated by *Maruyama* [3.457], there are three areas of interest regarding the electrical conductivity: (i) electrostatic discharge (for example, preventing fire or explosion hazards in combustible environments or perturbations in electronics, which requires an electrical resistivity of less than $10^{12} \Omega \text{ cm}$); (ii) electrostatic painting (which requires the material to be painted to have enough electrical conductivity – an electrical resistivity below $10^6 \Omega \text{ cm}$ – to prevent the charged paint droplets from being repelled); (iii) electromagnetic interference shielding (which is achieved for an electrical resistivity of less than $10 \Omega \text{ cm}$).

Materials are often required to be multifunctional; for example, to have both high electrical conductivity and high toughness, or high thermal conductivity and high thermal stability. An association of several materials, each of them bringing one of the desired features, generally meets this need. The exceptional features and properties of carbon nanotubes make them likely to be a perfect multifunctional material in many cases. For in-

stance, materials used in satellites are often required to be electrical conductive, mechanically self-supporting, able to transport away excess heat, and often to be robust against electromagnetic interference, while being of minimal weight and volume. All of these properties should be possible with a single nanotube-containing composite material instead of complex multimaterials combining layers of polymers, aluminium, copper, and so on. Table 3.5 provides an overview of various fields in which nanotube-based multifunctional materials should find application.

Nanoelectronics

As reported in Sects. 3.1.1 and 3.4.4, SWNT nanotubes can be either metallic (with an electrical conductivity higher than that of copper), or semiconducting. This has inspired the design of several components for nanoelectronics. First, metallic SWNTs can be used as mere ballistic conductors. Moreover, as early as 1995, realizing a rectifying diode by joining one metallic SWNT to one semiconductor SWNT (hetero-junction) was proposed by *Lambin* et al. [3.469], then later by *Chico* et al. [3.470] and *Yao* et al. [3.471]. Also, field effect transistors (FET) can be built by attaching a semiconductor SWNT across two electrodes (source and drain) deposited on an insulating substrate that serves as a gate electrode [3.472, 473]. The association of two such SWNT-based FETs makes a voltage inverter [3.474].

All of the latter developments are fascinating and provide promising outlets for nanotube-based electronics. However, progress is obviously needed before SWNT-based integrated circuits can be constructed on a routine basis. A key issue is the need to be able to selectively prepare either metallic or semiconductor nanotubes. Although a method of selectively destroying metallic SWNTs in bundles of undifferentiated SWNTs [3.475] has been proposed, the method is not scalable and selective synthesis would be preferable. Also, defect-free nanotubes are required. Generally speaking, this relates to another major challenge, which is to be able to fabricate integrated circuits including nanometer-size components (that only sophisticated imaging methods such as AFM are able to visualize) on an industrial scale. An overview of the issues related to the integration of carbon nanotubes into microelectronics systems has been written by *Graham* et al. [3.476].

Nanotools, Nanodevices and Nanosystems

Due to the ability of graphene to expand slightly when electrically charged, nanotubes have been found to act as actuators. *Kim* et al. [3.477] demonstrated this by

designing “nanotweezers”, which are able to grab, manipulate and release nano-objects (the “nanobead” that was handled for the demonstration was actually closer to a micrometer in size than a nanometer), as well as to measure their electrical properties. This was made possible by simply depositing two noninterconnected gold coatings onto a pulled glass micropipette (Fig. 3.31), and then attaching two MWNTs (or two SWNT-bundles) $\approx 20\text{--}50$ nm in diameter to each of the gold electrodes. Applying a voltage (0–8.5 V) between the two electrodes then makes the tube tips open and close reversibly in a controlled manner.

A similar experiment, again rather simple, was proposed by *Baughman* et al. the same year (1999) [3.478]. This consisted of mounting two SWNT-based paper strips (“bucky-paper”) on both sides of insulating double-sided tape. The two bucky-paper strips had been previously loaded with Na^+ and Cl^- , respectively. When 1 V was applied between the two paper strips, both of them expanded, but the strip loaded with Na^+ expanded a bit more, forcing the whole system to bend. Though performed in a liquid environment, this behavior has inspired the authors to predict a future use for their system in “artificial muscles.”

Another example of amazing nanotools is the nanothermometer proposed by *Gao* et al. [3.479]. A single MWNT was used, which was partially filled with liquid gallium. Temperature variations in the range 50–500 °C cause the gallium to reversibly move up and down within the nanotube cavity at reproducible levels with respect to the temperature values applied.

Of course, nanotools such as nanotweezers or nanothermometers are hardly commercial enough to justify

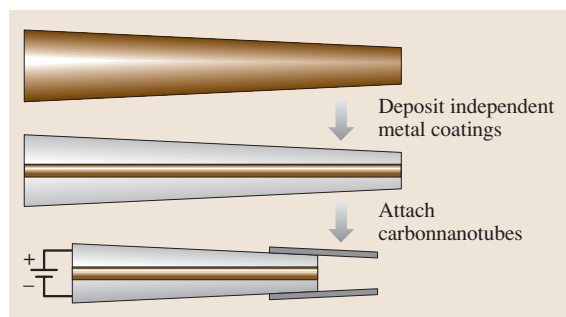


Fig. 3.31 Sketch explaining how the first nanotweezers were designed. The process involves modifying a glass micropipette (dark cone, *top*). Two Au coatings (in gray, *middle*) are deposited so that they are not in contact. Then a voltage is applied to the electrodes (from [3.477])

industrial investment. But such experiments are more than just amazing laboratory curiosities. They demonstrate the ability of carbon nanotubes to provide building blocks for future nanodevices, including nanomechanical systems.

Supercapacitors

Supercapacitors consist of two electrodes immersed in an electrolyte (such as 6M KOH), separated by an insulating ion-permeable membrane. Charging the capacitors is achieved by applying a potential between the two electrodes, which makes the cations and the anions move toward the oppositely charged electrode. Suitable electrodes should exhibit high electrical conductivities and high surface areas, since the capacitance is proportional to these parameters. Actually, the surface area should consist of an appropriate combination of mesopores (to allow the electrolyte components to circulate well, which is related to the charging speed) and micropores (whose walls provide the attractive surfaces and fixation sites for the ions). Based on early work by *Niu* et al. [3.480], such a combination was found to be provided by the specific architecture offered by packed and entangled h-MWNTs with poor nanotextures (see Sect. 3.1.2). However, activation pretreatments were necessary. For instance, a capacitor made from nanotubes with a surface area of 220 m²/g exhibited a capacitance of 20 F/g, which increased to 100 F/g after an activation treatment was applied to the nanotubes so that their surface area increased to 880 m²/g [3.159]. Alternatively, again due to their remarkable architectures derived from their huge aspect ratios, nanotubes can also be used as supports for conductive polymer coatings, such as polypyrrole or polyaniline [3.481], or additives to regular carbon electrodes [3.482], which make the material more open, allowing easier circulation and penetration of ions. Supercapacitors built from such composites can survive more than 2000 charging cycles, with current densities as high as 350 mA/g [3.483]. Capacitors including nanotubes have already shown capacitances as high as 180–200 F/g, equivalent to those obtained with electrodes built from regular carbon materials, but they have the advantage of faster charging [3.159]. Current work in this area will certainly lead to further optimization of both the nanotube material architecture and the nanotube-supported conductive polymers, meaning that the outlook for the commercial use of nanotubes as components for supercapacitors is positive, and this is ignoring the potential application of second-generation nanotubes (such as nanotube-based

nano-objects) in this field. A first attempt to use hybrid nanotubes (see Sect. 3.5.2) has already resulted in

improved properties with respect to genuine (undoped) nanotube-based systems [3.484].

3.7 Concluding Remarks

Carbon nanotubes have been the focus of a lot of research work (and therefore a lot of funding) for more than a decade now. Considering this investment of time and money, relatively few nanotube applications have reached the market yet. This may remind some of the disappointments associated with fullerene research, originally believed to be so promising, but which has resulted in no significant application after twenty years.

However, nanotubes exhibit an extraordinary diversity of morphologies, textures, structures and nanotextures, far beyond that provided by fullerenes. Indeed, the properties of nanotubes are yet to be fully identified, and we should not forget the potential of hybrid nanotubes, heteronanotubes and nanotube-containing composites. The history of nanotubes has only just begun.

References

- 3.1 L.V. Radushkevich, V.M. Lukyanovich: O strukture ugljeroda, obrazujucegosja pri termiceskom razlozenii okisi ugljeroda na zeleznom kontakte, Zurn. Fisic. Chim. **26**, 88–95 (1952)
- 3.2 T. V. Hughes, C. R. Chambers: US Patent 405, 480 (1889)
- 3.3 P. Schützenberger, L. Schützenberger: Sur quelques faits relatifs à l'histoire du carbone, C. R. Acad. Sci. Paris **111**, 774–778 (1890)
- 3.4 C. Pélabon, H. Pélabon: Sur une variété de carbone filamenteux, C. R. Acad. Sci. (Paris) **137**, 706–708 (1903)
- 3.5 R. T. K. Baker, P. S. Harris: The formation of filamentous carbon. In: *Chemistry and Physics of Carbon*, Vol. 14, ed. by P. L. Walker Jr., P. A. Thrower (Dekker, New York 1978) pp. 83–165
- 3.6 S. Iijima: Helical microtubules of graphite carbon, Nature **354**, 56–58 (1991)
- 3.7 S. Iijima, T. Ichihashi: Single-shell carbon nanotubes of 1-nm diameter, Nature **363**, 603–605 (1993)
- 3.8 D. S. Bethune, C. H. Kiang, M. S. de Vries, G. Gorman, R. Savoy, J. Vazquez, R. Bayers: Cobalt-catalysed growth of carbon nanotubes with single-atomic-layer walls, Nature **363**, 605–607 (1993)
- 3.9 J. Tersoff, R. S. Ruoff: Structural properties of a carbon-nanotube crystal, Phys. Rev. Lett. **73**, 676–679 (1994)
- 3.10 N. Wang, Z. K. Tang, G. D. Li, J. S. Chen: Single-walled 4 Å carbon nanotube arrays, Nature **408**, 50–51 (2000)
- 3.11 N. Hamada, S. I. Sawada, A. Oshiyama: New one-dimensional conductors, graphite microtubules, Phys. Rev. Lett. **68**, 1579–1581 (1992)
- 3.12 M. S. Dresselhaus, G. Dresselhaus, P. C. Eklund: *Science of Fullerenes and Carbon Nanotubes* (Academic, San Diego 1995)
- 3.13 R. C. Haddon: Chemistry of the fullerenes: The manifestation of strain in a class of continuous aromatic molecules, Science **261**, 1545–1550 (1993)
- 3.14 M. Monthieux, B. W. Smith, B. Burteaux, A. Claye, J. Fisher, D. E. Luzzi: Sensitivity of single-wall nanotubes to chemical processing: An electron microscopy investigation, Carbon **39**, 1261–1272 (2001)
- 3.15 H. Allouche, M. Monthieux: Chemical vapor deposition of pyrolytic carbon onto carbon nanotubes. Part II – Structure and texture, Carbon **43**, 1265–1278 (2005)
- 3.16 N. M. Rodriguez, A. Chambers, R. T. Baker: Catalytic engineering of carbon nanostructures, Langmuir **11**, 3862–3866 (1995)
- 3.17 M. Audier, A. Oberlin, M. Oberlin, M. Coulon, L. Bonnetain: Morphology and crystalline order in catalytic carbons, Carbon **19**, 217–224 (1981)
- 3.18 Y. Saito: Nanoparticles and filled nanocapsules, Carbon **33**, 979–988 (1995)
- 3.19 P. J. F. Harris: *Carbon Nanotubes and Related Structures* (Cambridge Univ. Press, Cambridge 1999)
- 3.20 H. W. Kroto, J. R. Heath, S. C. O'Brien, R. F. Curl, R. E. Smalley: C₆₀ Buckminsterfullerene, Nature **318**, 162–163 (1985)
- 3.21 W. Krätschmer, L. D. Lamb, K. Fostiropoulos, D. R. Huffman: Solid C₆₀: A new form of carbon, Nature **347**, 354–358 (1990)
- 3.22 L. Fulchieri, Y. Schwob, F. Fabry, G. Flamant, L. F. P. Chibante, D. Laplaze: Fullerene production in a 3-phase AC plasma process, Carbon **38**, 797–803 (2000)
- 3.23 K. Saidane, M. Razafinimanana, H. Lange, A. Huczko, M. Baltas, A. Gleizes, J. L. Meunier: Fullerene synthesis in the graphite electrode arc process: local plasma characteristics and correlation with yield, J Phys. D: Appl. Phys. **37**, 232–239 (2004)

- 3.24 T. Guo, P. Nikolaev, A.G. Rinzler, D. Tomanek, D.T. Colbert, R.E. Smalley: Self-assembly of tubular fullerenes, *J. Phys. Chem.* **99**, 10694–10697 (1995)
- 3.25 T. Guo, P. Nikolaev, A. Thess, D.T. Colbert, R.E. Smalley: Catalytic growth of single-walled nanotubes by laser vaporisation, *Chem. Phys. Lett.* **243**, 49–54 (1995)
- 3.26 A.G. Rinzler, J. Liu, H. Dai, P. Nikolaev, C.B. Huffman, F.J. Rodriguez-Macias, P.J. Boul, A.H. Lu, D. Heymann, D.T. Colbert, R.S. Lee, J.E. Fischer, A.M. Rao, P.C. Eklund, R.E. Smalley: Large scale purification of single wall carbon nanotubes: Process, product and characterization, *Appl. Phys. A* **67**, 29–37 (1998)
- 3.27 A. Thess, R. Lee, P. Nikolaev, H. Dai, P. Petit, J. Robert, C. Xu, Y.H. Lee, S.G. Kim, D.T. Colbert, G. Scuseria, D. Tomanek, J.E. Fischer, R.E. Smalley: Crystalline ropes of metallic carbon nanotubes, *Science* **273**, 487–493 (1996)
- 3.28 L.M. Chapelle, J. Gavillet, J.L. Cochon, M. Ory, S. Lefrant, A. Loiseau, D. Pigache: A continuous wave CO₂ laser reactor for nanotube synthesis, *Proc. Electronic Properties of Novel Materials–XVI Int. Winterschool – AIP Conf. Proc.*, ed. by H. Kuzmany, J. Fink, M. Mehring, S. Roth (Springer, Berlin Heidelberg 1999) 237–240
- 3.29 M. Yudasaka, T. Komatsu, T. Ichihashi, S. Iijima: Single wall carbon nanotube formation by laser ablation using double targets of carbon and metal, *Chem. Phys. Lett.* **278**, 102–106 (1997)
- 3.30 M. Castignolles, A. Foutel-Richard, A. Mavel, J.L. Cochon, D. Pigache, A. Loiseau, P. Bernier: Combined experimental and numerical study of the parameters controlling the C-SWNT synthesis via laser vaporization, *Proc. Electronic Properties of Novel Materials–XVI Int. Winterschool – AIP Conf. Proc.*, ed. by H. Kuzmany, J. Fink, M. Mehring, S. Roth (Springer, Berlin Heidelberg 2002) 385–389
- 3.31 T.W. Ebbesen, P.M. Ajayan: Large-scale synthesis of carbon nanotubes, *Nature* **358**, 220–221 (1992)
- 3.32 D. Ugarte: Morphology and structure of graphitic soot particles generated in arc-discharge C₆₀ production, *Chem. Phys. Lett.* **198**, 596–602 (1992)
- 3.33 T.W. Ebbesen: Carbon nanotubes, *Ann. Rev. Mater. Sci.* **24**, 235–264 (1994)
- 3.34 T. Beltz, J. Find, D. Herein, N. Pfänder, T. Rühle, H. Werner, M. Wohlers, R. Schlögl: On the production of different carbon forms by electric arc graphite evaporation, *Ber. Bunsen. Phys. Chem.* **101**, 712–725 (1997)
- 3.35 C. Journet, W.K. Maser, P. Bernier, A. Loiseau, L.M. de la Chapelle, S. Lefrant, P. Deniard, R. Lee, J.E. Fischer: Large-scale production of single-walled carbon nanotubes by the electric-arc technique, *Nature* **388**, 756–758 (1997)
- 3.36 K. Saïdane, M. Razafinimanana, H. Lange, M. Baltas, A. Gleizes, J.J. Gonzalez: Influence of the carbon arc current intensity on fullerene synthesis, *Proc. 24th Int. Conf. on Phenomena in Ionized Gases*, ed. by P. Pisarczyk, T. Pisarczyk, J. Wotowski, (Institute of Plasma Physics and Laser Microfusion, Warsaw 1999) 203–204
- 3.37 H. Allouche, M. Monthieux, M. Pacheco, M. Razafinimanana, H. Lange, A. Huczko, T. P. Teulet, A. Gleizes, T. Sogabe: Physical characteristics of the graphite-electrode electric-arc as parameters for the formation of single-wall carbon nanotubes, *Proc. Eurocarbon (Deutsche Keram. Ges.)* **2**, 1053–1054 (2000)
- 3.38 M. Razafinimanana, M. Pacheco, M. Monthieux, H. Allouche, H. Lange, A. Huczko, A. Gleizes: Spectroscopic study of an electric arc with Gd and Fe doped anodes for the carbon nanotube formation, *Proc. 25th Int. Conf. on Phenomena in Ionized Gases*, ed. by E. Goto (Nagoya Univ., Nagoya 2001) 297–298
- 3.39 M. Razafinimanana, M. Pacheco, M. Monthieux, H. Allouche, H. Lange, A. Huczko, P. Teulet, A. Gleizes, C. Goze, P. Bernier, T. Sogabe: Influence of doped graphite electrode in electric arc for the formation of single wall carbon nanotubes, *Proc. 6th Eur. Conf. on Thermal Plasma Processes – Progress in Plasma Processing of Materials*, New York 2000, ed. by P. Fauchais (Begell House, New York 2001) 649–654
- 3.40 M. Pacheco, H. Allouche, M. Monthieux, A. Razafinimanana, A. Gleizes: Correlation between the plasma characteristics and the morphology and structure of the carbon phases synthesised by electric arc discharge, *Proc. 25th Biennial Conf. on Carbon*, Lexington (Kentucky) 2001, ed. by F. Derbyshire (American Carbon Society 2001) Extend. Abstr.(CD-Rom), Novel/14.1
- 3.41 M. Pacheco, M. Monthieux, M. Razafinimanana, L. Donadieu, H. Allouche, N. Caprais, A. Gleizes: New factors controlling the formation of single-wall carbon nanotubes by arc plasma, *Proc. Carbon 2002 Int. Conf.*, Beijing 2002, ed. by H.-M. Cheng (Shanxi Chunqiu Audio-Visual Press, Beijing 2002) (CD-Rom/Oral/1014)
- 3.42 M. Monthieux, M. Pacheco, H. Allouche, M. Razafinimanana, N. Caprais, L. Donnadieu, A. Gleizes: New data about the formation of SWNTs by the electric arc method, *Electronic Properties of Molecular Nanostructures*, AIP Conf. Proc., ed. by H. Kuzmany, J. Fink, M. Mehring, S. Roth (Springer, Berlin Heidelberg 2002) 182–185
- 3.43 H. Lange, A. Huczko, M. Sioda, M. Pacheco, M. Razafinimanana, A. Gleizes: Influence of gadolinium on carbon arc plasma and formation of fullerenes and nanotubes, *Plasma Chem. Plasma Process* **22**, 523–536 (2002)
- 3.44 C. Journet: La production de nanotubes de carbone. Ph.D. Thesis (University of Montpellier II, Montpellier 1998)
- 3.45 T. Sogabe, T. Masuda, K. Kuroda, Y. Hirohaya, T. Hino, T. Ymashina: Preparation of B₄C-mixed

- graphite by pressureless sintering and its air oxidation behavior, *Carbon* **33**, 1783–1788 (1995)
- 3.46 M. Ishigami, J. Cumings, A. Zettl, S. Chen: A simple method for the continuous production of carbon nanotubes, *Chem. Phys. Lett.* **319**, 457–459 (2000)
- 3.47 Y. L. Hsin, K. C. Hwang, F. R. Chen, J. J. Kai: Production and in-situ metal filling of carbon nanotube in water, *Adv. Mater.* **13**, 830–833 (2001)
- 3.48 H. W. Zhu, X. S. Li, B. Jiang, C. L. Xu, C. L. Zhu, Y. F. Zhu, D. H. Wu, X. H. Chen: Formation of carbon nanotubes in water by the electric arc technique, *Chem. Phys. Lett.* **366**, 664–669 (2002)
- 3.49 W. K. Maser, P. Bernier, J. M. Lambert, O. Stephan, P. M. Ajayan, C. Colliex, V. Brotons, J. M. Planeix, B. Coq, P. Molinie, S. Lefrant: Elaboration and characterization of various carbon nanostructures, *Synth. Met.* **81**, 243–250 (1996)
- 3.50 J. Gavillet, A. Loiseau, J. Thibault, A. Maigné, O. Stéphan, P. Bernier: TEM study of the influence of the catalyst composition on the formation and growth of SWNT, *Proc. Electronic Properties Novel Materials–XVII Int. Winterschool – AIP Conf. Proc.*, ed. by H. Kuzmany, J. Fink, M. Mehring, S. Roth (Springer, Berlin Heidelberg 2002) 202–206
- 3.51 G. Flamant, J. F. Robert, S. Marty, J. M. Gineste, J. Giral, B. Rivoire, D. Laplaze: Solar reactor scaling up. The fullerene synthesis case study, *Energy* **29**, 801–809 (2004)
- 3.52 T. M. Gruenberger, J. Gonzalez-Aguilar, F. Fabry, L. Fulchieri, E. Grivei, N. Probst, G. Flamant, H. Okuno, J. C. Charlier: Production of carbon nanotubes and other nanostructures via continuous 3-phase AC plasma processing, *Fuller. Nanotub. Car. N.* **12**, 571–581 (2004)
- 3.53 H. Okuno, E. Grivel, F. Fabry, T. M. Gruenberger, J. J. Gonzalez-Aguilar, A. Palnichenko, L. Fulchieri, N. Probst, J. C. Chalier: Synthesis of carbon nanotubes and nano-necklaces by thermal plasma process, *Carbon* **42**, 2543–2549 (2004)
- 3.54 L. P. F. Chibante, A. Thess, J. M. Alford, M. D. Diener, R. E. Smalley: Solar generation of the fullerenes, *J. Phys. Chem.* **97**, 8696–8700 (1993)
- 3.55 C. L. Fields, J. R. Pitts, M. J. Hale, C. Bingham, A. Lewandowski, D. E. King: Formation of fullerenes in highly concentrated solar flux, *J. Phys. Chem.* **97**, 8701–8702 (1993)
- 3.56 P. Bernier, D. Laplaze, J. Auriol, L. Barbedette, G. Flamant, M. Lebrun, A. Brunelle, S. Della-Negra: Production of fullerenes from solar energy, *Synth. Met.* **70**, 1455–1456 (1995)
- 3.57 M. J. Heben, T. A. Bekkedhal, D. L. Schultz, K. M. Jones, A. C. Dillon, C. J. Curtis, C. Bingham, J. R. Pitts, A. Lewandowski, C. L. Fields: Production of single wall carbon nanotubes using concentrated sunlight, *Proc. Symp. Recent Adv. Chem. Phys. Fullerenes Rel. Mater.*, Pennington 1996, ed. by K. M. Kadish, R. S. Ruoff (Electrochemical Society, Pennington 1996) 803–811
- 3.58 D. Laplaze, P. Bernier, C. Journet, G. Vié, G. Flamant, E. Philippot, M. Lebrun: Evaporation of graphite using a solar furnace, *Proc. 8th Int. Symp. Solar Concentrating Technol.*, Köln 1996, ed. by M. Becker, M. Balmer (C. F. Müller Verlag, Heidelberg 1997) 1653–1656
- 3.59 D. Laplaze, P. Bernier, W. K. Maser, G. Flamant, T. Guillard, A. Loiseau: Carbon nanotubes: The solar approach, *Carbon* **36**, 685–688 (1998)
- 3.60 T. Guillard, S. Cetout, L. Alvarez, J. L. Sauvajol, E. Anglaret, P. Bernier, G. Flamant, D. Laplaze: Production of carbon nanotubes by the solar route, *Eur. Phys. J.* **5**, 251–256 (1999)
- 3.61 D. Luxembourg, G. Flamant, A. Guillot, D. Laplaze: Hydrogen storage in solar produced single-walled carbon nanotubes, *Mater. Sci. Eng. B* **108**, 114–119 (2004)
- 3.62 G. Flamant, M. Bijeire, D. Luxembourg: Modelling of a solar reactor for single wall nanotubes synthesis, *ASME J. Solar Energy Eng.* **128**, 1–124 (2006)
- 3.63 G. G. Tibbetts, M. Endo, C. P. Beetz: Carbon fibers grown from the vapor phase: A novel material, *SAMPE J.* **22**, 30 (1989)
- 3.64 R. T. K. Baker: Catalytic growth of carbon filaments, *Carbon* **27**, 315–323 (1989)
- 3.65 E. Flahaut: Synthèse par voie catalytique et caractérisation de composites nanotubes de carbone-metal-oxyde Poudres et matériaux denses. Ph.D. Thesis (Univers. Paul Sabatier, Toulouse 1999)
- 3.66 E. Flahaut, R. Bacsa, A. Peigney, Ch. Laurent: Gram-scale CCVD synthesis of double-walled carbon nanotubes, *Chem. Commun.*, 1442–1443 (2003)
- 3.67 R. T. K. Baker, P. S. Harris, R. B. Thomas, R. J. Waite: Formation of filamentous carbon from iron, cobalt, and chromium catalyzed decomposition of acetylene, *J. Catal.* **30**, 86–95 (1973)
- 3.68 T. Koyama, M. Endo, Y. Oyuma: Carbon fibers obtained by thermal decomposition of vaporized hydrocarbon, *Jap. J. Appl. Phys.* **11**, 445–449 (1972)
- 3.69 M. Endo, A. Oberlin, T. Koyama: High resolution electron microscopy of graphitizable carbon fiber prepared by benzene decomposition, *Jap. J. Appl. Phys.* **16**, 1519–1523 (1977)
- 3.70 N. M. Rodriguez: A review of catalytically grown carbon nanofibers, *J. Mater. Res.* **8**, 3233–3250 (1993)
- 3.71 W. R. Davis, R. J. Slawson, G. R. Rigby: An unusual form of carbon, *Nature* **171**, 756 (1953)
- 3.72 H. P. Boehm: Carbon from carbon monoxide disproportionation on nickel and iron catalysts; morphological studies and possible growth mechanisms, *Carbon* **11**, 583–590 (1973)
- 3.73 M. Audier, A. Oberlin, M. Coulon: Crystallographic orientations of catalytic particles in filamentous carbon; case of simple conical particles, *J. Cryst. Growth* **55**, 546–549 (1981)
- 3.74 M. Audier, M. Coulon: Kinetic and microscopic aspects of catalytic carbon growth, *Carbon* **23**, 317–323 (1985)

- 3.75 M. Audier, A. Oberlin, M. Coulon: Study of biconic microcrystals in the middle of carbon tubes obtained by catalytic disproportionation of CO, *J. Cryst. Growth* **57**, 524–534 (1981)
- 3.76 A. Thaib, G. A. Martin, P. Pinheiro, M. C. Schouler, P. Gadelle: Formation of carbon nanotubes from the carbon monoxide disproportionation reaction over $\text{CO}/\text{Al}_2\text{O}_3$ and Co/SiO_2 catalysts, *Catal. Lett.* **63**, 135–141 (1999)
- 3.77 P. Pinheiro, M. C. Schouler, P. Gadelle, M. Mermoux, E. Dooryh e: Effect of hydrogen on the orientation of carbon layers in deposits from the carbon monoxide disproportionation reaction over $\text{Co}/\text{Al}_2\text{O}_3$ catalysts, *Carbon* **38**, 1469–1479 (2000)
- 3.78 P. Pinheiro, P. Gadelle: Chemical state of a supported iron–cobalt catalyst during CO disproportionation. I. Thermodynamic study, *J. Phys. Chem. Solids* **62**, 1015–1021 (2001)
- 3.79 P. Pinheiro, P. Gadelle, C. Jeandey, J. L. Oddou: Chemical state of a supported iron–cobalt catalyst during CO disproportionation. II. Experimental study, *J. Phys. Chem. Solids* **62**, 1023–1037 (2001)
- 3.80 C. Laurent, E. Flahaut, A. Peigney, A. Rousset: Metal nanoparticles for the catalytic synthesis of carbon nanotubes, *New J. Chem.* **22**, 1229–1237 (1998)
- 3.81 A. Peigney, C. Laurent, F. Dobigeon, A. Rousset: Carbon nanotubes grown in situ by a novel catalytic method, *J. Mater. Res.* **12**, 613–615 (1997)
- 3.82 V. Ivanov, J. B. Nagy, P. Lambin, A. Lucas, X. B. Zhang, X. F. Zhang, D. Bernaerts, G. Van Tendeloo, S. Amelinckx, J. Van Landuyt: The study of nanotubules produced by catalytic method, *Chem. Phys. Lett.* **223**, 329–335 (1994)
- 3.83 V. Ivanov, A. Fonseca, J. B. Nagy, A. Lucas, P. Lambin, D. Bernaerts, X. B. Zhang: Catalytic production and purification of nanotubules having fullerene-scale diameters, *Carbon* **33**, 1727–1738 (1995)
- 3.84 K. Hernadi, A. Fonseca, J. B. Nagy, D. Bernaerts, A. Fudala, A. Lucas: Catalytic synthesis of carbon nanotubes using zeolite support, *Zeolites* **17**, 416–423 (1996)
- 3.85 H. Dai, A. G. Rinzler, P. Nikolaev, A. Thess, D. T. Colbert, R. E. Smalley: Single-wall nanotubes produced by metal-catalysed disproportionation of carbon monoxide, *Chem. Phys. Lett.* **260**, 471–475 (1996)
- 3.86 A. M. Cassel, J. A. Raymakers, J. Kong, H. Dai: Large scale CVD synthesis of single-walled carbon nanotubes, *J. Phys. Chem. B* **109**, 6484–6492 (1999)
- 3.87 B. Kitiyanan, W. E. Alvarez, J. H. Harwell, D. E. Resasco: Controlled production of single-wall carbon nanotubes by catalytic decomposition of CO on bimetallic Co–Mo catalysts, *Chem. Phys. Lett.* **317**, 497–503 (2000)
- 3.88 A. Govindaraj, E. Flahaut, C. Laurent, A. Peigney, A. Rousset, C. N. R. Rao: An investigation of carbon nanotubes obtained from the decomposition of methane over reduced $\text{Mg}_{1-x}\text{M}_x\text{Al}_2\text{O}_4$ spinel catalysts, *J. Mater. Res.* **14**, 2567–2576 (1999)
- 3.89 E. Flahaut, A. Peigney, C. Laurent, A. Rousset: Synthesis of single-walled carbon nanotube–Co–MgO composite powders and extraction of the nanotubes, *J. Mater. Chem.* **10**, 249–252 (2000)
- 3.90 J. Kong, A. M. Cassel, H. Dai: Chemical vapor deposition of methane for single-walled carbon nanotubes, *Chem. Phys. Lett.* **292**, 567–574 (1998)
- 3.91 E. Flahaut, A. Peigney, W. S. Bacsa, R. R. Bacsa, Ch. Laurent: CVD synthesis of carbon nanotubes from (Mg, Co, Mo)O catalysts: Influence of the proportions of cobalt and molybdenum, *J. Mater. Chem.* **14**, 646–653 (2004)
- 3.92 E. Flahaut, Ch. Laurent, A. Peigney: Catalytic CVD synthesis of double and triple-walled carbon nanotubes by the control of the catalyst preparation, *Carbon* **43**, 375–383 (2005)
- 3.93 R. Marangoni, P. Serp, R. Feurrer, Y. Kihn, P. Kalck, C. Vahlas: Carbon nanotubes produced by substrate free metalorganic chemical vapor deposition of iron catalyst and ethylene, *Carbon* **39**, 443–449 (2001)
- 3.94 R. Sen, A. Govindaraj, C. N. R. Rao: Carbon nanotubes by the metallocene route, *Chem. Phys. Lett.* **267**, 276–280 (1997)
- 3.95 Y. Y. Fan, H. M. Cheng, Y. L. Wei, G. Su, S. H. Shen: The influence of preparation parameters on the mass production of vapor grown carbon nanofibers, *Carbon* **38**, 789–795 (2000)
- 3.96 L. Ci, J. Wei, B. Wei, J. Liang, C. Xu, D. Wu: Carbon nanofibers and single-walled carbon nanotubes prepared by the floating catalyst method, *Carbon* **39**, 329–335 (2001)
- 3.97 M. Glerup, H. Kanzow, R. Almairac, M. Castignolles, P. Bernier: Synthesis of multi-walled carbon nanotubes and nano-fibres using aerosol method with metal-ions as the catalyst precursors, *Chem. Phys. Lett.* **377**, 293–298 (2003)
- 3.98 O. A. Nerushev, M. Sveningsson, L. K. L. Falk, F. Rohmund: Carbon nanotube films obtained by thermal vapour deposition, *J. Mater. Chem.* **11**, 1122–1132 (2001)
- 3.99 Z. Zhou, L. Ci, L. Song, X. Yan, D. Liu, H. Yuan, Y. Gao, J. Wang, L. Liu, W. Zhou, G. Wang, Si Xie: Producing cleaner double-walled carbon nanotubes in a floating catalyst system, *Carbon* **41**, 2607–2611 (2003)
- 3.100 F. Rohmund, L. K. L. Falk, F. E. B. Campbell: A simple method for the production of large arrays of aligned carbon nanotubes, *Chem. Phys. Lett.* **328**, 369–373 (2000)
- 3.101 G. G. Tibbetts, C. A. Bernardo, D. W. Gorkiewicz, R. L. Alig: Role of sulfur in the production of carbon fibers in the vapor phase, *Carbon* **32**, 569–576 (1994)
- 3.102 S. Bai, F. Li, Q. H. Yang, H. M. Cheng, J. B. Bai: Influence of ferrocene/benzene mole ratio in the synthesis of carbon nanostructures, *Chem. Phys. Lett.* **376**, 83–89 (2003)

- 3.103 W. Q. Han, P. Kholer-Riedlich, T. Seeger, F. Ernst, M. Ruhle, N. Grobert, W. K. Hsu, B. H. Chang, Y. Q. Zhu, H. W. Kroto, M. Terrones, H. Terrones: Aligned CN_x nanotubes by pyrolysis of ferrocene under NH_3 atmosphere, *Appl. Phys. Lett.* **77**, 1807–1809 (2000)
- 3.104 L. Ci, Z. Rao, Z. Zhou, D. Tang, X. Yan, Y. Liang, D. Liu, H. Yuan, W. Zhou, G. Wang, W. Liu, S. Xie: Double wall carbon nanotubes promoted by sulfur in a floating iron catalyst CVD system, *Chem. Phys. Lett.* **359**, 63–67 (2002)
- 3.105 S. Maruyama, R. Kojima, Y. Miyauchi, S. Chiashi, M. Kohno: Low-temperature synthesis of high-purity single-walled carbon nanotubes from alcohol, *Chem. Phys. Lett.* **360**, 229–234 (2002)
- 3.106 T. Kyotani, L. F. Tsai, A. Tomita: Preparation of ultrafine carbon tubes in nanochannels of an anodic aluminum oxide film, *Chem. Mater.* **8**, 2109–2113 (1996)
- 3.107 R. E. Smalley, J. H. Hafner, D. T. Colbert, K. Smith: (1998) Catalytic growth of single-wall carbon nanotubes from metal particles, US patent US19980601010903
- 3.108 P. Nikolaev: Gas-phase production of single-walled carbon nanotubes from carbon monoxide: a review of the HiPco process, *J. Nanosci. Nanotech.* **4**, 307–316 (2004)
- 3.109 W. K. Hsu, J. P. Hare, M. Terrones, H. W. Kroto, D. R. M. Walton, P. J. F. Harris: Condensed-phase nanotubes, *Nature* **377**, 687 (1995)
- 3.110 W. S. Cho, E. Hamada, Y. Kondo, K. Takayanagi: Synthesis of carbon nanotubes from bulk polymer, *Appl. Phys. Lett.* **69**, 278–279 (1996)
- 3.111 Y. L. Li, Y. D. Yu, Y. Liang: A novel method for synthesis of carbon nanotubes: Low temperature solid pyrolysis, *J. Mater. Res.* **12**, 1678–1680 (1997)
- 3.112 M. L. Terranova, S. Piccirillo, V. Sessa, P. Sbornicchia, M. Rossi, S. Botti, D. Manno: Growth of single-walled carbon nanotubes by a novel technique using nano-sized graphite as carbon source, *Chem. Phys. Lett.* **327**, 284–290 (2000)
- 3.113 R. L. Vander Wal, T. Ticich, V. E. Curtis: Diffusion flame synthesis of single-walled carbon nanotubes, *Chem. Phys. Lett.* **323**, 217–223 (2000)
- 3.114 H. Cui, G. Eres, J. Y. Howe, A. Puzos, M. Varela, D. B. Geohegan, D. H. Lowndes: Growth behavior of carbon nanotubes on multilayered metal catalyst film in chemical vapor deposition, *Chem. Phys. Lett.* **374**, 222–228 (2003)
- 3.115 Y. Y. Wei, G. Eres, V. I. Merkulov, D. H. Lowndes: Effect of film thickness on carbon nanotube growth by selective area chemical vapor deposition, *Appl. Phys. Lett.* **78**, 1394–1396 (2001)
- 3.116 I. T. Han, B. K. Kim, H. J. Kim, M. Yang, Y. W. Jin, S. Jung, N. Lee, S. K. Kim, J. M. Kim: Effect of Al and catalyst thickness on the growth of carbon nanotubes and application to gated field emitter arrays, *Chem. Phys. Lett.* **400**, 139–144 (2004)
- 3.117 W. Z. Li, S. S. Xie, L. X. Qian, B. H. Chang, B. S. Zou, W. Y. Zhou, R. A. Zha, G. Wang: Large scale synthesis of aligned carbon nanotubes, *Science* **274**, 1701–1703 (1996)
- 3.118 F. Zheng, L. Liang, Y. Gao, J. H. Sukamoto, L. Aardahl: Carbon nanotubes synthesis using mesoporous silica templates, *Nanolett.* **2**, 729–732 (2002)
- 3.119 S. H. Jeong, O.-K. Lee, K. H. Lee, S. H. Oh, C. G. Park: Preparation of aligned carbon nanotubes with prescribed dimension: Template synthesis and sonication cutting approach, *Chem. Mater.* **14**, 1859–1862 (2002)
- 3.120 A. M. Cassel, N. R. Franklin, T. W. Tomblor, E. M. Chan, J. Han, H. Dai: Directed growth of free-standing single-walled carbon nanotubes, *J. Am. Chem. Soc.* **121**, 7975–7976 (1999)
- 3.121 S. Fan, M. Chapline, N. Franklin, T. Tomblor, A. M. Cassel, H. Dai: Self-oriented regular arrays of carbon nanotubes and their field emission properties, *Science* **283**, 512–514 (1999)
- 3.122 N. S. Kim, Y. T. Lee, J. Park, H. Ryu, H. J. Lee, S. Y. Choi, J. Choo: Dependence of vertically aligned growth of carbon nanotubes on catalyst, *J. Phys. Chem. B* **106**, 9286–9290 (2002)
- 3.123 C. J. Lee, D. W. Kim, T. J. Lee, Y. C. Choi, Y. S. Park, Y. H. Lee, W. B. Choi, N. S. Lee, G.-S. Park, J. M. Kim: Synthesis of aligned carbon nanotubes using thermal chemical vapor deposition, *Chem. Phys. Lett.* **312**, 461–468 (1999)
- 3.124 W. D. Zhang, Y. Wen, S. M. Liu, W. C. Tjiu, G. Q. Xu, L. M. Gan: Synthesis of vertically aligned carbon nanotubes on metal deposited quartz plates, *Carbon* **40**, 1981–1989 (2002)
- 3.125 S. Huang, L. Dai, A. W. H. Mau: Controlled fabrication of large scale aligned carbon nanofiber/nanotube patterns by photolithography, *Adv. Mater.* **14**, 1140–1143 (2002)
- 3.126 T. Sun, G. Wang, H. Liu, L. Feng, D. Zhu: Control over the wettability of an aligned carbon nanotube film, *J. Am. Chem. Soc.* **125**, 14996–14997 (2003)
- 3.127 Y. Huh, J. Y. Lee, J. Cheon, Y. K. Hong, J. Y. Koo, T. J. Lee, C. J. Lee: Controlled growth of carbon nanotubes over cobalt nanoparticles by thermal chemical vapor deposition, *J. Mater. Chem.* **13**, 2297–2300 (2003)
- 3.128 Y. Kobayashi, H. Nakashima, D. Takagi, Y. Homma: CVD growth of single-walled carbon nanotubes using size-controlled nanoparticle catalyst, *Thin Solid Films* **464–465**, 286–289 (2004)
- 3.129 C. L. Cheung, A. Kurtz, H. Park, C. M. Lieber: Diameter-controlled synthesis of carbon nanotubes, *J. Phys. Chem B* **106**, 2429–2433 (2002)
- 3.130 Y. Huh, J. Y. Lee, J. Cheon, Y. K. Hong, J. Y. Koo, T. J. Lee, C. J. Lee: Controlled growth of carbon nanotubes over cobalt nanoparticles by thermal chemical vapor deposition, *J. Mater. Chem.* **13**, 2297–2300 (2003)

- 3.131 M. Paillet, V. Jourdain, P. Poncharal, J.-L. Sauvajol, A. Zahab, J. C. Meyer, S. Roth, N. Cordente, C. Amiens, B. Chaudret: Versatile synthesis of individual single-walled carbon nanotubes from nickel nanoparticles for the study of their physical properties, *J. Phys. Chem. B* **108**, 17112–17118 (2004)
- 3.132 S. Casimirius, E. Flahaut, C. Laurent, C. Vieu, F. Carcenac, C. Laberty-Robert: Optimized microcontact printing process for the patterned growth of individual SWNTs, *Microelectr. Eng.* **73–74**, 564–569 (2004)
- 3.133 Y. Lei, K. S. Yeong, J. T. L. Thong, W. K. Chim: Large-scale ordered carbon nanotubes arrays initiated from highly ordered catalyst arrays on silicon substrates, *Chem. Mater.* **16**, 2757–2761 (2004)
- 3.134 Q. Ye, A. M. Cassel, H. Liu, K. J. Chao, J. Han, M. Meyyappan: Large-scale fabrication of carbon nanotube probe tips for atomic force microscopy critical dimension imaging applications, *Nano Lett.* **4**, 1301–1308 (2004)
- 3.135 K. Hata, D. N. Futaba, K. Mizuno, T. Namai, M. Yumara, S. Iijima: Water-assisted highly efficient synthesis of impurity-free single-walled carbon nanotubes, *Science* **306**, 1362–1364 (2004)
- 3.136 C. N. R. Rao, R. Sen, B. C. Satishkumar, A. Govindaraj: Large aligned carbon nanotubes bundles from ferrocene pyrolysis, *Chem. Commun.*, 1525–1526 (1998)
- 3.137 R. Andrews, D. Jacques, A. M. Rao, F. Derbyshire, D. Qian, X. Fan, E. C. Dickey, J. Chen: Continuous production of aligned carbon nanotubes: A step closer to commercial realization, *Chem. Phys. Lett.* **303**, 467–474 (1999)
- 3.138 X. Zhang, A. Cao, B. Wei, Y. Li, J. Wei, C. Xu, D. Wu: Rapid growth of well-aligned carbon nanotube arrays, *Chem. Phys. Lett.* **362**, 285–290 (2002)
- 3.139 X. Zhang, A. Cao, Y. Li, C. Xu, J. Liang, D. Wu, B. Wei: Self-organized arrays of carbon nanotube ropes, *Chem. Phys. Lett.* **351**, 183–188 (2002)
- 3.140 K. S. Choi, Y. S. Cho, S. Y. Hong, J. B. Park, D. J. Kim: Effects of ammonia on the alignment of carbon nanotubes in metal-assisted chemical vapor deposition, *J. Eur. Ceram. Soc.* **21**, 2095–2098 (2001)
- 3.141 N. S. Kim, Y. T. Lee, J. Park, J. B. Han, Y. S. Choi, S. Y. Choi, J. Choo, G. H. Lee: Vertically aligned carbon nanotubes grown by pyrolysis of iron, cobalt, and nickel phthalocyanines, *J. Phys. Chem. B* **107**, 9249–9255 (2003)
- 3.142 C. Emmeger, J. M. Bonard, P. Mauron, P. Sudan, A. Lepora, B. Grobety, A. Züttel, L. Schlapbach: Synthesis of carbon nanotubes over Fe catalyst on aluminum and suggested growth mechanism, *Carbon* **41**, 539–547 (2003)
- 3.143 M. Endo, H. W. Kroto: Formation of carbon nanofibers, *J. Phys. Chem.* **96**, 6941–6944 (1992)
- 3.144 R. S. Wagner: VLS mechanisms of crystal growth. In: *Whisker Technology*, ed. by P. Levit A. (Wiley, New York 1970) pp. 47–72
- 3.145 Y. H. Lee, S. G. Kim, D. Tomanek: Catalytic growth of single-wall carbon nanotubes: An ab initio study, *Phys. Rev. Lett.* **78**, 2393–2396 (1997)
- 3.146 V. Jourdain, H. Kanzow, M. Castignolles, A. Loiseau, P. Bernier: Sequential catalytic growth of carbon nanotubes, *Chem. Phys. Lett.* **364**, 27–33 (2002)
- 3.147 H. Dai: Carbon Nanotubes: Synthesis, integration, and properties, *Acc. Chem. Res.* **35**, 1035–1044 (2002)
- 3.148 Y. Saito, M. Okuda, N. Fujimoto, T. Yoshikawa, M. Tomita, T. Hayashi: Single-wall carbon nanotubes growing radially from Ni fine particles formed by arc evaporation, *Jpn. J. Appl. Phys.* **33**, L526–L529 (1994)
- 3.149 J. Bernholc, C. Brabec, M. Buongiorno Nardelli, A. Maiti, C. Roland, B. J. Yakobson: Theory of growth and mechanical properties of nanotubes, *Appl. Phys. A* **67**, 39–46 (1998)
- 3.150 M. Pacheco: Synthèse des nanotubes de carbone par arc électrique. Ph.D. Thesis (Université Toulouse III, Toulouse 2003)
- 3.151 K. Méténier, S. Bonnamy, F. Béguin, C. Journet, P. Bernier, L. M. de la Chapelle, O. Chauvet, S. Lefrant: Coalescence of single walled nanotubes and formation of multi-walled carbon nanotubes under high temperature treatments, *Carbon* **40**, 1765–1773 (2002)
- 3.152 P. G. Collins, P. Avouris: Nanotubes for electronics, *Sci. Am.* **283**, 38–45 (2000)
- 3.153 K. A. Williams, P. C. Eklund: Monte Carlo simulation of H₂ physisorption in finite diameter carbon nanotube ropes, *Chem. Phys. Lett.* **320**, 352–358 (2000)
- 3.154 Q.-H. Yang, P. X. Hou, S. Bai, M. Z. Wang, H. M. Cheng: Adsorption and capillarity of nitrogen in aggregated multi-walled carbon nanotubes, *Chem. Phys. Lett.* **345**, 18–24 (2001)
- 3.155 S. Inoue, N. Ichikuni, T. Suzuki, T. Uematsu, K. Kaneko: Capillary condensation of N₂ on multiwalled carbon nanotubes, *J. Phys. Chem.* **102**, 4689–4692 (1998)
- 3.156 S. Agnihotri, J. P. Mota, M. Rostam-Abadi, M. J. Rood: Structural characterization of single-walled carbon nanotube bundles by experiment and molecular simulation, *Langmuir* **21**, 896–904 (2005)
- 3.157 M. Eswaramoorthy, R. Sen, C. N. R. Rao: A study of micropores in single-walled carbon nanotubes by the adsorption of gases and vapors, *Chem. Phys. Lett.* **304**, 207–210 (1999)
- 3.158 A. Peigney, Ch. Laurent, E. Flahaut, R. R. Bacsa, A. Rousset: Specific surface area of carbon nanotubes and bundles of carbon nanotubes, *Carbon* **39**, 507–514 (2001)
- 3.159 E. Frackowiak, S. Delpeux, K. Jurewicz, K. Szostak, D. Cazorla-Amoros, F. Béguin: Enhanced capacitance of carbon nanotubes through chemical activation, *Chem. Phys. Lett.* **336**, 35–41 (2002)
- 3.160 E. Raymundo-Piñero, P. Azaïs, T. Cacciaguerra, D. Cazorla-Amorós, A. Linares-Solano, F. Béguin: KOH and NaOH activation mechanisms of multi-

- walled carbon nanotubes with different structural organisation, *Carbon* **43**, 786–795 (2005)
- 3.161 S. Delpoux, K. Szostak, E. Frackowiak, F. Béguin: An efficient two-step process for producing opened multi-walled carbon nanotubes of high purity, *Chem. Phys. Lett.* **404**, 374–378 (2005)
- 3.162 Z. Chen, W. Thiel, A. Hirsch: Reactivity of the convex and concave surfaces of single-walled carbon nanotubes (SWCNTs) towards addition reactions: dependence on the carbon-atom pyramidalization, *Chem. Phys. Chem.* **1**, 93–97 (2003)
- 3.163 S. Park, D. Srivastava, K. Cho: Generalized reactivity of curved surfaces: carbon nanotubes, *Nano Lett.* **3**, 1273–1277 (2003)
- 3.164 X. Lu, Z. Chen, P. Schleyer: Are Stone–Wales defect sites always more reactive than perfect sites in the sidewalls of single-wall carbon nanotubes?, *J. Am. Chem. Soc.* **127**, 20–21 (2005)
- 3.165 M. Muris, N. Dupont–Pavlosky, M. Bienfait, P. Zepfenfeld: Where are the molecules adsorbed on single-walled nanotubes?, *Surf. Sci.* **492**, 67–74 (2001)
- 3.166 R. B. Hallock, Y. H. Yang: Adsorption of helium and other gases to carbon nanotubes and nanotubes bundles, *J. Low Temp. Phys.* **134**, 21–30 (2004)
- 3.167 A. Fujiwara, K. Ishii, H. Suematsu, H. Kataura, Y. Maniwa, S. Suzuki, Y. Achiba: Gas adsorption in the inside and outside of single-walled carbon nanotubes, *Chem. Phys. Lett.* **336**, 205–211 (2001)
- 3.168 C. M. Yang, H. Kanoh, K. Kaneko, M. Yudasaka, S. Iijima: Adsorption behaviors of HiPco single-walled carbon nanotubes aggregates for alcohol vapors, *J. Phys. Chem.* **106**, 8994–8999 (2002)
- 3.169 D. H. Yoo, G. H. Rue, M. H. W. Chan, Y. W. Hwang, H. K. Kim: Study of nitrogen adsorbed on open-ended nanotube bundles, *J. Phys. Chem. B* **107**, 1540–1542 (2003)
- 3.170 J. Jiang, S. I. Sandler: Nitrogen adsorption on carbon nanotubes bundles: role of the external surface, *Phys. Rev. B* **68**, 245412–1–245412–9 (2003)
- 3.171 J. Zhao, A. Buldum, J. Han, J. P. Lu: Gas molecule adsorption in carbon nanotubes and nanotube bundles, *Nanotechnology* **13**, 195–200 (2002)
- 3.172 C. Matranga, B. Bockrath: Hydrogen-bonded and physisorbed CO in single-walled carbon nanotubes bundles, *J. Phys. Chem. B* **109**, 4853–4864 (2005)
- 3.173 M. D. Ellison, M. J. Crotty, D. Koh, R. L. Spray, K. E. Tate: Adsorption of NH₃ and NO₂ on single-walled carbon nanotubes, *J. Phys. Chem. B* **108**, 7938–7943 (2004)
- 3.174 S. Picozzi, S. Santucci, L. Lozzi, L. Valentin, B. Delley: Ozone adsorption on carbon nanotubes: the role of Stone–Wales defects, *J. Chem. Phys.* **120**, 7147–7152 (2004)
- 3.175 N. Chakrapani, Y. M. Zhang, S. K. Nayak, J. A. Moore, D. L. Carroll, Y. Y. Choi, P. M. Ajayan: Chemisorption of acetone on carbon nanotubes, *J. Phys. Chem. B* **107**, 9308–9311 (2003)
- 3.176 A. Chambers, C. Park, R. T. K. Baker, N. Rodriguez: Hydrogen storage in graphite nanofibers, *J. Phys. Chem. B* **102**, 4253–4256 (1998)
- 3.177 J. Giraudet, M. Dubois, D. Claves, J. P. Pinheiro, M. C. Schouler, P. Gadelle, A. Hamwi: Modifying the electronic properties of multi-wall carbon nanotubes via charge transfer, by chemical doping with some inorganic fluorides, *Chem. Phys. Lett.* **381**, 306–314 (2003)
- 3.178 J. Hilding, E. A. Grulke, S. B. Sinnott, D. Qian, R. Andrews, M. Jagtoyen: Sorption of butane on carbon multiwall nanotubes at room temperature, *Langmuir* **17**, 7540–7544 (2001)
- 3.179 K. Masenelli–Varlot, E. McRae, N. Dupont–Pavlosky: Comparative adsorption of simple molecules on carbon nanotubes. Dependence of the adsorption properties on the nanotube morphology, *Appl. Surf. Sci.* **196**, 209–215 (2002)
- 3.180 D. J. Browning, M. L. Gerrard, J. B. Lakeman, I. M. Mellor, R. J. Mortimer, M. C. Turpin: Studies into the storage of hydrogen in carbon nanofibers: Proposal of a possible mechanism, *Nanolett.* **2**, 201–205 (2002)
- 3.181 F. H. Yang, R. T. Yang: Ab initio molecular orbital study of adsorption of atomic hydrogen on graphite: insight into hydrogen storage in carbon nanotubes, *Carbon* **40**, 437–444 (2002)
- 3.182 A. D. Lueking, R. T. Yang: Hydrogen spillover to enhance hydrogen storage – study of the effect of carbon physicochemical properties, *Appl. Catal. A* **265**, 259–268 (2004)
- 3.183 G. E. Froudakis: Why alkali-metal-doped carbon nanotubes possess high hydrogen uptake, *Nanolett.* **1**, 531–533 (2001)
- 3.184 H. Ulbricht, G. Moos, T. Hertel: Physisorption of molecular oxygen on single-wall carbon nanotube bundles and graphite, *Phys. Rev. B* **66**, 075404–1–075404–7 (2002)
- 3.185 H. Ulbricht, J. Kriebel, G. Moos, T. Hertel: Desorption kinetics and interaction of Xe with single-wall carbon nanotube bundles, *Chem. Phys. Lett.* **363**, 252–260 (2002)
- 3.186 R. Saito, G. Dresselhaus, M. S. Dresselhaus: *Physical Properties of Carbon Nanotubes* (Imperial College Press, London 1998)
- 3.187 A. Charlier, E. McRae, R. Heyd, M. F. Charlier, D. Moretti: Classification for double-walled carbon nanotubes, *Carbon* **37**, 1779–1783 (1999)
- 3.188 A. Charlier, E. McRae, R. Heyd, M. F. Charlier: Metal semi-conductor transitions under uniaxial stress for single- and double-walled carbon nanotubes, *J. Phys. Chem. Solids* **62**, 439–444 (2001)
- 3.189 P. Puech, H. Hubel, D. Dunstan, R. R. Bacsa, Ch. Laurent, W. S. Bacsa: Discontinuous tangential stress in double wall carbon nanotubes, *Phys. Rev. Lett.* **93**, 095506 (2004)

- 3.190 P. M. Ajayan, M. Terrones, A. de la Guardia, V. Hue, N. Grobert, B. Q. Wei, H. Lezec, G. Ramanath, T. W. Ebbesen: Nanotubes in a flash – Ignition and reconstruction, *Science* **296**, 705 (2002)
- 3.191 H. Ajiki, T. Ando: Electronic states of carbon nanotubes, *J. Phys. Soc. Jap.* **62**, 1255–1266 (1993)
- 3.192 S. M. Bachilo, M. S. Strano, C. Kittrell, R. H. Hauge, R. E. Smalley, R. B. Weisman: Structure-assigned optical spectra of single-walled carbon nanotubes, *Science* **298**, 2361 (2002)
- 3.193 M. Bockrath, D. H. Cobden, J. Lu, A. G. Rinzler, R. E. Smalley, L. Balents, P. L. McEuen: Luttinger liquid behaviour in carbon nanotubes, *Nature* **397**, 598–601 (1999)
- 3.194 C. T. White, T. N. Todorov: Carbon nanotubes as long ballistic conductors, *Nature* **393**, 240–242 (1998)
- 3.195 S. Frank, P. Poncharal, Z. L. Wang, W. A. de Heer: Carbon nanotube quantum resistors, *Science* **280**, 1744–1746 (1998)
- 3.196 W. Liang, M. Bockrath, D. Bozovic, J. H. Hafner, M. Tinkham, H. Park: Fabry–Perot interference in a nanotube electron waveguide, *Nature* **411**, 665–669 (2001)
- 3.197 L. Langer, V. Bayot, E. Grivei, J.–P. Issi, J.–P. Heremans, C. H. Olk, L. Stockman, C. van Haesendonck, Y. Buynseraeder: Quantum transport in a multi-walled carbon nanotube, *Phys. Rev. Lett.* **76**, 479–482 (1996)
- 3.198 K. Liu, S. Roth, G. S. Duesberg, G. T. Kim, D. Popa, K. Mukhopadhyay, R. Doome, J. B'Nagy: Antilocalization in multiwalled carbon nanotubes, *Phys. Rev. B* **61**, 2375–2379 (2000)
- 3.199 G. Fedorov, B. Lassagne, M. Sagnes, B. Raquet, J. M. Broto, F. Triozon, S. Roche, E. Flahaut: Gate-dependent magnetoresistance phenomena in carbon nanotubes, *Phys. Rev. Lett.* **94**, 66801–66804 (2005)
- 3.200 A. Javey, J. Guo, Q. Wang, M. Lundstrom, H. Dai: Ballistic carbon nanotube field-effect transistors, *Nature* **424**, 654–657 (2003)
- 3.201 Y. A. Kasumov, R. Deblock, M. Kociak, B. Reulet, H. Bouchiat, I. I. Khodos, Y. B. Gorbatov, V. T. Volkov, C. Journet, M. Burghard: Supercurrents through single-walled carbon nanotubes, *Science* **284**, 1508–1511 (1999)
- 3.202 B. W. Alphenaar, K. Tsukagoshi, M. Wagner: Magnetoresistance of ferromagnetically contacted carbon nanotubes, *Phys. Eng.* **10**, 499–504 (2001)
- 3.203 S. Berber, Y. Kwon, D. Tomanek: Unusually high thermal conductivity of carbon nanotubes, *Phys. Rev. Lett.* **84**, 4613–4616 (2000)
- 3.204 S. N. Song, X. K. Wang, R. P. H. Chang, J. B. Ketterson: Electronic properties of graphite nanotubules from galvanomagnetic effects, *Phys. Rev. Lett.* **72**, 697–700 (1994)
- 3.205 M.–F. Yu, O. Lourie, M. J. Dyer, K. Moloni, T. F. Kelley, R. S. Ruoff: Strength and breaking mechanism of multiwalled carbon nanotubes under tensile load, *Science* **287**, 637–640 (2000)
- 3.206 D. A. Walters, L. M. Ericson, M. J. Casavant, J. Liu, D. T. Colbert, K. A. Smith, R. E. Smalley: Elastic strain of freely suspended single-wall carbon nanotube ropes, *Appl. Phys. Lett.* **74**, 3803–3805 (1999)
- 3.207 B. G. Demczyk, Y. M. Wang, J. Cumingd, M. Hetamn, W. Han, A. Zettl, R. O. Ritchie: Direct mechanical measurement of the tensile strength and elastic modulus of multiwalled carbon nanotubes, *Mater. Sci. Eng. A* **334**, 173–178 (2002)
- 3.208 R. P. Gao, Z. L. Wang, Z. G. Bai, W. A. De Heer, L. M. Dai, M. Gao: Nanomechanics of individual carbon nanotubes from pyrolytically grown arrays, *Phys. Rev. Lett.* **85**, 622–625 (2000)
- 3.209 M. M. J. Treacy, T. W. Ebbesen, J. M. Gibson: Exceptionally high Young's modulus observed for individual carbon nanotubes, *Nature* **381**, 678–680 (1996)
- 3.210 N. Yao, V. Lordie: Young's modulus of single-wall carbon nanotubes, *J. Appl. Phys.* **84**, 1939–1943 (1998)
- 3.211 O. Lourie, H. D. Wagner: Transmission electron microscopy observations of fracture of single-wall carbon nanotubes under axial tension, *Appl. Phys. Lett.* **73**, 3527–3529 (1998)
- 3.212 S. C. Tsang, Y. K. Chen, P. J. F. Harris, M. L. H. Green: A simple chemical method of opening and filling carbon nanotubes, *Nature* **372**, 159–162 (1994)
- 3.213 M. Monthieux: Filling single-wall carbon nanotubes, *Carbon* **40**, 1809–1823 (2002)
- 3.214 W. K. Hsu, S. Y. Chu, E. Munoz-Picone, J. L. Boldu, S. Firth, P. Franchi, B. P. Roberts, A. Schilder, H. Terrones, N. Grobert, Y. Q. Zhu, M. Terrones, M. E. McHenry, H. W. Kroto, D. R. M. Walton: Metallic behaviour of boron-containing carbon nanotubes, *Chem. Phys. Lett.* **323**, 572–579 (2000)
- 3.215 R. Czerw, M. Terrones, J. C. Charlier, X. Blasé, B. Foley, R. Kamalakaran, N. Grobert, H. Terrones, D. Tekleab, P. M. Ajayan, W. Blau, M. Rühle, D. L. Carroll: Identification of electron donor states, in N-doped carbon nanotubes, *Nanolett.* **1**, 457–460 (2001)
- 3.216 O. Stephan, P. M. Ajayan, C. Colliex, P. Redlich, J. M. Lambert, P. Bernier, P. Lefin: Doping graphitic and carbon nanotube structures with boron and nitrogen, *Science* **266**, 1683–1685 (1994)
- 3.217 A. Loiseau, F. Willaime, N. Demoncy, N. Schramchenko, G. Hug, C. Colliex, H. Pascard: Boron nitride nanotubes, *Carbon* **36**, 743–752 (1998)
- 3.218 C. C. Tang, L. M. de la Chapelle, P. Li, Y. M. Liu, H. Y. Dang, S. S. Fan: Catalytic growth of nanotube and nanobamboo structures of boron nitride, *Chem. Phys. Lett.* **342**, 492–496 (2001)
- 3.219 K. Suenaga, C. Colliex, N. Demoncy, A. Loiseau, H. Pascard, F. Willaime: Synthesis of nanoparticles and nanotubes with well separated layers

- of boron-nitride and carbon, *Science* **278**, 653–655 (1997)
- 3.220 D. Golberg, Y. Bando, L. Bourgeois, K. Kurashima, T. Sato: Large-scale synthesis and HRTEM analysis of single-walled B- and N-doped carbon nanotube bundles, *Carbon* **38**, 2017–2027 (2000)
- 3.221 R.S. Lee, J. Gavillet, M. Lamy de la Chapelle, A. Loiseau, J.-L. Cochon, D. Pigache, J. Thibault, F. Willaime: Catalyst-free synthesis of boron nitride single-wall nanotubes with a preferred zig-zag configuration, *Phys. Rev. B* **64**, 121405.1–121405.4 (2001)
- 3.222 B. Burteaux, A. Claye, B.W. Smith, M. Monthieux, D. E. Luzzi, J. E. Fischer: Abundance of encapsulated C₆₀ in single-wall carbon nanotubes, *Chem. Phys. Lett.* **310**, 21–24 (1999)
- 3.223 D. Ugarte, A. Châtelain, W. A. de Heer: Nanocapillarity and chemistry in carbon nanotubes, *Science* **274**, 1897–1899 (1996)
- 3.224 J. Cook, J. Sloan, M. L. H. Green: Opening and filling carbon nanotubes, *Fuller. Sci. Technol.* **5**, 695–704 (1997)
- 3.225 P. M. Ajayan, S. Iijima: Capillarity-induced filling of carbon nanotubes, *Nature* **361**, 333–334 (1993)
- 3.226 P. M. Ajayan, T. W. Ebbesen, T. Ichihashi, S. Iijima, K. Tanigaki, H. Hiura: Opening carbon nanotubes with oxygen and implications for filling, *Nature* **362**, 522–525 (1993)
- 3.227 S. Seraphin, D. Zhou, J. Jiao, J. C. Withers, R. Loufty: Yttrium carbide in nanotubes, *Nature* **362**, 503 (1993)
- 3.228 S. Seraphin, D. Zhou, J. Jiao, J. C. Withers, R. Loufty: Selective encapsulation of the carbides of yttrium and titanium into carbon nanoclusters, *Appl. Phys. Lett.* **63**, 2073–2075 (1993)
- 3.229 R.S. Ruoff, D. C. Lorents, B. Chan, R. Malhotra, S. Subramoney: Single-crystal metals encapsulated in carbon nanoparticles, *Science* **259**, 346–348 (1993)
- 3.230 A. Loiseau, H. Pascard: Synthesis of long carbon nanotubes filled with Se, S, Sb, and Ge by the arc method, *Chem. Phys. Lett.* **256**, 246–252 (1996)
- 3.231 N. Démoncy, O. Stephan, N. Brun, C. Colliex, A. Loiseau, H. Pascard: Filling carbon nanotubes with metals by the arc discharge method: The key role of sulfur, *Eur. Phys. J. B* **4**, 147–157 (1998)
- 3.232 E. Flahaut, J. Sloan, K. S. Coleman, V. C. Williams, S. Friedrichs, N. Hanson, M. L. H. Green: 1D p-block halide crystals confined into single walled carbon nanotubes, *Proc. Mater. Res. Soc. Symp.* **633**, A13.15.1–A13.15.6 (2001)
- 3.233 C. H. Kiang, J. S. Choi, T. T. Tran, A. D. Bacher: Molecular nanowires of 1 nm diameter from capillary filling of single-walled carbon nanotubes, *J. Phys. Chem. B* **103**, 7449–7551 (1999)
- 3.234 Z. L. Zhang, B. Li, Z. J. Shi, Z. N. Gu, Z. Q. Xue, L. M. Peng: Filling of single-walled carbon nanotubes with silver, *J. Mater. Res.* **15**, 2658–2661 (2000)
- 3.235 A. Govindaraj, B. C. Satishkumar, M. Nath, C. N. R. Rao: Metal nanowires and intercalated metal layers in single-walled carbon nanotubes bundles, *Chem. Mater.* **12**, 202–205 (2000)
- 3.236 J. Mittal, M. Monthieux, H. Allouche: Room temperature filling of single-wall carbon nanotubes with chromium oxide in open air, *Chem. Phys. Lett.* **339**, 311–318 (2001)
- 3.237 E. Dujardin, T. W. Ebbesen, H. Hiura, K. Tanigaki: Capillarity and wetting of carbon nanotubes, *Science* **265**, 1850–1852 (1994)
- 3.238 J. Sloan, A. I. Kirkland, J. L. Hutchison, M. L. H. Green: Integral atomic layer architectures of 1D crystals inserted into single walled carbon nanotubes, *Chem. Commun.*, 1319–1332 (2002)
- 3.239 J. Sloan, M. C. Novotny, S. R. Bailey, G. Brown, C. Xu, V. C. Williams, S. Friedrichs, E. Flahaut, R. L. Calender, A. P. E. York, K. S. Coleman, M. L. H. Green, R. E. Dunin-Borkowski, J. L. Hutchison: Two layer 4 : 4 co-ordinated KI crystals grown within single walled carbon nanotubes, *Chem. Phys. Lett.* **329**, 61–65 (2000)
- 3.240 G. Brown, S. R. Bailey, J. Sloan, C. Xu, S. Friedrichs, E. Flahaut, K. S. Coleman, J. L. Hutchinson, R. E. Dunin-Borkowski, M. L. H. Green: Electron beam induced in situ clusterisation of 1D ZrCl₄ chains within single-walled carbon nanotubes, *Chem. Commun.*, 845–846 (2001)
- 3.241 J. Sloan, D. M. Wright, H. G. Woo, S. Bailey, G. Brown, A. P. E. York, K. S. Coleman, J. L. Hutchison, M. L. H. Green: Capillarity and silver nanowire formation observed in single walled carbon nanotubes, *Chem. Commun.*, 699–700 (1999)
- 3.242 X. Fan, E. C. Dickey, P. C. Eklund, K. A. Williams, L. Grigorian, R. Buczko, S. T. Pantelides, S. J. Pennycook: Atomic arrangement of iodine atoms inside single-walled carbon nanotubes, *Phys. Rev. Lett.* **84**, 4621–4624 (2000)
- 3.243 G. Brown, S. R. Bailey, M. Novotny, R. Carter, E. Flahaut, K. S. Coleman, J. L. Hutchison, M. L. H. Green, J. Sloan: High yield incorporation and washing properties of halides incorporated into single walled carbon nanotubes, *Appl. Phys. A* **76**, 457–462 (2003)
- 3.244 J. Sloan, D. E. Luzzi, A. I. Kirkland, J. L. Hutchison, M. L. H. Green: Imaging and characterization of molecules and one-dimensional crystals formed within carbon nanotubes, *Mater. Res. Soc. Bull.* **29**, 265–271 (2004)
- 3.245 J. Chancolon, F. Archaimbault, A. Pineau, S. Bonnamy: Confinement of selenium into carbon nanotubes, *Fuller. Nanotub. Car. N.* **13**, 189–194 (2005)
- 3.246 B. W. Smith, M. Monthieux, D. E. Luzzi: Encapsulated C₆₀ in carbon nanotubes, *Nature* **396**, 323–324 (1998)
- 3.247 B. W. Smith, D. E. Luzzi: Formation mechanism of fullerene peapods and coaxial tubes: A path to large scale synthesis, *Chem. Phys. Lett.* **321**, 169–174 (2000)
- 3.248 K. Hirahara, K. Suenaga, S. Bandow, H. Kato, T. Okazaki, H. Shinohara, S. Iijima: One-dimensional metallo-fullerene crystal generated inside single-

- walled carbon nanotubes, *Phys. Rev. Lett.* **85**, 5384–5387 (2000)
- 3.249 B. W. Smith, M. Monthioux, D. E. Luzzi: Carbon nanotube encapsulated fullerenes: A unique class of hybrid material, *Chem. Phys. Lett.* **315**, 31–36 (1999)
- 3.250 D. E. Luzzi, B. W. Smith: Carbon cage structures in single wall carbon nanotubes: A new class of materials, *Carbon* **38**, 1751–1756 (2000)
- 3.251 S. Bandow, M. Takisawa, K. Hirahara, M. Yudasoka, S. Iijima: Raman scattering study of double-wall carbon nanotubes derived from the chains of fullerenes in single-wall carbon nanotubes, *Chem. Phys. Lett.* **337**, 48–54 (2001)
- 3.252 Y. Sakurabayashi, M. Monthioux, K. Kishita, Y. Suzuki, T. Kondo, M. Le Lay: Tayloring double wall carbon nanotubes?. In: *Molecular Nanostructures*, Amer. Inst. Phys. Conf. Proc., Vol. 685, ed. by H. Kuzmany, J. Fink, M. Mehring, S. Roth (Springer, Berlin Heidelberg 2003) pp. 302–305
- 3.253 B. W. Smith, D. E. Luzzi, Y. Achiba: Tumbling atoms and evidence for charge transfer in $\text{La}_2@\text{C}_{80}@\text{SWNT}$, *Chem. Phys. Lett.* **331**, 137–142 (2000)
- 3.254 K. Suenaga, M. Tence, C. Mory, C. Colliex, H. Kato, T. Okazaki, H. Shinohara, K. Hirahara, S. Bandow, S. Iijima: Element-selective single atom imaging, *Science* **290**, 2280–2282 (2000)
- 3.255 D. E. Luzzi, B. W. Smith, R. Russo, B. C. Satishkumar, F. Stercel, N. R. C. Nemes: Encapsulation of metallofullerenes and metallocenes in carbon nanotubes, *Proc. Electronic Properties of Novel Materials–XVI Int. Winterschool – AIP Conf. Proc.*, ed. by H. Kuzmany, J. Fink, M. Mehring, S. Roth (Springer, Berlin Heidelberg 2001) 622–626
- 3.256 D. J. Hornbaker, S.-J. Kahng, S. Misra, B. W. Smith, A. T. Johnson, E. J. Mele, D. E. Luzzi, A. Yazdani: Mapping the one-dimensional electronic states of nanotube peapod structures, *Science* **295**, 828–831 (2002)
- 3.257 H. Kondo, H. Kino, T. Ohno: Transport properties of carbon nanotubes encapsulating C_{60} and related materials, *Phys. Rev. B* **71**, 115413 (2005)
- 3.258 S. H. Jhang, S. W. Lee, D. S. Lee, Y. W. Park, G. H. Jeong, T. Hirata, R. Hatakeyama, U. Dettlaff, S. Roth, M. S. Kabir, E. E. B. Campbell: Random telegraph noise in carbon nanotube peapod transistors, *Fuller. Nanotub. Car. N.* **13**, 195–198 (2005)
- 3.259 G. H. Jeong, R. Hatakeyama, T. Hirata, K. Tohji, K. Motomiya, N. Sato, Y. Kawazoe: Structural deformation of single-walled carbon nanotubes and fullerene encapsulation due to magnetized plasma ion irradiation, *Appl. Phys. Lett.* **79**, 4213–4215 (2001)
- 3.260 Y. P. Sun, K. Fu, Y. Lin, W. Huang: Functionalized carbon nanotubes: Properties and applications, *Acc. Chem. Res.* **35**, 1095–1104 (2002)
- 3.261 S. Osswald, E. Flahaut, H. Ye, Y. Gogotsi: Elimination of D-band in Raman spectra of double-wall carbon nanotubes by oxidation, *Chem. Phys. Lett.* **402**, 422–427 (2005)
- 3.262 J. Chen, M. A. Hamon, M. Hui, C. Yongsheng, A. M. Rao, P. C. Eklund, R. C. Haddon: Solution properties of single-walled carbon nanotubes, *Science* **282**, 95–98 (1998)
- 3.263 J. Chen, A. M. Rao, S. Lyuksyutov, M. E. Itkis, M. A. Hamon, H. Hu, R. W. Cohn, P. C. Eklund, D. T. Colbert, R. E. Smalley, R. C. Haddon: Dissolution of full-length single-walled carbon nanotubes, *J. Phys. Chem. B* **105**, 2525–2528 (2001)
- 3.264 F. Pompeo, D. E. Resasco: Water solubilization of single-walled carbon nanotubes by functionalization with glucosamine, *Nanolett.* **2**, 369–373 (2002)
- 3.265 Y. P. Sun, W. Huang, Y. Lin, K. Fu, A. Kitaygorodskiy, L. A. Riddle, Y. J. Yu, D. L. Carroll: Soluble dendron-functionalized carbon nanotubes: Preparation, characterization, and properties, *Chem. Mater.* **13**, 2864–2869 (2001)
- 3.266 K. Fu, W. Huang, Y. Lin, L. A. Riddle, D. L. Carroll, Y. P. Sun: Defunctionalization of functionalized carbon nanotubes, *Nanolett.* **1**, 439–441 (2001)
- 3.267 P. W. Chiu, G. S. Duesberg, U. Dettlaff-Weglikowska, S. Roth: Interconnection of carbon nanotubes by chemical functionalization, *Appl. Phys. Lett.* **80**, 3811–3813 (2002)
- 3.268 E. T. Mickelson, C. B. Huffman, A. G. Rinzler, R. E. Smalley, R. H. Hauge, J. L. Margrave: Fluorination of single-wall carbon nanotubes, *Chem. Phys. Lett.* **296**, 188–194 (1998)
- 3.269 V. N. Khabashesku, W. E. Billups, J. L. Margrave: Fluorination of single-wall carbon nanotubes and subsequent derivatization reactions, *Acc. Chem. Res.* **35**, 1087–1095 (2002)
- 3.270 P. J. Boul, J. Liu, E. T. Michelson, C. B. Huffman, L. M. Ericson, I. W. Chiang, K. A. Smith, D. T. Colbert, R. H. Hauge, J. L. Margrave, R. E. Smalley: Reversible side-wall functionalization of buckytubes, *Chem. Phys. Lett.* **310**, 367–372 (1999)
- 3.271 J. L. Bahr, J. Yang, D. V. Kosynkin, M. J. Bronikowski, R. E. Smalley, J. M. Tour: Functionalization of carbon nanotubes by electrochemical reduction of aryl diazonium salts: A bucky paper electrode, *J. Am. Chem. Soc.* **123**, 6536–6542 (2001)
- 3.272 M. Holzinger, O. Vostrowsky, A. Hirsch, F. Hennrich, M. Kappes, R. Weiss, F. Jellen: Sidewall functionalization of carbon nanotubes, *Angew. Chem. Int. Ed.* **40**, 4002–4005 (2001)
- 3.273 Y. Chen, R. C. Haddon, S. Fang, A. M. Rao, P. C. Eklund, W. H. Lee, E. C. Dickey, E. A. Grulke, J. C. Pendergrass, A. Chavan, B. E. Haley, R. E. Smalley: Chemical attachment of organic functional groups to single-walled carbon nanotube material, *J. Mater. Res.* **13**, 2423–2431 (1998)
- 3.274 C. Velasco-Santos, A. L. Martinez-Hernandez, M. Lozada-Cassou, A. Alvarez-Castillo, V. M. Castano: Chemical functionalization of carbon nanotubes through an organosilane, *Nanotechnology* **13**, 495–498 (2002)

- 3.275 A. Star, J. F. Stoddart, D. Steuerman, M. Diehl, A. Boukai, E. W. Wong, X. Yang, S. W. Chung, H. Choi, J. R. Heath: Preparation and properties of polymer-wrapped single-walled carbon nanotubes, *Angew. Chem. Int. Ed.* **41**, 1721–1725 (2002)
- 3.276 A. Pénicaud, P. Poulin, A. Derré, E. Anglaret, P. Petit: Spontaneous dissolution of a single-wall carbon nanotube salt, *J. Amer. Chem. Soc.* **127**, 8–9 (2005)
- 3.277 R. Stevens, C. Nguyen, A. Cassel, L. Delzeit, M. Meyyappan, J. Han: Improved fabrication approach for carbon nanotube probe devices, *Appl. Phys. Lett.* **77**, 3453–3455 (2000)
- 3.278 J. H. Hafner, C. L. Cheung, A. T. Wooley, C. M. Lieber: Structural and functional imaging with carbon nanotube AFM probes, *Progr. Biophys. Molec. Biol.* **77**, 73–110 (2001)
- 3.279 S. S. Wong, E. Joselevich, A. T. Woodley, C. L. Cheung, C. M. Lieber: Covalently functionalized nanotubes as nanometre-size probes in chemistry and biology, *Nature* **394**, 52–55 (1998)
- 3.280 C. L. Cheung, J. H. Hafner, C. M. Lieber: Carbon nanotube atomic force microscopy tips: Direct growth by chemical vapor deposition and application to high-resolution imaging, *Proc. Natl. Acad. Sci. USA* **97**, 3809–3813 (2000)
- 3.281 W. A. de Heer, A. Châtelain, D. Ugarte: A carbon nanotube field-emission electron source, *Science* **270**, 1179–1180 (1995)
- 3.282 J. M. Bonard, J. P. Salvetat, T. Stockli, W. A. de Heer, L. Forro, A. Chatelâin: Field emission from single-wall carbon nanotube films, *Appl. Phys. Lett.* **73**, 918–920 (1998)
- 3.283 W. Zhu, C. Bower, O. Zhou, G. Kochanski, S. Jin: Large current density from carbon nanotube field emitters, *Appl. Phys. Lett.* **75**, 873–875 (1999)
- 3.284 Y. Saito, R. Mizushima, T. Tanaka, K. Tohji, K. Uchida, M. Yumura, S. Uemura: Synthesis, structure, and field emission of carbon nanotubes, *Fuller. Sci. Technol.* **7**, 653–664 (1999)
- 3.285 J. Kong, N. R. Franklin, C. Zhou, M. G. Chapline, S. Peng, K. Cho, H. Dai: Nanotube molecular wire as chemical sensors, *Science* **287**, 622–625 (2000)
- 3.286 P. G. Collins, K. Bradley, M. Ishigami, A. Zettl: Extreme oxygen sensitivity of electronic properties of carbon nanotubes, *Science* **287**, 1801–1804 (2000)
- 3.287 H. Chang, J. D. Lee, S. M. Lee, Y. H. Lee: Adsorption of NH₃ and NO₂ molecules on carbon nanotubes, *Appl. Phys. Lett.* **79**, 3863–3865 (2001)
- 3.288 C. Cantalini, L. Valentini, L. Lozzi, I. Armentano, J. M. Kenny, S. Santucci: NO₂ gas sensitivity of carbon nanotubes obtained by plasma enhanced chemical vapor deposition, *Sensor. Actuat. B* **93**, 333–337 (2003)
- 3.289 J. Li, Y. Lu, Q. Ye, M. Cinke, J. Han, M. Meyyappan: Carbon nanotubes sensors for gas and organic vapor detection, *Nano Lett.* **3**, 929–933 (2003)
- 3.290 O. K. Varghese, P. D. Kichambre, D. Gong, K. G. Ong, E. C. Dickey, C. A. Grimes: Gas sensing characteristics of multi-wall carbon nanotubes, *Sensor. Actuat. B* **81**, 32–41 (2001)
- 3.291 K. G. Ong, K. Zeng, C. A. Grimes: A wireless, passive carbon nanotube-based gas sensor, *IEEE Sens. J.* **2/2**, 82–88 (2002)
- 3.292 J. Kong, M. G. Chapline, H. Dai: Functionalized carbon nanotubes for molecular hydrogen sensors, *Adv. Mater.* **13**, 1384–1386 (2001)
- 3.293 A. Modi, N. Koratkar, E. Lass, B. Wei, P. M. Ajayan: Miniaturized gas ionisation sensors using carbon nanotubes, *Nature* **424**, 171–174 (2003)
- 3.294 F. Rodriguez-Reinoso: The role of carbon materials in heterogeneous catalysis, *Carbon* **36**, 159–175 (1998)
- 3.295 E. Auer, A. Freund, J. Pietsch, T. Tacke: Carbon as support for industrial precious metal catalysts, *Appl. Catal. A* **173**, 259–271 (1998)
- 3.296 J. M. Planeix, N. Coustel, B. Coq, B. Botrons, P. S. Kumbhar, R. Dutartre, P. Geneste, P. Bernier, P. M. Ajayan: Application of carbon nanotubes as supports in heterogeneous catalysis, *J. Am. Chem. Soc.* **116**, 7935–7936 (1994)
- 3.297 P. Serp, M. Corrias, P. Kalck: Carbon nanotubes and nanofibers in catalysis, *Appl. Catal. A* **253**, 337–358 (2003)
- 3.298 K. P. De Jong, J. W. Geus: Carbon nanofibers: catalytic synthesis and applications, *Catal. Rev.* **42**, 481–510 (2000)
- 3.299 N. F. Goldshleger: Fullerene and fullerene-based materials in catalysis, *Fuller. Sci. Technol.* **9**, 255–280 (2001)
- 3.300 M. F. R. Pereira, J. L. Figueiredo, J. J. M. Órfão, P. Serp, P. Kalck, Y. Kihn: Catalytic activity of carbon nanotubes in the oxidative dehydrogenation of ethylbenzene, *Carbon* **42**, 2807–2813 (2004)
- 3.301 G. Mestl, N. I. Maksimova, N. Keller, V. V. Roddatis, R. Schlögl: Carbon nanofilaments in heterogeneous catalysis: An industrial application for new carbon materials?, *Angew. Chem. Int. Ed. Engl.* **40**, 2066–2068 (2001)
- 3.302 N. Muradov: Catalysis of methane decomposition over elemental carbon, *Catal. Commun.* **2**, 89–94 (2001)
- 3.303 J. E. Fischer, A. T. Johnson: Electronic properties of carbon nanotubes, *Curr. Opin. Solid State Mater. Sci.* **4**, 28–33 (1999)
- 3.304 M. Menon, A. N. Andriotis, G. E. Froudakis: Curvature dependence of the metal catalyst atom interaction with carbon nanotubes walls, *Chem. Phys. Lett.* **320**, 425–434 (2000)
- 3.305 Z. Liu, X. Lin, J. Y. Lee, W. Zhang, M. Han, L. M. Gan: Preparation and characterization of platinum-based electrocatalysts on multiwalled carbon nanotubes for proton exchange membrane fuel cells, *Langmuir* **18**, 4054–4060 (2002)

- 3.306 R. Giordano, P. Serp, P. Kalck, Y. Kihn, J. Schreiber, C. Marhic, J.-L. Duvail: Preparation of rhodium supported on carbon nanotubes catalysts via surface mediated organometallic reaction, *Eur. J. Inorg. Chem.*, 610–617 (2003)
- 3.307 H.-B. Chen, J.D. Lin, Y. Cai, X.Y. Wang, J. Yi, J. Wang, G. Wei, Y.Z. Lin, D.W. Liao: Novel multi-walled nanotube-supported and alkali-promoted Ru catalysts for ammonia synthesis under atmospheric pressure, *Appl. Surf. Sci.* **180**, 328–335 (2001)
- 3.308 Y. Zhang, H. B. Zhang, G. D. Lin, P. Chen, Y. Z. Yuan, K. R. Tsai: Preparation, characterization and catalytic hydroformylation properties of carbon nanotubes-supported Rh-phosphine catalyst, *Appl. Catal. A* **187**, 213–224 (1999)
- 3.309 T. Kyotani, S. Nakazaki, W.-H. Xu, A. Tomita: Chemical modification of the inner walls of carbon nanotubes by HNO₃ oxidation, *Carbon* **39**, 782–785 (2001)
- 3.310 Z.J. Liu, Z.Y. Yuan, W. Zhou, L.M. Peng, Z. Xu: Co/carbon nanotubes monometallic system: The effects of oxidation by nitric acid, *Phys. Chem. Chem. Phys.* **3**, 2518–2521 (2001)
- 3.311 Carillo, J.A. Swartz, J.M. Gamba, R.S. Kane, N. Chakrapani, B. Wei, P.M. Ajayan: Noncovalent functionalization of graphite and carbon nanotubes with polymer multilayers and gold nanoparticles, *Nano Lett.* **3**, 1437–1440 (2003)
- 3.312 M.S. Dresselhaus, K.A. Williams, P.C. Eklund: Hydrogen adsorption in carbon materials, *Mater. Res. Soc. Bull.* **24**, 45–50 (1999)
- 3.313 H.-M. Cheng, Q.-H. Yang, C. Liu: Hydrogen storage in carbon nanotubes, *Carbon* **39**, 1447–1454 (2001)
- 3.314 G.G. Tibbetts, G.P. Meisner, C.H. Olk: Hydrogen storage capacity of carbon nanotubes, filaments, and vapor-grown fibers, *Carbon* **39**, 2291–2301 (2001)
- 3.315 F. L. Darkrim, P. Malbrunot, G. P. Tartaglia: Review of hydrogen storage adsorption in carbon nanotubes, *Int. J. Hydrogen Energy* **27**, 193–202 (2002)
- 3.316 G.E. Froudakis: Hydrogen interaction with carbon nanotubes: a review of ab initio studies, *J. Phys.: Condens. Matter* **14**, R453–R465 (2002)
- 3.317 M. Hirscher, M. Becher: Hydrogen storage in carbon nanotubes, *J. Nanosci. Nanotechnol.* **3(1–2)**, 3–17 (2003)
- 3.318 C. Park, P.E. Anderson, C.D. Tan, R. Hidalgo, N. Rodriguez: Further studies of the interaction of hydrogen with graphite nanofibers, *J. Phys. Chem. B* **103**, 10572–1058 (1999)
- 3.319 A.D. Lueking, R.T. Yang, N.M. Rodriguez, R.T.K. Baker: Hydrogen storage in graphite nanofibers: effect of synthesis catalyst and pretreatment conditions, *Langmuir* **20(3)**, 714–721 (2004)
- 3.320 A.D. Lueking, R.T. Yang: Hydrogen storage in carbon nanotubes: residual metal content and pretreatment temperature, *AIChE J.* **49(6)**, 1556–1568 (2003)
- 3.321 C.C. Ahn, Y. Ye, B.V. Ratnakumar, C. Witham, R.C. Bowman, B. Fultz: Hydrogen adsorption measurements on graphite nanofibers, *Appl. Phys. Lett.* **73**, 3378–3380 (1998)
- 3.322 Q. Wang, J.K. Johnson: Computer simulations of hydrogen adsorption on graphite nanofibers, *J. Phys. Chem. B* **103**, 277–281 (1999)
- 3.323 M. Rzepka, P. Lamp, M.A. de la Casa-Lillo: Physisorption of hydrogen on microporous carbon and carbon nanotubes, *J. Phys. Chem. B* **102**, 10894–10898 (1998)
- 3.324 A.C. Dillon, K.M. Jones, T.A. Bekkedahl, C.H. Kiang, D.S. Bethune, M.J. Heben: Storage of hydrogen in single-walled carbon nanotubes, *Nature* **386**, 377–379 (1997)
- 3.325 K. Shen, T. Pietrass: ¹H and ²H NMR of hydrogen adsorption on carbon nanotubes, *J. Phys. Chem. B* **108**, 9937–9942 (2004)
- 3.326 Y. Ye, C.C. Ahn, C. Witham, R.C. Bowman, B. Fultz, J. Liu, A.G. Rinzler, D. Colbert, K.A. Smith, R.E. Smalley: Hydrogen adsorption and cohesive energy of single-walled carbon nanotubes, *Appl. Phys. Lett.* **74**, 2307–2309 (1999)
- 3.327 C. Liu, Y.Y. Fan, M. Liu, H.T. Cong, H.M. Cheng, M.S. Dresselhaus: Hydrogen storage in single-walled carbon nanotubes at room temperature, *Science* **286**, 1127–1129 (1999)
- 3.328 M. Hirscher, M. Becher, M. Haluska, U. Dettlaff-Weglikowska, A. Quintel, G.S. Duesberg, Y.M. Choi, P. Dwonos, M. Hulman, S. Roth, I. Stepanek, P. Bernier: Hydrogen storage in sonicated carbon materials, *Appl. Phys. A* **72**, 129–132 (2001)
- 3.329 H.G. Schimmel, G.J. Kearley, M.G. Nijkamp, C.T. Visser, K.P. de Jong, F.M. Mulder: Hydrogen adsorption in carbon nanostructures: comparison of nanotubes, fibers, and coals, *Chem. Eur. J.* **9**, 4764–4770 (2003)
- 3.330 M.R. Smith Jr, E.W. Bittner, W. Shi, J.K. Johnson, B.C. Bockrath: Chemical activation of single-walled nanotubes for hydrogen adsorption, *J. Phys. Chem. B* **107**, 3752–3760 (2003)
- 3.331 A. Ansón, M.A. Callejas, A.M. Benito, W.K. Maser, M.T. Izquierdo, B. Rubio, J. Jagiello, M. Tomes, J.B. Parra, M.T. Martinez: Hydrogen adsorption studies on single wall carbon nanotubes, *Carbon* **42**, 1243–1248 (2004)
- 3.332 C.Q. Ning, F. Wei, G.H. Luo, Q.X. Wang, Y.L. Wu, H. Yu: Hydrogen storage in multi-wall carbon nanotubes using samples up to 85 g, *Appl. Phys. A* **78**, 955–959 (2004)
- 3.333 P.A. Gordon, R.B. Saeger: Molecular modeling of adsorptive energy storage: Hydrogen storage in single-walled carbon nanotubes, *Ind. Eng. Chem. Res.* **38**, 4647–4655 (1999)
- 3.334 P. Marinelli, R. Pellenq, J. Conard: *H stocké dans les carbones un site légèrement métastable*, AF-14-020 (National Conference on Materials, Tours, France 2002)

- 3.335 S. M. Lee, H. Y. Lee, T. Frauenheim, M. Elstner, Y. G. Hwang: Hydrogen storage in single-walled and multi walled carbon nanotubes, Proc. of Material Research Society Symposium **593**, 187–192 (1999)
- 3.336 S. M. Lee, H. Y. Lee: Hydrogen storage in single-walled carbon nanotubes, Appl. Phys. Lett. **76**, 2877–2879 (2000)
- 3.337 S. M. Lee, K. S. Park, Y. C. Choi, Y. S. Park, J. M. Bok, D. J. Bae, K. S. Nahm, Y. G. Choi, C. S. Yu, N. Kim, T. Frauenheim, Y. H. Lee: Hydrogen adsorption in carbon nanotubes, Synth. Met. **113**, 209–216 (2000)
- 3.338 X. Zhang, D. Cao, J. Chen: Hydrogen adsorption storage on single-walled carbon nanotube arrays by a combination of classical potential and density functional theory, J. Phys. Chem. B **107**, 4942–4950 (2003)
- 3.339 H. M. Cheng, G. P. Pez, A. C. Cooper: Mechanism of hydrogen sorption in single-walled carbon nanotubes, J. Am. Chem. Soc. **123**, 5845–5846 (2001)
- 3.340 M. A. de la Casa-Lillo, F. Lamari-Darkrim, D. Cazorla-Amoros, A. Linares-Solano: Hydrogen storage in activated carbons and activated carbon fibers, J. Phys. Chem. B **106**, 10930–10934 (2002)
- 3.341 A. Kusnetzova, D. B. Mawhinney, V. Naumenko, J. T. Yates, J. Liu, R. E. Smalley: Enhancement of adsorption inside of single-walled nanotubes: Opening the entry ports, Chem. Phys. Lett. **321**, 292–296 (2000)
- 3.342 G. E. Gadd, M. Blackford, S. Moricca, N. Webb, P. J. Evans, A. M. Smith, G. Jacobsen, S. Leung, A. Day, Q. Hua: The world's smallest gas cylinders?, Science **277**, 933–936 (1997)
- 3.343 Z. Mao, S. B. Sinnott: A computational study of molecular diffusion and dynamic flow through carbon nanotubes, J. Phys. Chem. B **104**, 4618–4624 (2000)
- 3.344 Z. Mao, S. B. Sinnott: Separation of organic molecular mixtures in carbon nanotubes and bundles: Molecular dynamics simulations, J. Phys. Chem. B **105**, 6916–6924 (2001)
- 3.345 H. Chen, D. S. Sholl: Rapid diffusion of CH₄/H₂ mixtures in single-walled carbon nanotubes, J. Am. Chem. Soc. **126**, 7778–7779 (2004)
- 3.346 C. Gu, G.-H. Gao, Y. X. Yu, T. Nitta: Simulation for separation of hydrogen and carbon monoxide by adsorption on single-walled carbon nanotubes, Fluid Phase Equil. **194/197**, 297–307 (2002)
- 3.347 R. Q. Long, R. T. Yang: Carbon nanotubes as superior sorbent for dioxine removal, J. Am. Chem. Soc. **123**, 2058–2059 (2001)
- 3.348 Y. H. Li, S. Wang, A. Cao, D. Zhao, X. Zhang, C. Xu, Z. Luan, D. Ruan, J. Liang, D. Wu, B. Wei: Adsorption of fluoride from water by amorphous alumina supported on carbon nanotubes, Chem. Phys. Lett. **350**, 412–416 (2001)
- 3.349 Y. H. Li, S. Wang, J. Wei, X. Zhang, C. Xu, Z. Luan, D. Wu, B. Wei: Lead adsorption on carbon nanotubes, Chem. Phys. Lett. **357**, 263–266 (2002)
- 3.350 C. Park, E. S. Engel, A. Crowe, T. R. Gilbert, N. M. Rodriguez: Use of carbon nanofibers in the removal of organic solvents from water, Langmuir **16**, 8050–8056 (2000)
- 3.351 X. Peng, Y. Li, Z. Luan, Z. Di, H. Wang, B. Tian, Z. Jia: Adsorption of 1,2-dichlorobenzene from water to carbon nanotubes, Chem. Phys. Lett. **376**, 154–158 (2003)
- 3.352 P. Kondratyuk, J. T. Yates: Nanotubes as molecular sponges: the adsorption of CCl₄, Chem. Phys. Lett. **383**, 314–316 (2004)
- 3.353 A. Huczko, H. Lange, E. Calko, H. Grubek-Jaworska, P. Droszcz: Physiological testing of carbon nanotubes: are they asbestos-like?, Full. Sci. Technol. **9**, 251–254 (2001)
- 3.354 A. A. Shvedova, V. Castranova, E. R. Kisin, D. Schwegler-Berry, A. R. Murray, V. Z. Gandelman, A. M. Maynard, P. Baron: Exposure to carbon nanotube material: assessment of nanotube cytotoxicity using human keratinocyte cells, Toxicol. Env. Health A **66**, 1909–1926 (2003)
- 3.355 C. W. Lam, J. T. James, R. McCluskey, R. L. Hunter: Pulmonary toxicity of single-wall carbon nanotubes in mice 7 and 90 days after intratracheal instillation, Toxicol. Sci. **77**, 126–134 (2004)
- 3.356 D. Pantarotto, J. P. Briand, M. Prato, A. Bianco: Translocation of bioactive peptides across cell membranes by carbon nanotubes, Chem. Commun., 16–17 (2004)
- 3.357 C. Salvador-Morales, E. Flahaut, E. Sim, J. Sloan, M. L. H. Green, R. B. Sim: Complement activation and protein adsorption by carbon nanotubes, Molec. Immun. **43**, 193–201 (2006)
- 3.358 M. P. Mattson, R. C. Haddon, A. M. Rao: Molecular functionalization of carbon nanotubes and use as substrates for neuronal growth, J. Molec. Neurosci. **14**, 175–182 (2000)
- 3.359 J. J. Davis, M. L. H. Green, H. A. O. Hill, Y. C. Leung, P. J. Sadler, J. Sloan, A. V. Xavier, S. C. Tsang: The immobilization of proteins in carbon nanotubes, Inorg. Chim. Acta **272**, 261–266 (1998)
- 3.360 R. J. Chen, Y. Zhang, D. Wang, H. Dai: Noncovalent sidewall functionalization of single-walled carbon nanotubes for protein immobilization, J. Am. Chem. Soc. **123**, 3838–3839 (2001)
- 3.361 M. Shim, N. W. S. Kam, R. J. Chen, Y. Li, H. Dai: Functionalization of carbon nanotubes for biocompatibility and biomolecular recognition, Nanolett. **2**, 285–288 (2002)
- 3.362 C. Dwyer, M. Guthold, M. Falvo, S. Washburn, R. Superfine, D. Erie: DNA-functionalized single-walled carbon nanotubes, Nanotechnology **13**, 601–604 (2002)
- 3.363 H. Huang, S. Taylor, K. Fu, Y. Lin, D. Zhang, T. W. Hanks, A. M. Rao, Y. Sun: Attaching proteins to carbon nanotubes via diimide-activated amidation, Nanolett. **2**, 311–314 (2002)

- 3.364 C. V. Nguyen, L. Delzeit, A. M. Cassell, J. Li, J. Han, M. Meyyappan: Preparation of nucleic acid functionalized carbon nanotube arrays, *Nanolett.* **2**, 1079–1081 (2002)
- 3.365 B. R. Azamian, J. J. Davis, K. S. Coleman, C. B. Bagshaw, M. L. H. Green: Bioelectrochemical single-walled carbon nanotubes, *J. Am. Chem. Soc.* **124**, 12664–12665 (2002)
- 3.366 E. Katz, I. Willner: Biomolecule-functionalized carbon nanotubes: Applications in nanobioelectronics, *Chem. Phys. Chem.* **5**, 1084–1104 (2004)
- 3.367 J. Wang: Carbon-nanotube based electrochemical biosensors: a review, *Electroanalysis* **17**, 7–14 (2005)
- 3.368 T. Laha, A. Agarwal, T. McKechnie, S. Seal: Synthesis and characterization of plasma spray formed carbon nanotube reinforced aluminum composite, *Mater. Sci. Eng. A* **381**, 249–258 (2004)
- 3.369 T. Noguchi, A. Magario, S. Fukazawa, S. Shimizu, J. Beppu, M. Seki: Carbon nanotube/aluminium composites with uniform dispersion, *Mater. Transact.* **45**, 602–604 (2004)
- 3.370 Y. B. Li, Q. Ya, B. Q. Wei, J. Liang, D. H. Wu: Processing of a carbon nanotubes-Fe₈₂P₁₈ metallic glass composite, *J. Mater. Sci. Lett.* **17**, 607–609 (1998)
- 3.371 K. T. Kim, K. H. Lee, S. I. Cha, C.-B. Mo, S. H. Hong: Characterization of carbon nanotubes/Cu nanocomposites processed by using nano-sized Cu powders, *Mater. Res. Soc. Symp. Proc.* **821**, 111–116 (2004)
- 3.372 F. Zhang, J. Shen, J. Sun: Processing and properties of carbon nanotubes-nano-WC-Co composites, *Mater. Sci. Eng. A* **381**, 86–91 (2004)
- 3.373 C. L. Xu, B. Q. Wei, R. Z. Ma, J. Liang, X. K. Ma, D. H. Wu: Fabrication of aluminum-carbon nanotube composites and their electrical properties, *Carbon* **37**, 855–858 (1999)
- 3.374 T. Kuzumaki, K. Miyazawa, H. Ichinose, K. Ito: Processing of carbon nanotube reinforced aluminum composite, *J. Mater. Res.* **13**, 2445–2449 (1998)
- 3.375 T. Kuzumaki, O. Ujiie, H. Ichinose, K. Ito: Mechanical characteristics and preparation of carbon nanotube fiber-reinforced Ti composite, *Adv. Eng. Mater.* **2**, 416–418 (2000)
- 3.376 S.-N. Li, S.-Z. Song, T.-Q. Yu, H.-M. Chen, Y.-S. Zhang, J.-L. Shen: Properties of structure of magnesium matrix composite reinforced with CNTs, *J. Wuhan Univ. Technol., Mater. Sci. Ed.* **19**, 65–68 (2004)
- 3.377 E. Carreno-Morelli, J. Yang, E. Couteau, K. Hernadi, J. W. Seo, C. Bonjour, L. Forro, R. Schaller: Carbon nanotube/magnesium composites, *Phys. Stat. Solidi A* **201**, R53–R55 (2004)
- 3.378 Z. Bian, R. J. Wang, W. H. Wang, T. Zhang, A. Inoue: Carbon-nanotube-reinforced Zr-based bulk metallic glass composites and their properties, *Adv. Funct. Mater.* **14**, 55–63 (2004)
- 3.379 S. R. Dong, J. P. Tu, X. B. Zhang: An investigation of the sliding wear behavior of Cu-matrix composite reinforced by carbon nanotubes, *Mater. Sci. Eng. A* **313**, 83–87 (2001)
- 3.380 J. Wang, G. Chen, M. Wang, M. P. Chatrathi: Carbon-nanotube/copper composite electrodes for capillary electrophoresis microchip detection of carbohydrates, *Analyst (Cambridge)* **129**, 512–515 (2004)
- 3.381 Q. Ngo, B. A. Cruden, A. M. Cassell, M. D. Walker, Q. Ye, J. E. Koehne, M. Meyyappan, J. Li, C. Y. Yang: Thermal conductivity of carbon nanotube composite films, *Mater. Res. Soc. Symp. Proc.* **812**, 179–184 (2004)
- 3.382 X. H. Chen, C. S. Chen, H. N. Xiao, F. Q. Cheng, G. Zhang, G. J. Yi: Corrosion behavior of carbon nanotubes-Ni composite coating, *Surf. Coat. Technol.* **191**, 351–356 (2005)
- 3.383 J.-P. Tu, T.-Z. Zou, L.-Y. Wang, W.-X. Chen, Z.-D. Xu, F. Liu, X.-B. Zhang: Friction and wear behavior of Ni-based carbon nanotube composite coatings, *Zhejiang Daxue Xuebao, Gongxueban* **38**, 931–934 (2004)
- 3.384 Z. Yang, H. Xu, M.-K. Li, Y.-L. Shi, Y. Huang, H.-L. Li: Preparation and properties of Ni-P/single-walled carbon nanotubes composite coatings by means of electroless plating, *Thin Solid Films* **466**, 86–91 (2004)
- 3.385 A. Peigney: Tougher ceramics with carbon nanotubes, *Nature Mater.* **2**, 15–16 (2003)
- 3.386 G. D. Zhan, J. D. Kuntz, J. Wan, A. K. Mukherjee: Single-wall carbon nanotubes as attractive toughening agents in alumina-based composites, *Nature Mater.* **2**, 38–42 (2003)
- 3.387 J. Sun, L. Gao, W. Li: Colloidal processing of carbon nanotube/alumina composites, *Chem. Mater.* **14**, 5169–5172 (2002)
- 3.388 J. Ning, J. Zhang, Y. Pan, J. Guo: Surfactants assisted processing of carbon nanotube-reinforced SiO₂ matrix composites, *Ceram. Int.* **30**, 63–67 (2004)
- 3.389 V. G. Gavalas, R. Andrews, D. Bhattacharyya, L. G. Bachas: Carbon nanotube sol-gel composite materials, *Nanolett.* **1**, 719–721 (2001)
- 3.390 S. Rul, Ch. Laurent, A. Peigney, A. Rousset: Carbon nanotubes prepared in-situ in a cellular ceramic by the gel casting-foam method, *J. Eur. Ceram. Soc.* **23**, 1233–1241 (2003)
- 3.391 R. Z. Ma, J. Wu, B. Q. Wei, J. Liang, D. H. Wu: Processing and properties of carbon nanotube/nano-SiC ceramic, *J. Mater. Sci.* **33**, 5243–5246 (1998)
- 3.392 R. W. Siegel, S. K. Chang, B. J. Ash, J. Stone, P. M. Ajayan, R. W. Doremus, L. S. Schadler: Mechanical behavior of polymer and ceramic matrix nanocomposites, *Scr. Mater.* **44**, 2061–2064 (2001)
- 3.393 X. Wang, N. P. Pature, H. Tanaka: Contact-damage-resistant ceramic/single-wall carbon nanotubes and ceramic/graphite composites, *Nature Mater.* **3**, 539–544 (2004)
- 3.394 C. Laurent, A. Peigney, O. Dumortier, A. Rousset: Carbon nanotubes-Fe-alumina nanocomposites.

- Part II: Microstructure and mechanical properties of the hot-pressed composites, *J. Eur. Ceram. Soc.* **18**, 2005–2013 (1998)
- 3.395 A. Peigney, C. Laurent, A. Rousset: Synthesis and characterization of alumina matrix nanocomposites containing carbon nanotubes, *Key Eng. Mater.* **132–136**, 743–746 (1997)
- 3.396 A. Peigney, C. Laurent, E. Flahaut, A. Rousset: Carbon nanotubes in novel ceramic matrix nanocomposites, *Ceram. Intern.* **26**, 677–683 (2000)
- 3.397 S. Rul: Synthèse de composites nanotubes de carbone-métal-oxyde. Ph.D. Thesis (Université Toulouse III, Toulouse 2002)
- 3.398 E. Flahaut, A. Peigney, C. Laurent, C. Marlière, F. Chastel, A. Rousset: Carbon nanotube-metal-oxide nanocomposites: Microstructure, electrical conductivity and mechanical properties, *Acta Mater.* **48**, 3803–3812 (2000)
- 3.399 R. R. Bacsa, C. Laurent, A. Peigney, W. S. Bacsa, T. Vaugien, A. Rousset: High specific surface area carbon nanotubes from catalytic chemical vapor deposition process, *Chem. Phys. Lett.* **323**, 566–571 (2000)
- 3.400 P. Coquay, A. Peigney, E. De Grave, R. E. Vandenberghe, C. Laurent: Carbon nanotubes by a CVD method. Part II: Formation of nanotubes from (Mg,Fe)O catalysts, *J. Phys. Chem. B* **106**, 13199–13210 (2002)
- 3.401 E. Flahaut, Ch. Laurent, A. Peigney: Double-walled carbon nanotubes in composite powders, *J. Nanosci. Nanotech.* **3**, 151–158 (2003)
- 3.402 A. Peigney, P. Coquay, E. Flahaut, R. E. Vandenberghe, E. De Grave, C. Laurent: A study of the formation of single- and double-walled carbon nanotubes by a CVD method, *J. Phys. Chem. B* **105**, 9699–9710 (2001)
- 3.403 A. Peigney, S. Rul, F. Lefevre-Schlick, C. Laurent: Densification during hot-pressing of carbon nanotube metal-ceramic composites, *J. Europ. Ceram. Soc.*, submitted (2006)
- 3.404 Z. Xia, L. Riester, W. A. Curtin, H. Li, B. W. Sheldon, J. Liang, B. Chang, J. M. Xu: Direct observation of toughening mechanisms in carbon nanotube ceramic matrix composites, *Acta Mater.* **52**, 931–944 (2004)
- 3.405 S. Rul, F. Lefevre-Schlick, E. Capria, C. Laurent, A. Peigney: Percolation of single-walled carbon nanotubes in ceramic matrix nanocomposites, *Acta Materialia* **52**, 1061–1067 (2004)
- 3.406 A. Peigney, E. Flahaut, C. Laurent, F. Chastel, A. Rousset: Aligned carbon nanotubes in ceramic-matrix nanocomposites prepared by high-temperature extrusion, *Chem. Phys. Lett.* **352**, 20–25 (2002)
- 3.407 G.-D. Zhan, J. D. Kuntz, J. E. Garay, A. K. Mukherjee: Electrical properties of nanoceramics reinforced with ropes of single-walled carbon nanotubes, *Appl. Phys. Lett.* **83**, 1228–1230 (2003)
- 3.408 Q. Huang, L. Gao: Manufacture and electrical properties of multiwalled carbon nanotube/BaTiO₃ nanocomposite ceramics, *J. Mater Chem.* **14**, 2536–2541 (2004)
- 3.409 S. L. Huang, M. R. Koblischka, K. Fossheim, T. W. Ebbesen, T. H. Johansen: Microstructure and flux distribution in both pure and carbon-nanotube-embedded Bi₂Sr₂CaCu₂O_{8+δ} superconductors, *Physica C* **311**, 172–186 (1999)
- 3.410 T. Seeger, G. de la Fuente, W. K. Maser, A. M. Benito, M. A. Callejas, M. T. Martinez: Evolution of multiwalled carbon-nanotube/SiO₂ composites via laser treatment, *Nanotechnology* **14**, 184–187 (2003)
- 3.411 G.-D. Zhan, J. D. Kuntz, H. Wang, C.-M. Wang, A. K. Mukherjee: Anisotropic thermal properties of single-wall-carbon-nanotube-reinforced nanoceramics, *Phil. Mag. Lett.* **84**, 419–423 (2004)
- 3.412 A. Weidenkaff, S. G. Ebbinghaus, T. Lippert: Ln_{1-x}A_xCoO₃ (Ln = Er, La; A = Ca, Sr)/carbon nanotube composite materials applied for rechargeable Zn/Air batteries, *Chem. Mater.* **14**, 1797–1805 (2002)
- 3.413 D. S. Lim, J. W. An, H. J. Lee: Effect of carbon nanotube addition on the tribological behavior of carbon/carbon composites, *Wear* **252**, 512–517 (2002)
- 3.414 R. Andrews, D. Jacques, A. M. Rao, T. Rantell, F. Derbyshire, Y. Chen, J. Chen, R. C. Haddon: Nanotube composite carbon fibers, *Appl. Phys. Lett.* **75**, 1329–1331 (1999)
- 3.415 P. M. Ajayan, O. Stephan, C. Colliex, D. Trauth: Aligned carbon nanotube arrays formed by cutting a polymer resin-nanotube composite, *Science* **265**, 1212–14 (1994)
- 3.416 R. Haggemueller, H. H. Gommans, A. G. Rinzler, J. E. Fischer, K. I. Winey: Aligned single-wall carbon nanotubes in composites by melt processing methods, *Chem. Phys. Lett.* **330**, 219–225 (2000)
- 3.417 L. S. Schadler, S. C. Giannaris, P. M. Ajayan: Load transfer in carbon nanotube epoxy composites, *Appl. Phys. Lett.* **73**, 3842–3844 (1998)
- 3.418 S. J. V. Frankland, A. Caglar, D. W. Brenner, M. Griebel: Molecular simulation of the influence of chemical cross-links on the shear strength of carbon nanotube-polymer interfaces, *J. Phys. Chem. B* **106**, 3046–3048 (2002)
- 3.419 H. D. Wagner: Nanotube-polymer adhesion: A mechanics approach, *Chem. Phys. Lett.* **361**, 57–61 (2002)
- 3.420 P. M. Ajayan, L. S. Schadler, C. Giannaris, A. Rubio: Single-walled carbon nanotube-polymer composites: Strength and weakness, *Adv. Mater.* **12**, 750–753 (2000)
- 3.421 X. Gong, J. Liu, S. Baskaran, R. D. Voise, J. S. Young: Surfactant-assisted processing of carbon nanotube/polymer composites, *Chem. Mater.* **12**, 1049–1052 (2000)
- 3.422 E. T. Thostenson, W. Z. Li, D. Z. Wang, Z. F. Ren, T. W. Chou: Carbon nanotube/carbon fiber hybrid multiscale composites, *J. Appl. Phys.* **91**, 6034–6037 (2002)

- 3.423 S. Barrau, P. Demont, A. Peigney, C. Laurent, C. Lacabanne: Effect of palmitic acid on the electrical conductivity of carbon nanotubes-polyepoxy composite, *Macromolecules* **36**, 9678–9680 (2003)
- 3.424 S. Barrau, P. Demont, A. Peigney, C. Laurent, C. Lacabanne: DC and AC conductivity of carbon nanotubes-polyepoxy composites, *Macromolecules* **36**, 5187–5194 (2003)
- 3.425 J. Sandler, M. S. P. Shaffer, T. Prasse, W. Bauhofer, K. Schulte, A. H. Windle: Development of a dispersion process for carbon nanotubes in an epoxy matrix and the resulting electrical properties, *Polymer* **40**, 5967–5971 (1999)
- 3.426 M. J. Biercuk, M. C. Llaguno, M. Radosavljevic, J. K. Hyun, A. T. Johnson, J. E. Fischer: Carbon nanotube composites for thermal management, *Appl. Phys. Lett.* **80**, 2767–2769 (2002)
- 3.427 F. H. Gojny, K. Schulte: Functionalisation effect on the thermo-mechanical behaviour of multi-wall carbon nanotube/epoxy-composites, *Compos. Sci. Technol.* **64**, 2303–2308 (2004)
- 3.428 F. H. Gojny, M. H. G. Wichmann, U. Kopke, B. Fiedler, K. Schulte: Carbon nanotube-reinforced epoxy-composites: enhanced stiffness and fracture toughness at low nanotube content, *Compos. Sci. Technol.* **64**, 2363–2371 (2004)
- 3.429 G. Pecastaings, P. Delhaes, A. Derre, H. Saadaoui, F. Carmona, S. Cui: Role of interfacial effects in carbon nanotube/epoxy nanocomposite behavior, *J. Nanosci. Nanotech.* **4**, 838–843 (2004)
- 3.430 Z. Jin, K. P. Pramoda, G. Xu, S. H. Goh: Dynamic mechanical behavior of melt-processed multi-walled carbon nanotube/poly(methyl methacrylate) composites, *Chem. Phys. Lett.* **337**, 43–47 (2001)
- 3.431 Z. Jin, K. P. Pramoda, S. H. Goh, G. Xu: Poly(vinylidene fluoride)-assisted melt-blending of multi-walled carbon nanotube/poly(methyl methacrylate) composites, *Mater. Res. Bull.* **37**, 271–278 (2002)
- 3.432 C. A. Cooper, D. Ravich, D. Lips, J. Mayer, H. D. Wagner: Distribution and alignment of carbon nanotubes and nanofibrils in a polymer matrix, *Compos. Sci. Technol.* **62**, 1105–1112 (2002)
- 3.433 J. M. Benoit, B. Corraze, S. Lefrant, W. J. Blau, P. Bernier, O. Chauvet: Transport properties of PMMA-carbon nanotubes composites, *Synth. Met.* **121**, 1215–1216 (2001)
- 3.434 J. M. Benoit, B. Corraze, O. Chauvet: Localization, Coulomb interactions, and electrical heating in single-wall carbon nanotubes/polymer composites, *Phys. Rev. B* **65**, 241405/1–241405/4 (2002)
- 3.435 F. Du, R. C. Scogna, W. Zhou, S. Brand, J. E. Fischer, K. I. Winey: Nanotube networks in polymer nanocomposites: rheology and electrical conductivity, *Macromolecules* **37**, 9048–9055 (2004)
- 3.436 T. Kashiwagi, F. Du, K. I. Winey, K. M. Groth, J. R. Shields, R. H. Harris Jr., J. F. Douglas: Flammability properties of PMMA-single walled carbon nanotube nanocomposites, *Polymer. Mater. Sci. Eng.* **91**, 90–91 (2004)
- 3.437 M. S. P. Shaffer, A. H. Windle: Fabrication and characterization of carbon nanotube/poly(vinyl alcohol) composites, *Adv. Mater.* **11**, 937–941 (1999)
- 3.438 L. Jin, C. Bower, O. Zhou: Alignment of carbon nanotubes in a polymer matrix by mechanical stretching, *Appl. Phys. Lett.* **73**, 1197–1199 (1998)
- 3.439 H. D. Wagner, O. Lourie, Y. Feldman, R. Tenne: Stress-induced fragmentation of multiwall carbon nanotubes in a polymer matrix, *Appl. Phys. Lett.* **72**, 188–190 (1998)
- 3.440 H. D. Wagner, O. Lourie, X. F. Zhou: Macrofragmentation and microfragmentation phenomena in composite materials, *Compos. Part A* **30A**, 59–66 (1998)
- 3.441 J. R. Wood, Q. Zhao, H. D. Wagner: Orientation of carbon nanotubes in polymers and its detection by Raman spectroscopy, *Compos. Part A* **32A**, 391–399 (2001)
- 3.442 Q. Zhao, J. R. Wood, H. D. Wagner: Using carbon nanotubes to detect polymer transitions, *J. Polym. Sci. Part B* **39**, 1492–1495 (2001)
- 3.443 M. Cochet, W. K. Maser, A. M. Benito, M. A. Callejas, M. T. Martinez, J. M. Benoit, J. Schreiber, O. Chauvet: Synthesis of a new polyaniline/nanotube composite: In-situ polymerisation and charge transfer through site-selective interaction, *Chem. Commun.*, 1450–1451 (2001)
- 3.444 D. Qian, E. C. Dickey, R. Andrews, T. Rantell: Load transfer and deformation mechanisms in carbon nanotube-polystyrene composites, *Appl. Phys. Lett.* **76**, 2868–2870 (2000)
- 3.445 V. Datsyuk, Christelle Guerret-Piecourt, S. Dagreou, L. Billon, J.-C. Dupin, E. Flahaut, A. Peigney, C. Laurent: Double walled carbon nanotube/polymer composites via in-situ nitroxide mediated polymerisation of amphiphilic block copolymers, *Carbon* **43**, 873–876 (2005)
- 3.446 R. Blake, Y. K. Gun'ko, J. Coleman, M. Cadec, A. Fonseca, J. B. Nagy, W. J. Blau: A generic organometallic approach toward ultra-strong carbon nanotube polymer composites, *J. Am. Chem. Soc.* **126**, 10226–10227 (2004)
- 3.447 T. Kashiwagi, E. Grulke, J. Hilding, K. Groth, R. Harris, K. Butler, J. Shields, S. Kharchenko, J. Douglas: Thermal and flammability properties of polypropylene/carbon nanotube nanocomposites, *Polymer* **45**, 4227–4239 (2004)
- 3.448 C. Wei, D. Srivastava, K. Cho: Thermal expansion and diffusion coefficients of carbon nanotube-polymer composites, *Los Alamos Nat. Lab., Preprint Archive, Condensed Matter (archiv:cond-mat/0203349)*, 1–11 (2002)
- 3.449 J. C. Grunlan, M. V. Bannon, A. R. Mehrabi: Latex-based, single-walled nanotube composites: processing and electrical conductivity, *Polym. Prepr.* **45**, 154–155 (2004)

- 3.450 J. C. Grunlan, A. R. Mehrabi, M. V. Bannon, J. L. Bahr: Water-based single-walled-nanotube-filled polymer composite with an exceptionally low percolation threshold, *Adv. Mater. (Weinheim)* **16**, 150–153 (2004)
- 3.451 C. Pirlot, I. Willems, A. Fonseca, J. B. Nagy, J. Delhalle: Preparation and characterization of carbon nanotube/polyacrylonitrile composites, *Adv. Eng. Mater.* **4**, 109–114 (2002)
- 3.452 H. Lam, H. Ye, Y. Gogotsi, F. Ko: Structure and properties of electrospun single-walled carbon nanotubes reinforced nanocomposite fibrils by co-electrospinning, *Polym. Prepr.* **45**, 124–125 (2004)
- 3.453 L. Cao, H. Chen, M. Wang, J. Sun, X. Zhang, F. Kong: Photoconductivity study of modified carbon nanotube/oxotitanium phthalocyanine composites, *J. Phys. Chem. B* **106**, 8971–8975 (2002)
- 3.454 I. Musa, M. Baxendale, G.A.J. Amaratunga, W. Eccleston: Properties of regular poly(3-octylthiophene)/multi-wall carbon nanotube composites, *Synth. Met.* **102**, 1250 (1999)
- 3.455 E. Kymakis, I. Alexandou, G.A.J. Amaratunga: Single-walled carbon nanotube-polymer composites: Electrical, optical and structural investigation, *Synth. Met.* **127**, 59–62 (2002)
- 3.456 K. Yoshino, H. Kajii, H. Araki, T. Sonoda, H. Take, S. Lee: Electrical and optical properties of conducting polymer-fullerene and conducting polymer-carbon nanotube composites, *Fuller. Sci. Technol.* **7**, 695–711 (1999)
- 3.457 B. Maruyama, K. Alam: Carbon nanotubes and nanofibers in composite materials, *SAMPE J.* **38**, 59–70 (2002)
- 3.458 S. A. Curran, P. M. Ajayan, W. J. Blau, D. L. Carroll, J. N. Coleman, A. B. Dalton, A. P. Davey, A. Drury, B. McCarthy, S. Maier, A. Strevens: A composite from poly(m-phenylenevinylene-co-2,5-dioctoxy-p-phenylenevinylene) and carbon nanotubes. A novel material for molecular optoelectronics, *Adv. Mater.* **10**, 1091–1093 (1998)
- 3.459 P. Fournet, D.F. O'Brien, J. N. Coleman, H. H. Horhold, W. J. Blau: A carbon nanotube composite as an electron transport layer for M3EH-PPV based light-emitting diodes, *Synth. Met.* **121**, 1683–1684 (2001)
- 3.460 H. S. Woo, R. Czerw, S. Webster, D. L. Carroll, J. Balato, A. E. Strevens, D. O'Brien, W. J. Blau: Hole blocking in carbon nanotube-polymer composite organic light-emitting diodes based on poly(m-phenylene vinylene-co-2,5-dioctoxy-p-phenylene vinylene), *Appl. Phys. Lett.* **77**, 1393–1395 (2000)
- 3.461 H. S. Woo, R. Czerw, S. Webster, D. L. Carroll, J. W. Park, J. H. Lee: Organic light emitting diodes fabricated with single wall carbon nanotubes dispersed in a hole conducting buffer: The role of carbon nanotubes in a hole conducting polymer, *Synth. Met.* **116**, 369–372 (2001)
- 3.462 H. Ago, K. Petritsch, M. S. P. Shaffer, A. H. Windle, R. H. Friend: Composites of carbon nanotubes and conjugated polymers for photovoltaic devices, *Adv. Mater.* **11**, 1281–1285 (1999)
- 3.463 B. Vigolo, A. Pénicaud, C. Coulon, C. Sauder, R. Paillet, C. Journet, P. Bernier, P. Poulin: Macroscopic fibers and ribbons of oriented carbon nanotubes, *Science* **290**, 1331–1334 (2000)
- 3.464 B. Vigolo, P. Poulin, M. Lucas, P. Launois, P. Bernier: Improved structure and properties of single-wall carbon nanotube spun fibers, *Appl. Phys. Lett.* **11**, 1210–1212 (2002)
- 3.465 P. Poulin, B. Vigolo, P. Launois: Films and fibers of oriented single wall nanotubes, *Carbon* **40**, 1741–1749 (2002)
- 3.466 K. Jiang, Q. Li, S. Fan: Spinning continuous carbon nanotube yarn, *Nature* **419**, 801 (2002)
- 3.467 M. Zhang, K. R. Atkinson, R. H. Baughman: Multi-functional carbon nanotube yarns by downsizing an ancient technology, *Science* **306**, 1356–1361 (2004)
- 3.468 J. Steinmetz, M. Glerup, M. Paillet, P. Bernier, M. Holzinger: Production of pure nanotube fibers using a modified wet-spinning method, *Carbon* **43**, 2397–2400 (2005)
- 3.469 P. Lambin, A. Fonseca, J. P. Vigneron, J. B'Nagy, A. A. Lucas: Structural and electronic properties of bent carbon nanotubes, *Chem. Phys. Lett.* **245**, 85–89 (1995)
- 3.470 L. Chico, V. H. Crespi, L. X. Benedict, S. G. Louie, M. L. Cohen: Pure carbon nanoscale devices: Nanotube heterojunctions, *Phys. Rev. Lett.* **76**, 971–974 (1996)
- 3.471 Z. Yao, H. W. C. Postma, L. Balents, C. Dekker: Carbon nanotube intramolecular junctions, *Nature* **402**, 273–276 (1999)
- 3.472 S. J. Tans, A. R. M. Verschueren, C. Dekker: Room temperature transistor based on single carbon nanotube, *Nature* **393**, 49–52 (1998)
- 3.473 R. Martel, T. Schmidt, H. R. Shea, T. Hertel, P. Avouris: Single and multi-wall carbon nanotube field effect transistors, *Appl. Phys. Lett.* **73**, 2447–2449 (1998)
- 3.474 V. Derycke, R. Martel, J. Appenzeller, P. Avouris: Carbon nanotube inter- and intramolecular logic gates, *Nanolett.* **1**, 453–456 (2001)
- 3.475 P. G. Collins, M. S. Arnold, P. Avouris: Engineering carbon nanotubes using electrical breakdown, *Science* **292**, 706–709 (2001)
- 3.476 A. P. Graham, G. S. Duesberg, W. Hoenlein, F. Kreupl, M. Liebau, R. Martin, B. Rajasekharan, W. Pamler, R. Seidel, W. Steinhögl, E. Unger: How do carbon nanotubes fit into the semiconductor roadmap?, *Appl. Phys. A* **80**, 1141–1151 (2005)
- 3.477 P. Kim, C. M. Lieber: Nanotube nanotweezers, *Science* **286**, 2148–2150 (1999)
- 3.478 R. H. Baughman, C. Changxing, A. A. Zakhidov, Z. Iqbal, J. N. Barisci, G. M. Spinks, G. G. Wallace,

- A. Mazzoldi, D. de Rossi, A. G. Rinzler, O. Jaschinski S. Roth, M. Kertesz: Carbon nanotubes actuators, *Science* **284**, 1340–1344 (1999)
- 3.479 Y. Gao, Y. Bando: Carbon nanothermometer containing gallium, *Nature* **415**, 599 (2002)
- 3.480 C. Niu, E. K. Sichel, R. Hoch, D. Moy, H. Tennent: High power electro-chemical capacitors based on carbon nanotube electrodes, *Appl. Phys. Lett.* **70**, 1480–1482 (1997)
- 3.481 E. Frackowiak, F. Béguin: Electrochemical storage of energy in carbon nanotubes and nanostructured carbons, *Carbon* **40**, 1775–1787 (2002)
- 3.482 C. Portet, P.L. Taberna, P. Simon, E. Flahaut: Influence of carbon nanotubes addition on carbon-carbon supercapacitor performances in organic electrolyte, *J. Power. Sources* **139**, 371–378 (2005)
- 3.483 E. Frackowiak, K. Jurewicz, K. Szostak, S. Delpeux, F. Béguin: Nanotubular materials as electrodes for supercapacitors, *Fuel Process. Technol.* **77**, 213–219 (2002)
- 3.484 J. Mittal, E. Frackowiak, M. Monthieux, G. Lota: High performance supercapacitor from hybrid-nanotube-based electrodes, *Nanotechnol.* (2006) submitted